Design and Construction of a Supersonic Wind Tunnel with Diagnostics

A Major Qualifying Project

Submitted to the Faculty

of

Worcester Polytechnic Institute

in partial fulfillment of the requirements for the

Degrees of Bachelor of Science

in Aerospace and Mechanical Engineering

by

William Bugden

Katherine Fitton

Geordie Folinas

Nathan Fournier

Gallagher Hogan

Markus Ito

Joshua Lambert

Neel Patel

Dong-Uk Shin

Grant Wong

Earl Ziegler

April 17, 2013

Approved:

Prof. John Blandino, MQP Advisor

Abstract

The goal of this project was to design, construct, and conduct preliminary testing of a supersonic wind tunnel (SWT) in which flow properties could be measured and the flow qualitatively imaged. The current experimental facilities at Worcester Polytechnic Institute (WPI) do not include a supersonic wind tunnel. The SWT built in this project represents a new facility that can be used for research and teaching in the future. In addition to observing supersonic flow characteristics, the behavior of test objects in these flows can also be investigated. The wind tunnel is an indraft type that uses the pressure ratio created between a vacuum chamber and the ambient air to generate a flow. The tunnel was designed and built to be modular, allowing future users to switch the current channel contours with alternative, test-specific designs. The tunnel uses a Pitot-static probe system to acquire pressure measurements which are then used to calculate Mach number. In addition to the pressure measurements, a schlieren optical system was built to allow imaging of flow structures. To ensure proper performance under a range of ambient conditions, a humidity control system was designed and built to prevent condensation in the channel.

Acknowledgements

Table of Contents

List of Figures

List of Tables

1 Introduction

The goals of this project were to design and construct a supersonic wind tunnel with diagnostic and visualization systems to characterize flow properties. The supersonic wind tunnel was designed to interface with a vacuum chamber in the Vacuum Test Facility (VTF) at Worcester Polytechnic Institute. A pressure differential between the ambient air and the air in the vacuum drives the flow in the wind tunnel. Characterizing flow properties involved the use of a Pitot-static probe and static pressure taps. It also included an application of the schlieren technique, which is a non-intrusive method of qualitatively visualizing the flow through the test section.

The above goals were accomplished by splitting the project into three areas of focus, leading to the creation of three teams to design and construct each major component of the final product. These major components included the wind tunnel channel and flange, the probes and data acquisition system, and the schlieren flow visualization system.

1. The first team was responsible for the design and fabrication of the wind tunnel channel and flange. First, this team developed an understanding of the theory behind supersonic wind tunnel design. An analytical tool was then used to determine tunnel dimensions and contours based on the desired Mach number in the test section. The tunnel was designed and necessary components were fabricated and assembled.

2. The second team created the probe measurement system. They completed an in-depth literature review on the use of Pitot-static probes in supersonic flow applications. The design of the system included a Pitot-static probe and pressure taps interfacing with the side of the channel. It also included a data acquisition system (DAQ) that took the

required pressure measurements and calculated flow properties based on the relationships between pressure and Mach number.

3. The third team produced the schlieren system. The theory of schlieren imaging was investigated to understand the necessary optical equipment to qualitatively visualize the flow. The system was placed on a custom table designed to align with the test section of the channel. The required parts for the system and table were ordered. The optical parts were arranged on t-slotted extrusions to create a z-type imaging system and the table and mounting parts were fabricated and assembled.

Compressible flow in a supersonic wind tunnel creates condensation in the channel, which negatively affects the performance quality of the full system. In order to guarantee proper functionality of the wind tunnel, diagnostics, and flow visualization, the project also required the implementation of a humidity control system. The initial calculations and theory behind supersonic humidity control systems were investigated. The system required for this wind tunnel was then designed and assembled to interface directly with the inflow of the channel.

The wind tunnel was first run without the humidity control system to verify that there were no air leakages. The tunnel was then connected to the humidity control system and tested to ensure that no condensation formed in the channel. The Pitot-static probe system and schlieren system were commissioned separately through bench top tests to confirm proper operation. Once all three areas of focus had completed their work separately, the systems were interfaced and tested. Having met these objectives, future work can extend the capabilities of the tunnel and diagnostic systems, at which point, the tunnel can be used to make measurements in research applications.

2 Previous Work

The following sections outline the previous MQP projects involving supersonic wind tunnels advised by Professor Blandino at WPI. These projects include the first design of a supersonic wind tunnel to interface with the vacuum chamber in the VTF and a continuation project that designed a supersonic wind tunnel with variable contours in the nozzle and test section.

2.1 Summer 2009

In the summer of 2009 Peter Moore designed and constructed a supersonic wind tunnel [1]. The goal was to design a supersonic wind tunnel that could be used with WPI's large vacuum chamber which is the primary component of the VTF located in HL016. As part of this MQP, a detailed analysis of various different types of supersonic wind tunnels was conducted, keeping in mind the constraints imposed on the project from existing hardware that was going to be incorporated into the design. It was decided to use an indraft style tunnel design because of its compatibility with the vacuum chamber and the reduced complexity of using a vacuum tank.

The design of the tunnel geometry involved using the method of characteristics, a numerical procedure for solving inviscid, two-dimensional compressible flow problems. By using this method it is possible to calculate the contour of the tunnel in order to minimize oblique shocks in the convergent section. Once the geometry had been calculated, it was then imported into SolidWorks where the remaining channel and flange features were modeled and prepared for fabrication. The completed tunnel consisted of a mounting flange which mated with the vacuum tank, two identical upper and lower tunnel halves which are sandwiched between two sheets of clear acrylic, and an end piece which incorporated a ball valve to start the flow.

The finished tunnel was never tested during this MQP, the intention being to simulate the compressible air flow in COMSOL Multiphysics software. Ultimately it was discovered that the current version of COMSOL available at the time did not support high speed compressible flow, so standard isentropic flow relations were used to provide an estimate of the flow properties one might expect. The results of the 2009 MQP were available to the next MQP group who would be building on the work that had already been completed. The issues of condensation and measurement of the airflow in the tunnel were identified but left for future groups to consider due to the time and budget constraints of the MQP. The implementation of a supersonic diffuser to increase run time was also proposed as an option for the following group to pursue.

2.2 Academic Year 2009-2010

The main objective of the 2009-2010 project was to build a small-scale supersonic wind tunnel. The wind tunnel was constructed with the intent of providing a means of changing the channel geometry. The project was a continuation of a previous MQP group from the summer of 2009, which already built a wind tunnel with the objective of obtaining one specific Mach number. The group working over the 2009-2010 academic year decided to design a supersonic wind tunnel with variable contours that would allow for testing at various Mach numbers [2].

Before constructing the wind tunnel, the group studied many types of wind tunnels and analyzed the performance of each tunnel. They continued with the selection of the indraft type wind tunnel due to its simpler design and the availability of the vacuum chamber. Before constructing the wind tunnel, the group performed the calculations related to various conditions such as run-time, test section area, and appropriate Mach number to check the constraints for designing [2]. These calculations showed that adding a diffuser would increase the run-time [2].

When designing the tunnel, the group used the same cross sectional areas as those used by the previous MQP and therefore was able to reuse the ball valve and the end piece. Due to the placement of the ball vale at the inlet, the tunnel had to be sealed against the atmosphere. If the test section is left unsealed, the air leakage would not allow the tunnel to obtain the required pressure difference to drive the flow. The group used a rubber O-ring system on the edges of each contour and compressed the contours between the two side plates which were constructed based on the design generated by the previous MQP. The student group also added the variable contour sections to attain the different Mach numbers in the test area. The contoured sections were used in the throat, expansion section, straightening section, and diffuser section and were adjusted by pivoting screw adjustment mechanisms [2]. With each shape, the Mach number was calculated based on the method of characteristics.

The 2009-2010 group found that the fixed geometry tunnel built by Peter Moore was not able to sustain the required pressure difference due to a significant leak. Even though the group of students updated the sealing design by modifying the O-ring system and compressing the side panels in order to alleviate the leaking problem, they could not completely resolve the sealing issues. Overall, the functionality of the moveable contours on the tunnel could not be fully tested due to the sealing problem.

3 Wind Tunnel Channel and Flange Design

The first major area of focus in this project was the design of the wind tunnel itself. This required a thorough understanding of compressible flow regimes as they pertain to wind tunnel design. A lengthy literature review was conducted, and the findings were summarized and applied to the goals and facility conditions of this project to design and construct an indraft supersonic wind tunnel to be compatible with the vacuum chamber in WPI's VTF.

3.1 Compressible Flow Regimes

Material flow characteristics differ for various substances such as solids, liquids, and gases. Matter consists of molecules that are bonded together by intermolecular forces. Solids are comprised of molecules bonded together in relatively fixed positions. Liquids include molecules that are cohesively bonded, rather than held together in fixed positions. Due to this inherent nature, liquids can usually be approximated as incompressible substances. Gases consist of molecules moving in random motion with negligible cohesive forces. Depending on the speed of the gas, it can be approximated as either an incompressible or compressible substance [4].

3.1.1 Incompressible and Compressible Flows

An incompressible substance is one that does not experience significant density changes throughout the substance, or the medium. This situation can be found in low speed flows, where the kinetic energy is negligible to the thermal energy found in the medium [2]. Changes in density begin to take place when imposed with a pressure gradient. Higher speed flows, where the kinetic energy is comparable in magnitude to the thermal energy, will have varying densities throughout the medium and are thus considered compressible substances [2].

When a body is placed in a gas flow, disturbances will form and propagate through the medium. A given disturbance will affect those molecules closest to the body and will collide with the surrounding molecules [4]. In incompressible flows, the distance between the molecules will be maintained through propagation of the disturbance, but in compressible flows, the molecules will contract closer to each other before returning to their original distance after the disturbance [4]. This can be shown in Figure 1.
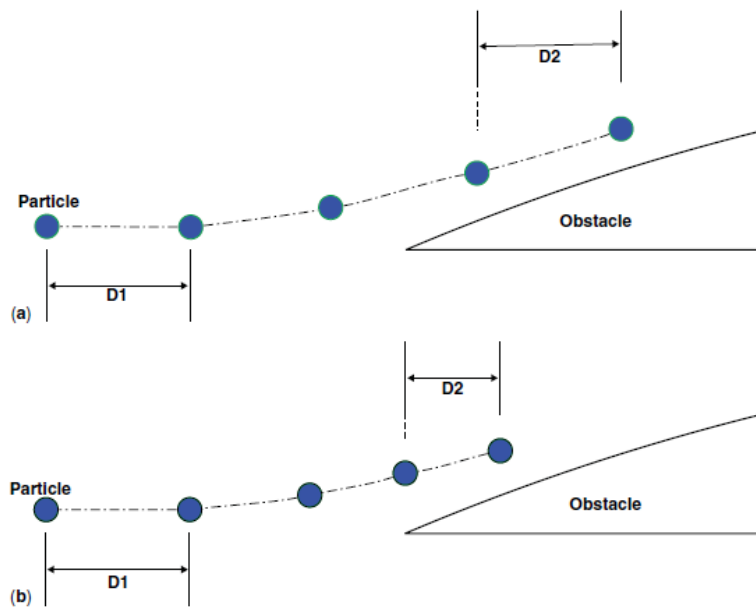
Figure 1: Molecules moving around an obstacle in a) incompressible flow and b) compressible flow (Ref [4], © 2010, Encyclopedia of Aerospace Engineering)

The speed at which a disturbance propagates through a medium is the speed of sound. The non-dimensional number that expresses free-stream velocity with respect to the speed of sound of a medium is the Mach number (M), which is determined to be:

$$M = \frac{u_\infty}{a} \tag{3.1}$$

where u_∞ is the free-stream velocity and a is the speed of sound of the medium [2,3]. In the case where the free-stream velocity is equal to or greater than the speed of sound in the medium, particles collide and accumulate. This creates a "speed barrier" region, or a shock wave that propagates through the flow [4]. This large disturbance makes for a discontinuous variation of properties in the flow.

3.1.2 Mach Number Flow Regimes

Flow properties can be established by the value of the Mach number. Flows that have a low Mach number, $M < 0.3$, can be assumed incompressible flow, while anything above this is considered compressible flow. The compressible flow regime can be further broken down into subsonic flow, $M < 1$, transonic flow, $0.7 < M < 1.2$, and supersonic flow, $M > 1$ [2,3].

Subsonic flows are characterized by smooth streamlines and have continuous variation of properties, rather than large disturbances that cause discontinuous variations [2]. When introduced to a body in the flow, disturbances will propagate further upstream of the body than flows with higher Mach numbers. This phenomenon is shown in Figure 2 for all Mach number regimes.
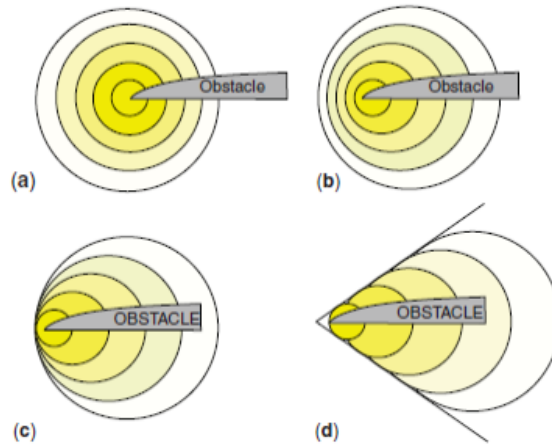
Figure 2: Disturbance propagation and shock wave formation upstream of body in a) M < 0.3, b) 0.3 < M < 0.7, c) 0.7 < M < 1.2, d) M > 1.2 (Ref [4], © 2010, Encyclopedia of Aerospace Engineering)

Transonic flows are an organization grouping used to make flow properties simpler through assumptions. They consist of mixed subsonic and supersonic flow regions. Shocks can occur in these flows but often do not have a strong enough pressure gradient to assume flow properties similar to those of supersonic flows. These regions are difficult to model mathematically because they have characteristics of subsonic and supersonic flows.

Supersonic flows may involve the formation of shock waves in the flow, since the free-stream velocity exceeds the speed of sound in the medium and creates highly compressed air at the front of the body. In cases where the Mach number exceeds 5, the flow is referred to as hypersonic [2]. These flows must account for the distance the molecules travel between consecutive collisions [4]. The effects of shock waves on flow properties and the different types of shocks will be discussed further in Section 3.1.3 Shock Waves.

3.1.3 Shock Waves

The most important effects of compressibility are not seen until the speed of sound has been broken, but the effects should be taken into consideration beginning at approximately M = 0.85. When a fluid flows over an object at Mach 1 and higher, clusters of very weak "Mach waves" begin to form. Individually, these Mach waves have little effect on the flow properties, but a high concentration of these Mach waves can converge and create what is known as a "shock wave". Shock waves always develop when the flow over an object is supersonic, and the flow through a shock wave can no longer be considered isentropic. The two types of shock waves are normal shocks and oblique shocks. Normal shocks form perpendicular to the direction of the flow, while oblique shocks are inclined at a certain angle α to the direction of the flow.

The velocity upstream of a shock wave is always supersonic. However, the downstream conditions are dependent upon the nature of the shock wave. The velocity downstream of an oblique shock may be subsonic, in which case the fluid is said to have passed through a strong shock, or it may be supersonic, in which case the fluid is said to have passed through a weak shock. The component of the downstream velocity that is perpendicular to the shock is always subsonic. In two-dimensional flow around a blunt body (Figure 3), a normal shock forms directly in front of the body and extends around the body as an oblique shock, and then further down as a Mach wave. As a result, the strength of the wave decreases from its highest level directly in front of the body to its lowest level around the sides of the body. Figure 3 provides a visual description of this behavior.
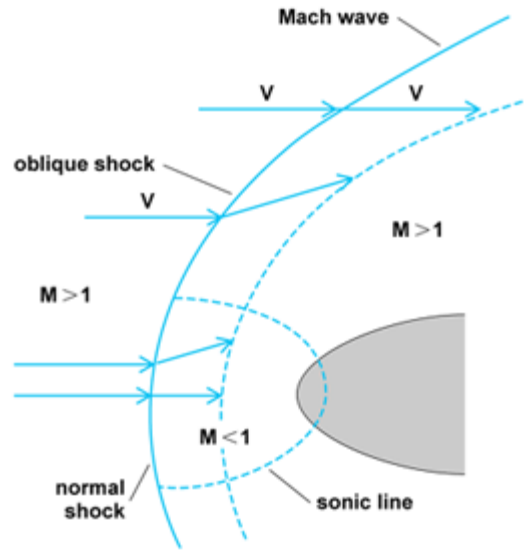
Figure 3: Shock waves over a blunt body (Ref [5], © 2012, Saad)

When supersonic flow is forced through contoured nozzle, as is the case in a wind tunnel, the flow expands or compresses across a series of Mach waves. This particular regime of compressible flow is known as Prandtl-Meyer flow. Figure 4 summarizes the basic types of flow patterns in Prandtl-Meyer flow. Supersonic flow over a convex curve will result in a series of expansion Mach waves (part (a) Figure 4), which make up what is known as a Prandtl-Meyer fan. The flow along these Mach waves is considered uniform, and the properties change gradually throughout the expansion fan. Supersonic flow over a concave curve will result in what is known as Prandtyl-Meyer compression (part (c) Figure 4). In this case, the compression waves meet further away from the surface of the wall to form an oblique shock.
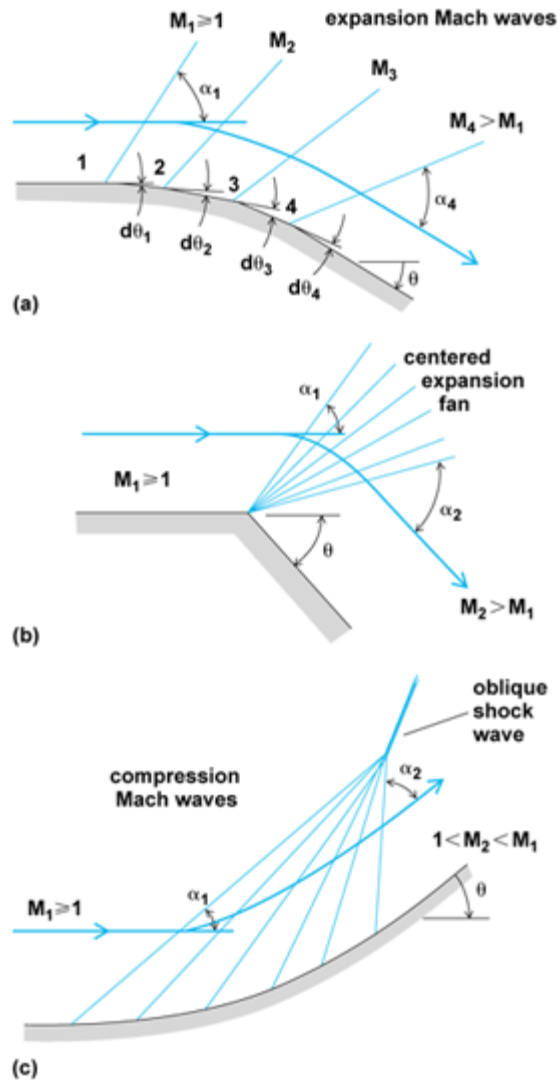
Figure 4: Prandtyl-Meyer flow (Ref [5], © 2012, Saad)

Another special type of shock wave that is important to discuss for the scope of this project is a humidity-induced condensation shock wave. At certain inlet humidity levels, in addition to fog in the test section, a γ-shaped condensation shock wave can form upstream of a normal shock, interacting with it and causing unexpected variations in flow properties.
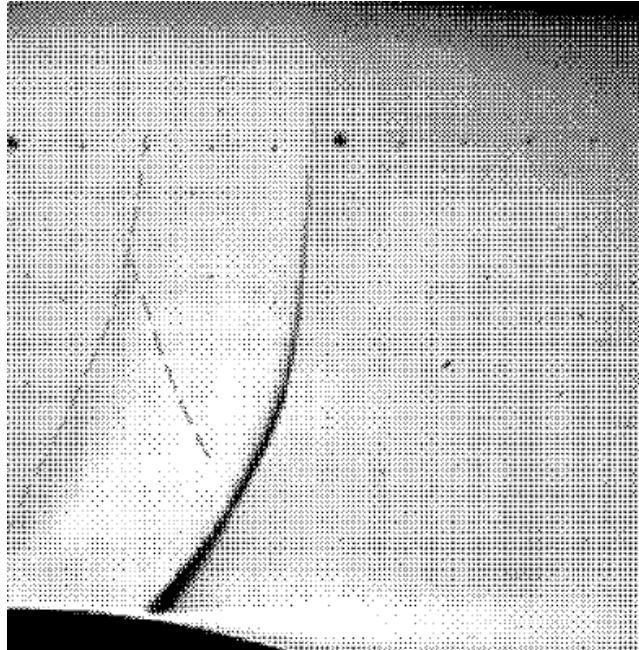
Figure 5: Condensation shock wave at 50% relative humidity (Ref [6], © 2008, Huang)

A condensation shock wave can form at inlet humidity levels over forty percent, resulting in weakening shock wave strength in the test section of the tunnel and highly unstable flow. The shock wave is visible due to condensing water droplets, and it does not require any special optics to see a condensation shock wave. An example of a condensation shock can be seen in Figure 5 above. For the purpose of obtaining reliable results, it is critical to monitor and control the humidity at the inlet of the tunnel to avoid the onset of such condensation. This will be discussed more in Section 6 Humidity Measurement and Control.

3.2 Introduction to Supersonic Wind Tunnels

Wind tunnels are devices used in aerodynamics research that allow investigators to study the effects of air moving over an object under controlled conditions. A supersonic wind tunnel additionally includes compressible flow effects when operating at normal conditions [1]. Before

designing a supersonic wind tunnel, it is important to understand how supersonic flows are generated in a nozzle. It is known that air flow is caused by a pressure differential, where air flows from an area of high pressure to an area of low pressure. Using this, a supersonic flow can be generated simply by creating a large enough pressure differential. However, in order to produce a supersonic flow, there must first be a sonic flow – that is the flow must reach the speed of sound. Sonic velocity can only be reached at the minimum cross-sectional area – or throat – of the duct. Therefore the nozzle must first converge to a critical point to produce sonic flow and then diverge to produce supersonic flow.

3.2.1 Types of Supersonic Wind Tunnels

There are three major types of wind tunnels, continuous, blowdown, and indraft. For this project the wind tunnel must be compatible with the vacuum chamber in the VTF. Both continuous and blowdown wind tunnels require a sizeable compressor to pump air at a high pressure through the nozzle. Blowdown tunnels create a pressure differential between the compressed air and air at atmospheric pressure to produce flow. An intermittent indraft wind tunnel utilizes the pressure difference between the ambient air and a vacuum chamber to run the tunnel. Continuous tunnels are closed circuit systems that do not draw or exhaust air into the atmosphere but instead recycle the air utilizing a return passage. Neither continuous nor blowdown wind tunnels are practical for use on a vacuum chamber. Therefore the most feasible wind tunnel type for this project would be the intermittent indraft wind tunnel.

3.2.2 Intermittent Indraft Wind Tunnels

To create a pressure difference in the intermittent indraft wind tunnel, the vacuum chamber is initially closed off by a valve and is then pumped down to a suitably low pressure. When the valve is opened, the tank will attempt to reach equilibrium causing air to flow from the atmosphere, through the wind tunnel, and into the tank until the tank reaches atmospheric pressure. However the tunnel will not produce a supersonic flow throughout the entire duration of the run time, therefore a critical time frame must be established to collect the relevant data. This time frame, or test time of the tunnel, is a measure of how long there is supersonic flow in the test section, which only exists until the pressure ratio lowers to a value where a normal shock forms and begins to move into the test section. At this point the flow conditions throughout the test section would not be uniform.

Figure 6 pictures the standard layout of an indraft wind tunnel followed by the components of the tunnel discussed in further detail.
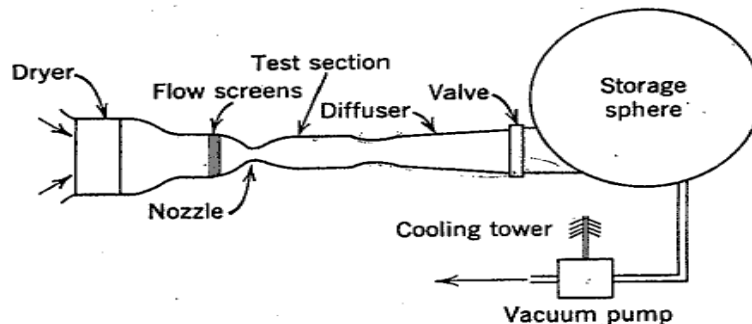
Figure 6: Diagrammatic layout of intermittent indraft wind tunnel, (Ref [7], © 1965, John Wiley & Sons, Inc**.)**

Air Drier

Driers are used to alleviate the negative effects that humidity has on supersonic wind tunnels [7]. If no method is used to enhance the air quality, then the maximum Mach number at which the wind tunnel can operate without the condensation of the air is Mach 1.6. There are two approaches for solving condensation problems within supersonic wind tunnels; the first method removes the water from the incoming air chemically, and the second method is evaporating the water from the incoming air. The amount of moisture in the air is dependent on the temperature, and independent of pressure.

Upstream Ball Valve

This project's wind tunnel uses a manually opening ball valve upstream of the channel that was capable of sealing against the pressure of the vacuum chamber. This valve is brazed to a copper pipe, which inserts into the tunnel inlet, and used to start and stop the flow of air into the wind tunnel. An advantage of having the valve upstream of the tunnel rather than downstream is that leaks can be determined and resolved within the tunnel.

Nozzle

The converging-diverging nozzle of the wind tunnel is the section in which the air accelerates from a subsonic flow, to a sonic flow, and finally to a supersonic flow. The method of characteristics described in the methodology is necessary for the design portion of the throat and test section. They are configured as a permanent assembly to reduce the amount of leaks.

Test Section

The main focus when designing the test section of the tunnel was to create enough space to accommodate any models or probes. The probes that were targeted for implementation were the Pitot pressure probe and the hot-wire probe. It should be noted that the location of the model or probe must be centered in the tunnel and a reasonable distance from the walls, because a supersonic boundary layer forms due to friction between the channel surfaces and the air, which can cause a loss in velocity and momentum. The test window that allows the test section to be monitored visually could create disturbances that would strike the model in some cases. However, because the inner walls of the test section are flush to the rest of the tunnel, there are no disturbances [7].

Windows

The viewing windows, or ports, on a supersonic wind tunnel are extremely common because they allow the optical analysis of the model in the test section, as well as enable the spectator to make general observations about the movements of the model or air flow over the model. The viewing window used in this project was selected to allow for proper visibility with the schlieren system as well as being able to withstand the pressure differential of the vacuum chamber.

Diffuser

A diffuser is used to extend the test time of a supersonic wind tunnel. The diffuser allows for the vacuum chamber to reach higher pressures before the test section no longer flows at supersonic speeds; this is compared to a case where there is no diffuser. A diffuser within the

tunnel should have a cross sectional area that is less than the test section's area, but greater than

the throat of the nozzle. The advantages of utilizing a diffuser are that it will decrease the overall

pressure difference that is needed to operate the tunnel as well as increase the test time.

Vacuum Chamber

The designed wind tunnel was created to mate with the vacuum chamber in WPI's VTF,

shown in Figure 7. This vacuum chamber is a 2.3 m^3 enclosure in which the air inside is

evacuated by means of a rotary mechanical pump and positive displacement blower. This part of

the system serves as the gas reservoir that was back-filled during each test run and can be

initially pumped down to 50 milliTorr for the wind tunnel tests [1].

Figure 7: WPI's vacuum chamber [1]

This project's wind tunnel was integrated onto the vacuum chambers door flange (port)

and was designed to be removable. The flange on the door of the tunnel was chosen because the

location helped to reduce subsonic expansion flows that enter the vacuum chamber and rebound

18

off of the walls, which can disrupt diagnostic readings inside of the wind tunnel. This ultimately is due to the fact that the vacuum chamber is 50 inches wide by 72 inches long, and the flange location allows for the flow to dissipate lengthwise.

3.2.3 Convergent-Divergent Nozzle Flow

The area-velocity relation is given in Equation 3.2 taken from Pope [7]. This equation shows the effect of the cross-sectional area of a nozzle on the velocity of the flow.

$$\frac{dA}{A} = (M^2 - 1)\frac{du}{u} \tag{3.2}$$

Equation 3.2 shows that with M < 1, the velocity of the flow will increase as the area of the duct decreases. This relation remains true until a critical cross-sectional area is reached, where M = 1. This critical point is known as the "throat", and at this condition the flow is said to be "choked." The area ratio that corresponds to this is given by Equation 3.3 from Pope [7], where A is the cross-sectional area at the inlet and A* is the area of the throat:

$$\frac{A}{A^*} = \frac{1}{M}\left\{\frac{1 + [(\gamma - 1)/2]M^2}{[(\gamma + 1)/2]}\right\}^{[(\gamma+1)/2(\gamma-1)]} \tag{3.3}$$

This same relation can then be used to calculate cross-sectional area of the test section to achieve the desired Mach number and vice versa. However, designing a supersonic wind tunnel is more complicated than knowing this A/A* value. This is because increases in supersonic flow velocity do not occur through planes normal to the duct axis, but instead propagate along Mach lines inclined at an angle α, which can be calculated by using the Mach number in the following equation:

$$\alpha = \sin^{-1}\left(\frac{1}{M}\right)$$

(3.4)

Therefore, an increase in area does not affect the centerline flow until characteristic lines cross again. The behavior of these characteristic lines is shown for both a gradual expansion nozzle and a minimum-length nozzle in Figure 8.
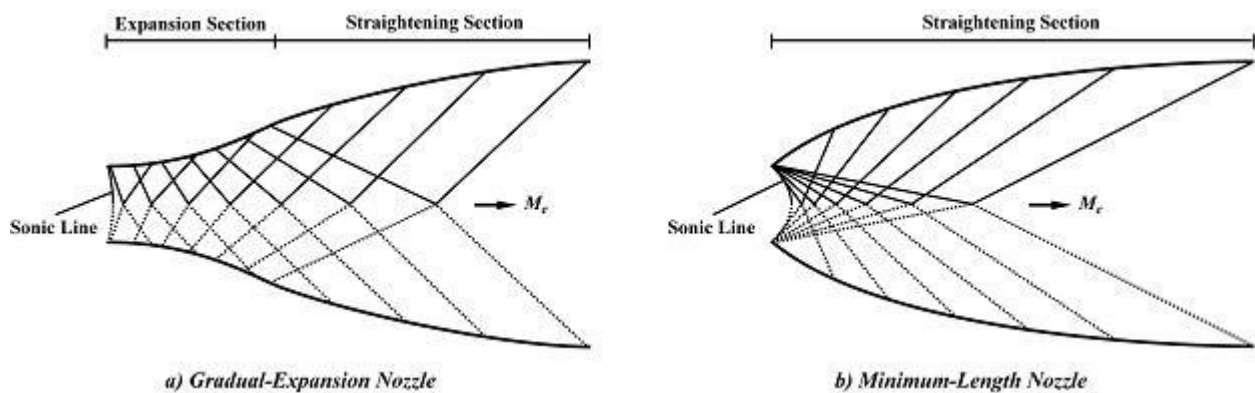
Figure 8: Characteristic lines in expanding supersonic flow (Ref [8], © 2012 NPTEL)

Gradual-expansion nozzles are commonly used where it is important to maintain a high-quality flow at the desired exit conditions. As a result, it is better suited for use in supersonic wind tunnels. A minimum-length nozzle would more likely be applied in rocket nozzles, where size and weight are design constraints. In both types of nozzle, however, there is what is known as "simple" and "non-simple" regions. A non-simple region would have Mach wave reflections and intersections. One goal in designing a nozzle is to minimize these non-simple regions, which can be accomplished by designing the contour of the tunnel such that Mach waves are not produced nor reflected while the flow is straightened [8].

3.2.4 Method of Characteristics

In order to shape the contour of the tunnel to these specifications, the method of characteristics can be employed. Figure 9 shows the basic layout of the characteristic lines in a typical method of characteristics schematic. For the purpose of this project, MATLAB will be used to do these calculations and contour the tunnel. The MATLAB code can be found in the 2010 Supersonic Wind Tunnel MQP, and the results can be seen in Section 3.1.1 Incompressible and Compressible Flows [2].
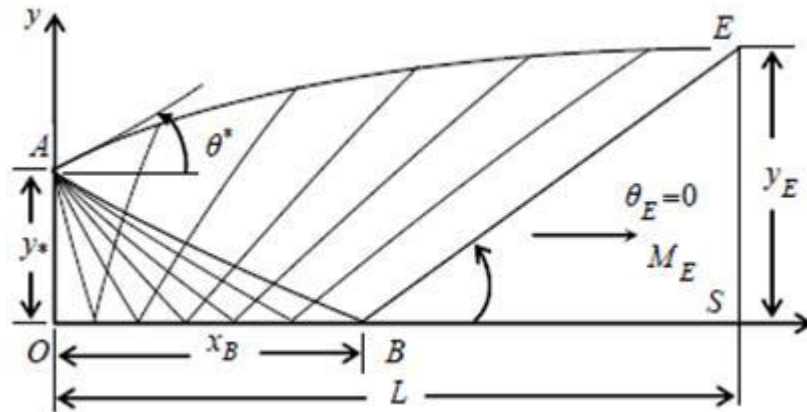
Figure 9: Method of characteristics schematic (Ref [8], © 2012 NPTEL)

3.3 Wind Tunnel Design Implementation

Upon completion of the literature review on supersonic wind tunnel theory, calculations were performed to design the channel for the wind tunnel. From there, the overall design of the wind tunnel was created. This design also accounted for more specific constraints by including detailed design components. From there the tunnel was manufactured and subject to a specific testing procedure for proper performance.

3.3.1 Initial Calculations

With a set geometric design for an intermittent indraft supersonic wind tunnel, the theoretical flow properties, test time, and run time were calculated using atmospheric and vacuum chamber conditions. These calculations are valuable to the project since the goal is to design proper diagnostics for this specific supersonic wind tunnel.

Theoretical Flow Properties

Before constructing the wind tunnel, initial conditions had to be set, constraints had to be known, parameters had to be determined, and properties had to be established. The initial conditions included constant inlet pressure, air density, temperature and constant vacuum chamber volume. Initial analysis of flow properties assumed the International Standard Atmosphere (ISA) from the International Organization for Standardization (ISO) of atmospheric pressure to be 101.325 kPa and have a temperature of 288.15 Kelvin, which is stated in ISO 2533:1975 [9]. During actual testing, the atmospheric pressure was taken to produce more accurate calculation results. The constraints on the WPI's VTF are a volume of 2.3 m^3 and a minimum vacated pressure of 50 milliTorr [2]. Another constraint that was placed on the tunnel for design purposes was a constant width of one and a half inches throughout the entire tunnel. This constant width simplified construction by having two flat pieces of material pressed and sealed against the contours of the tunnel. This also means that the tunnel flow should approximate a two-dimensional flow field, along with rectangular cross-sections. The desired attributes of the tunnel were determined so as to reach a Mach number of 2 in the test section and to extend the test time as much as possible. Using the method of characteristics (which is described in Section 3.2.3 Convergent-Divergent Nozzle Flow), the diverging portion of the

nozzle was defined using MATLAB code created by the 2009-2010 Supersonic Wind Tunnel

MQP [2]. The program created plotted points that started with the throat of the nozzle, and then

formed an expansion section, followed by a straightening section using the desired Mach number

along with other variables as a guide. Once the diverging section was defined, a smooth splined

converging section was added upstream, in front of the throat, to finish creating the converging-

diverging nozzle. The converging section was designed to fit into the ball valve and diffuser

assembly, which was taken off of the previous year's wind tunnel. Downstream of the diffuser, a

straight test section was made long enough for the flow to even out, and for the Pitot-static and

stagnations probes to be inserted. At the end of the test section, a diffuser was created to increase

test time and to slow the airflow speed prior to entering the vacuum chamber. The diffuser is not

necessary for the wind tunnel to operate in supersonic conditions, but in order to fit the tunnel

correctly onto the flange this design implementation was mandatory and beneficial. With the

design specifications, calculated data points, and sizing constraints, the geometry of the wind

tunnel was created using SolidWorks and machined in WPI's Washburn machine shop. The

contour consisted of an inlet, converging-diverging nozzle, test section, diffuser, and exit.

Knowing the areas of different sections, theoretical, isentropic flow properties were calculated

using the following equations [7].

$$\frac{A}{A^*} = \frac{1}{M}\left\{\frac{1 + [(\gamma - 1)/2]M^2}{[(\gamma + 1)/2]}\right\}^{[(\gamma+1)/2(\gamma-1)]} \tag{3.5}$$

$$\frac{T_0}{T} = 1 + \frac{\gamma - 1}{2}M^2 \tag{3.6}$$

$$\frac{P_0}{P} = \left(1 + \frac{\gamma - 1}{2}M^2\right)^{\frac{\gamma}{\gamma-1}} \tag{3.7}$$

$$\frac{\rho_0}{\rho} = \left(1 + \frac{\gamma - 1}{2} M^2\right)^{\frac{1}{\gamma - 1}} \tag{3.8}$$

$$\dot{m} = \frac{P_{atm} A^*}{\sqrt{T_{atm}}} \sqrt{\frac{\gamma}{R} \left(\frac{2}{\gamma + 1}\right)^{\frac{\gamma + 1}{\gamma - 1}}} \tag{3.9}$$

These equations are written in terms of Mach number, M, and the constant specific heat ratio, γ. Equation (3.5) is the area ratio equation, where the area at a location divided by the area at the throat, A^*, can be determined by the Mach number and vice versa. Equation (3.6), (3.7), and (3.8) determined the temperature, pressure, and air density ratios respectively. These ratios have the stagnation condition in the numerator and the local static condition in the denominator of the left hand side of the equations. The stagnation conditions are taken as standard atmospheric conditions. Because the Mach number is dependent on the area ratio, and the static conditions are dependent on the Mach number, the contour of the wind tunnel, which was established by the method of characteristics MATLAB code and design constraints, dictates all of the static conditions to the extent that isentropic flow can be assumed. In Figure 10, these properties are plotted versus distance into the wind tunnel from the inlet to the test section using the same code that defined the contour of diverging nozzle.
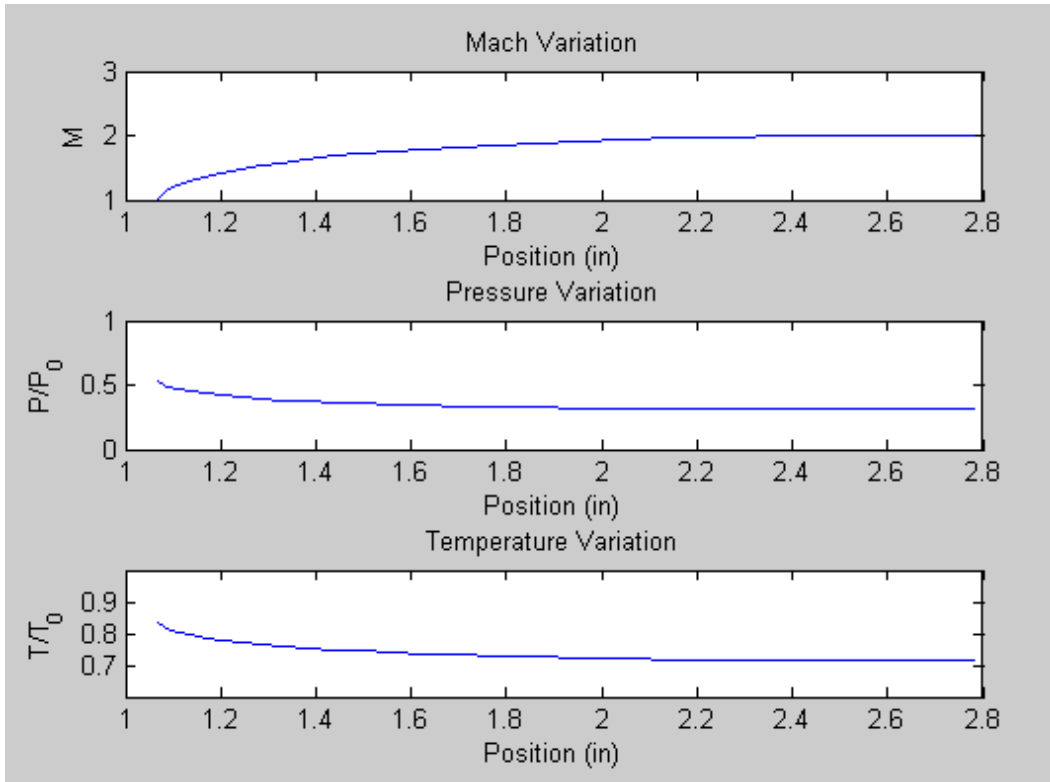
Figure 10: Mach number, pressure, and temperature ratio along the diverging section of the nozzle

Run Time

The run time encompasses the initial pump down of the vacuum chamber, the test time, and the duration of the vacuum chamber pressure equalizing with atmospheric pressure. Prior to testing, the supersonic wind tunnel must be attached to the vacuum chamber. This requires a few minutes for the wind tunnel flange to be bolted onto the frame of the vacuum chamber, the Pitot probes to be secured and hooked up, the Schlieren system to be properly aligned, and the desiccant air drier to be mounted. Once the wind tunnel is set up, the vacuum chamber uses a combined rotary mechanical pump and a positive displacement blower to extract air at over 25 m^3/sec, depending on the pressure of the tank, to reach an initial test pressure of 50 milliTorr. The pumping speed (m^3/sec), versus pressure (mmHg), is seen in Figure 11, depicting the Series

1700 Mechanical Booster Vacuum Pump's pumping speed [10]. Equation (3.10) shows the basic pumping time in seconds, t, as a function of volume in cubic meters, V, pumping speed in m^3/sec, S, initial pressure in Torr, P_i, and final pressure in Torr, P_f [10].
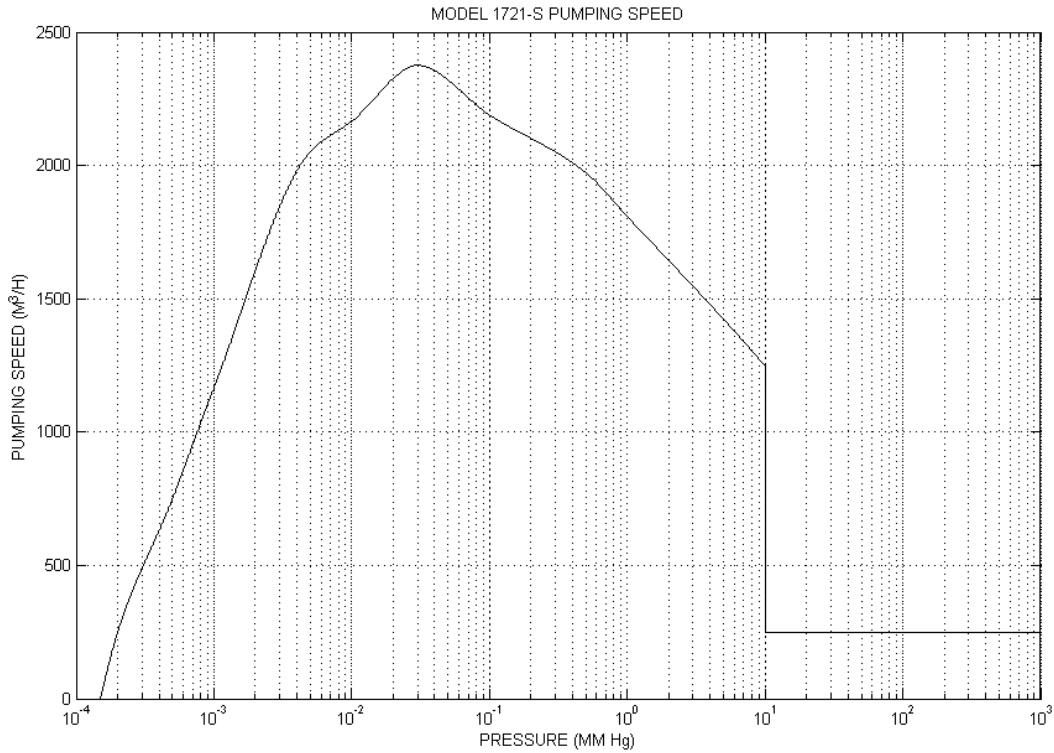
Figure 11: Pressure vs. pumping speed of the vacuum pump (Ref [10], © 1980, Penwalt Corp.)

$$t = \frac{V}{S} ln \frac{P_i}{P_f}$$
(3.10)

When the pump has reduced the pressure to 50 milliTorr, it is turned off, and the valve of the wind tunnel is opened to start the test. The air then flows through the tunnel and re-pressurizes the vacuum chamber. The test time is estimated from Equation (3.13) to last approximately 15 seconds until the shock wave reaches the diffuser (Equation (3.13) and test time is discussed in entirety in *Test Time*). The normal shock wave migrates back from the diffuser, through the test section, until it reaches the converging-diverging nozzle. Once the shock wave attempts to move in front of the throat of the nozzle, the pressure differential no

26

longer is able to sustain supersonic flow, the shock wave dissipates, and the flow unchokes and becomes subsonic. The remaining run time is the duration where the pressure in the vacuum chamber equalizes with the atmosphere with a decreasing mass flow rate until it is ceased. Once the flow stops, the run time has concluded, and either the wind tunnel is disconnected, or another test is started.

Test Time

The test time is established as the amount of time the test section retains supersonic flow at the design Mach number. When the valve opens, the difference in pressure between the atmosphere and the vacuum causes the air to flow through the converging-diverging nozzle, the test section, and the diffuser of the wind tunnel, and into the vacuum chamber. Initially the pressure ratio is large enough that it produces a shock wave that travels from the throat to the exit of the tunnel and dissipates inside of the vacuum chamber. Once this is done, the supersonic flow starts, reaching the desired Mach number on a time scale much shorter than the duration of supersonic flow overall. The test time is defined to start after the test section has reached its design value of Mach number. As the supersonic flow reaches the chamber, the back pressure in the vacuum is less than the pressure at the exit of the tunnel. This under-expanded flow causes the expansion fans to form at the exit. As the constant mass flow fills up the tank, the back pressure rises until it is equivalent to the exit pressure. In this instant, a straight jet of supersonic flow forms ideally; this case is called the design condition. As the chamber keeps filling up with air, the back pressure becomes greater than the exit pressure, and oblique shocks form at specific angles and patterns, called shock diamonds, to compensate for the over-expanded condition. With increasing back pressure, the oblique shocks coalesce into a normal shock that is

perpendicular to the flow. In front of the normal shock is supersonic flow, and behind it is subsonic flow. As the pressure in the chamber continues to rise, the normal shock moves upstream toward the throat of the nozzle passing by the test section [11]. Since the normal shock wave alter the flow from supersonic to subsonic, the test section flow is no longer supersonic. This event therefore defines the end of the useful test time.

The test time was calculated by manipulating the continuity equation (or mass conservation equation). The unaltered continuity equation, Equation (3.11), has the control volume, CV, integral encompassing the air density multiplied by the change in the volume of the vacuum chamber according to distance, and the control surface, CS, is the flux mass flow rate through the throat of the converging-diverging nozzle of the wind tunnel.

$$\frac{\partial}{\partial t} \iiint_{CV(t)} \rho \, d\forall_{chamber} + \oiint_{CS(t)} \rho \vec{V_r} \cdot \hat{n} \, dS = 0 \tag{3.11}$$

After assuming the volume of the vacuum chamber is constant and taking the control surface at the throat of the nozzle, this equation reduces down to the integral equations of Equation (3.12), where $\forall_{chamber}$ is the volume of the chamber, $d\rho$ is the differential of air density, $\dot{m}$ is the mass flow rate from Equation (3.9), and where i is the initial density of the vacuum chamber air right before the valve is opened, d is the density of the vacuum chamber when the normal shock wave reaches the diffuser, dt is the differential of time, and t is the test time that is being calculated.

$$\forall_{chamber} \int_{i}^{d} d\rho = \dot{m} \int_{0}^{t} dt \tag{3.12}$$

28

The result of this integration results in an expression for the test time in terms of the volume of the chamber,$\forall_{chamber}$, the pressure at the diffuser, P_d, the mass flow rate, $\dot{m}$, the static temperature of the flow at the diffuser, T_d, and the initial pressure inside the vacuum chamber, P_i. The full derivation of Equation (3.13) can be found in the Appendix A: Derivation of Equation for Test Time.

$$t = \frac{\forall_{chamber} P_d}{\dot{m} R T_d}\left(1 - \frac{P_i}{P_d}\right) \tag{3.13}$$

The test time calculated using Equation (3.13) results in a test time of 15.2 seconds. This calculated test time for an intermittent supersonic wind tunnel is quite considerable compared to other wind tunnels. This can be attributed to a large vacuum chamber and a small throat area.

3.3.2 Initial Overall Design

This MQP used a design strategy similar to the 2009 Supersonic Wind tunnel MQP: a fixed geometry tunnel that operates at a single Mach number [1]. This method was selected based on the challenges and time constraints presented with the design of a variable geometry tunnel. Since the main goal of this project is to be able to measure the flow in the tunnel and confirm that it is reaching the desired Mach number, it was decided that a variable geometry tunnel would add too much complexity to the MQP within the allotted project timeline.

One of the more significant issues noted by the previous MQP group was the presence of severe leakages between various components of the 2009 supersonic wind tunnel. Since the valve is placed upstream of the test section, the entire wind tunnel must be able to withstand the 50 milliTorr design initial vacuum. To solve this problem, this wind tunnel incorporated Buna N Nitrile O-rings between the side mating surfaces to prevent leakage, instead of using an adhesive sealant. These were used instead of an adhesive sealant to allow for a modular design of the side

panel, allowing for easy removal and access to the interior of the wind tunnel. The end blocks still use an adhesive sealant since they are designed to be non-removable. The sealing surfaces will also be limited to single surface for each individual O-ring so as to simplify assembly and ensure an airtight connection.

The stainless steel flange that was intended to interface between the vacuum tank and the wind tunnel, shown in Figure 12, was never used due to manufacturing problems in the 2009-2010 MQP. This project will be refurbishing the flange and integrating it into our tunnel for connection to the vacuum chamber. The wind tunnel length has also been extended by approximately 4 inches allowing for a longer test section. This is important because the addition of measuring probes and other instrumentation will reduce the area where the test piece can be placed.
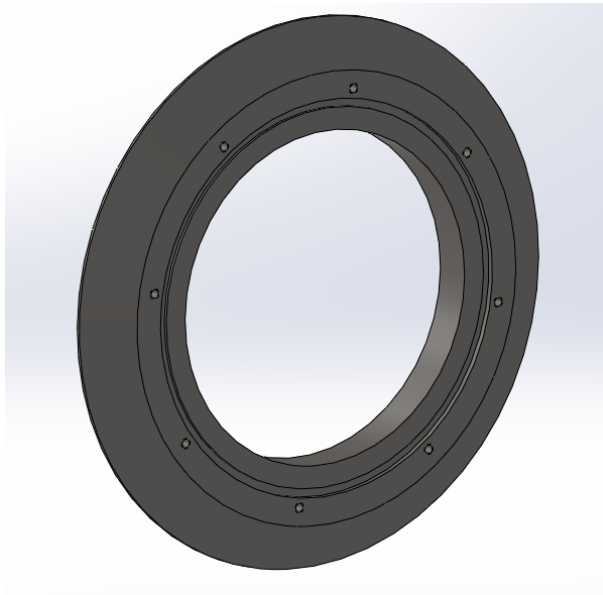
Figure 12: Stainless steel flange for vacuum chamber

3.3.3 Detailed Design of Complete Tunnel

The wind tunnel is comprised of three separate sections and an air drier which maintain the modularity of the entire assembly while keeping it airtight. The first section is the flange assembly, which is composed of the stainless steel mounting flange and the aluminum adapter flange. The second section is the tunnel core, which contains all the components for generating, measuring, and containing the supersonic flow. The final section is the valve assembly, which consists of the valve adapter block and the ball valve used to start and stop the airflow. Figure 13 shows an exploded view highlighting these three sections.
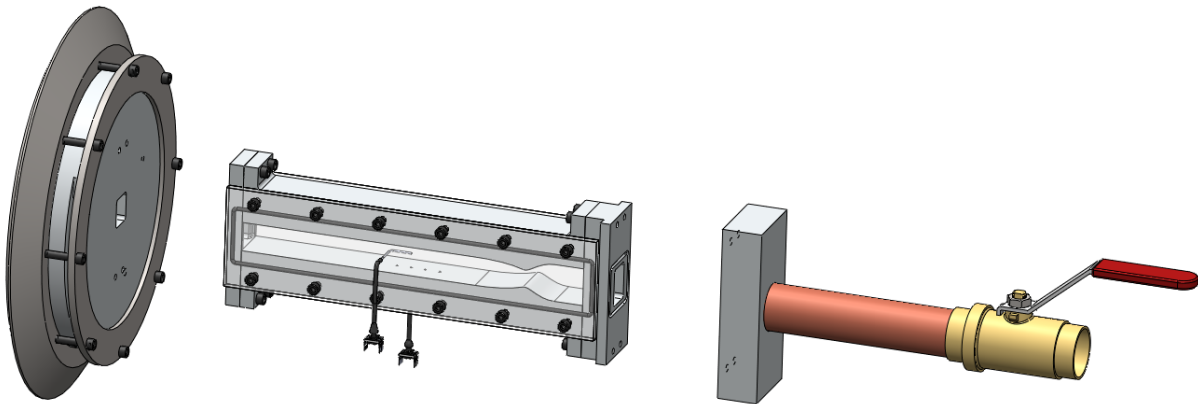
Figure 13: Wind tunnel exploded view

The flange assembly consists of two parts that not only support the weight of the entire wind tunnel, but also connect it to the vacuum chamber. This connection was made using the finished stainless steel flange recovered from the 2009-2010 MQP group. In addition, the flange also serves a secondary purpose; the wind tunnel can be removed and replaced with an acrylic window to facilitate observation of other experiments in the vacuum chamber [2].

The most important part of the wind tunnel is the core, where the airflow is channeled through the converging-diverging geometry before entering the test section. The tunnel core consists of upper and lower contours which have the converging–diverging geometry, two end blocks, and two windows which permit the viewing of the test section. Each of these components is sealed to the others through a combination of silicon adhesive, (used to secure the end blocks to the contours) or O-rings (window faces and external end block faces). The O-rings are seated in specially designed grooves which restrict their movement and ensure good compression when the tunnel is assembled.

The valve assembly has two parts, both of which were used in the previous iteration of the supersonic wind tunnel. Minor modifications were made to both parts to ensure that it would mate cleanly with the wind tunnel and any other components placed upstream, such as the air drier. These modifications involved resurfacing the valve adapter which transitions from the rectangular tunnel inlet to the valve pipe so it would mate cleanly with the wind tunnel, and re-drilling bolt holes.

3.3.4 Wind Tunnel Testing Procedure

Preliminary testing of the wind tunnel was carried out once the assembly is complete. The stainless steel flange was tested first with the acrylic window to check the seal between the flange and the chamber. A quick vacuum test was done to ensure that the window seal and the chamber seal could hold vacuum. The wind tunnel was then secured to the vacuum chamber in place of the window. The displacement blower was switched on and the chamber was pumped down. During this phase any large leaks would have been immediately audible. The vacuum chamber was pumped down to 50 milliTorr, which is the maximum recommended vacuum when

using the displacement blower. At this point the pump was shut off and a final check of all the seals was conducted using the high accuracy pressure gauge. The tunnel was certified as ready to begin running tests for the air drier and schlieren system since it held vacuum within 100 milliTorr of the final vacuum pressure for 1 minute after the pump is shut off.

4 Wind Tunnel Diagnostics

The second area of focus of this project was the design of a quantitative diagnostics system for measuring flow properties. The flow through a supersonic wind tunnel can be characterized through certain flow measurement techniques. Those explored in this project include Pitot-static pressure probe measurements and hot wire anemometry. The findings of a thorough literature review are reported below, along with the methodology used to design the system for this project.

4.1 Types of Flow Measurements

The two main diagnostic techniques investigated in this project were hot wire anemometry and pressure measurements with a Pitot-static probe. A hot-wire anemometer is used to determine the velocity and temperature of the specified test section inside of the wind tunnel. This is a result of the fact the voltage across the wire is proportional to the velocity of the flow. The wire resistance is dependent on its temperature, and the velocity affects the rate of the heat transfer or cooling. While this method effectively measures flow properties, the cost of the system was beyond the allotted budget of this project. Future projects have the option of investigating the implementation of a hot wire anemometer in the wind tunnel. The specific

information and related equations for hot wires are detailed in subsequent sections for use in future work.

This project will use of a Pitot-static pressure probe and static pressure ports to take measurements within the flow in order to calculate the Mach number. This allows the difference of static and stagnation pressures to be calculated and measured during the experiment. Based on the probe data, calculations can be made to find the Mach number of the free stream flow inside of the tunnel. The Pitot probe is normally installed in the direction of the flow, and the static pressure ports are aligned orthogonally to the flow direction. This process will allow for the calculation of the ratio of the static and stagnation pressures, and thus the Mach number, at the specified section where measurements are taken.

4.1.1 Hot-wire Anemometry

A hot-wire anemometer is a probe consisting of two prongs that suspend a thin wire of a few micrometers in diameter, as seen in Figure 14 [12]. It measures the forced convection between the heat generated from electrical current through the wire and the adjacent flow, by tracking the changes in electrical properties of the wire. This can be used to determine the magnitude of temperature, velocity, turbulence, or mass-flow properties of the flow direction perpendicular to the wire. The hot-wire is oriented perpendicular to the direction of the flow, but more complex geometries exist that orient the wire at angles relative to the flow. These geometries may be used to measure the flow properties in directions that are not in line with the flow. Also, an array of several wires can be used to simultaneously measure the flow in multiple dimensions.
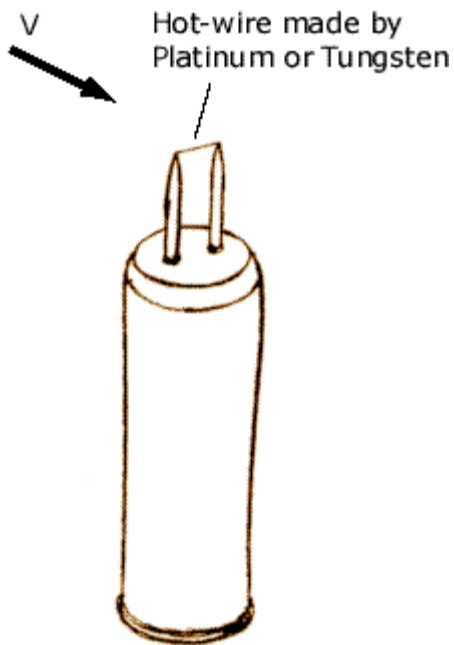
Figure 14: Hot-wire anemometer with a single wire [12]

Hot-wire anemometers are typically available in one of three modes. Each mode maintains some part of the probe characteristics constant in order to measure how the power is dissipated by convection. Constant Current Anemometers (CCA) were the first developed and those whose behavior is best characterized. Constant Temperature Anemometers (CTA) were used in studies during the 1930's. These anemometers offered a higher frequency response, but required more complex hardware to maintain the temperature of the wire. The Constant Voltage Anemometer is the most recently developed, and while it offers many positive attributes like high frequency response and low noise, its behavior in supersonic flows is less understood. Most studies use CCAs and CTAs because of their proven history.

Typical Challenges Involved

Several challenges arise when measuring properties in supersonic flow. The greatest challenge is the emergence of shock waves on intrusive measuring probes at Mach numbers greater than one. For subsonic flow, the convective heat transfer from the wire is a function of velocity, wire temperature, air temperature, and density of the flow. However, higher Mach numbers generate shock waves in front of the support prongs which complicate the relationship. The wire itself does not suffer significantly from this effect at low supersonic flows (M < 1.4), but shock wave strength increases and detaches from the wire as the Mach number increases, resulting in disturbances of the flow where convection becomes a function of mass flow rate and Mach number [13].

Due to the complexity of these flows, the behavior of the probe must be well understood before taking measurement. Therefore, a great deal of time is spent calibrating the probes before using them to take data. In particular, the team must understand how the resistance of the particular probe varies with temperature. Because the resistance does not vary linearly, second order effects are taken into account such that the equation follows the form:

$$\frac{R}{R_{ref}} = 1 + \alpha\left(T_w - T_{Ref}\right) + \beta\left(T_w - T_{ref}\right)^2 \qquad (4.1)$$

Where α and β are experimentally found constants, and $(T_w - T_{Ref})$ is the difference between the wire temperature and a reference temperature. However, velocity is still not present in this relationship, so we must include convective heat transfer relations. As stated earlier, the level of convective heat transfer for a CTA will vary with mass flow and temperature in flows where Mach number is higher than 1.4. The relationship between these and the voltage across the wire take the form:

$$\frac{E'}{E} = S_m \times \frac{m'}{m} + S_{T0} \times \frac{T_0'}{T_0} \qquad (4.2)$$

Where S_m and S_{T0} are constants, E', m', and T_0' are instantaneous values, m is mass flow, and T_0 is total temperature. Many factors go into the calculation of the highly complicated S constants, and velocity measurements are extracted from these values. Steinback and Nagabushana derive the velocity values from the values of the S constants [13].

4.1.2 Pitot-Static Probe

One of the most common instruments used to measure both the stagnation (total) pressure p_0 and static pressure p of a flow is the Pitot-static probe, or Prandtl tube, shown in Figure 15. This device is used to calculate the free stream velocity of the flow, either in a wind tunnel or mounted on an aircraft.
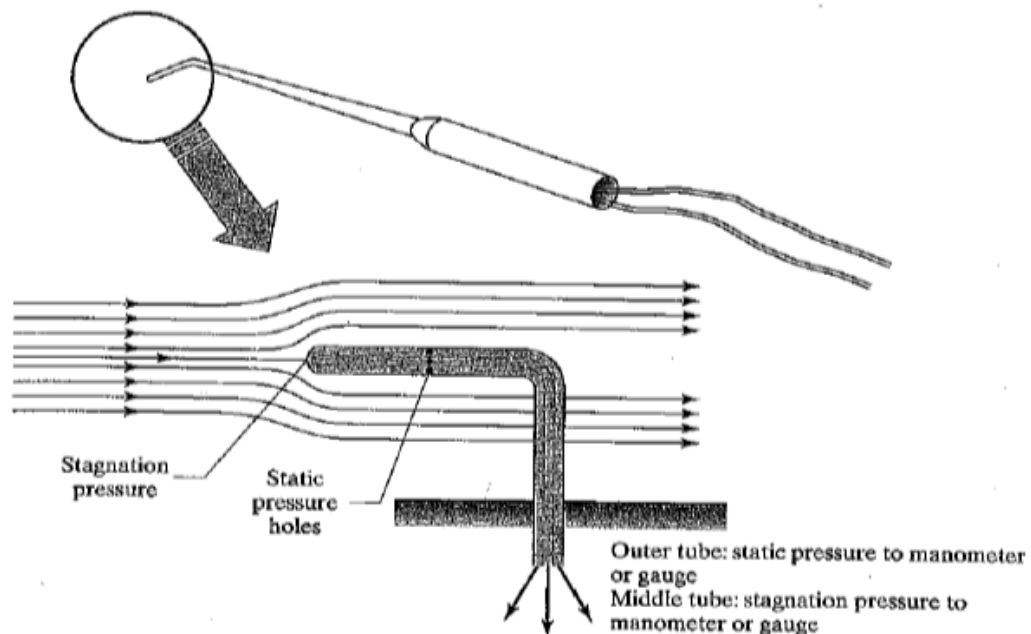
Figure 15: Pitot-static tube [14]

Pitot tubes are most commonly inserted through the wall of the tunnel and bent at a 90 degree angle to point directly into the flow. They may have several small holes drilled around the perimeter of the tube perpendicular to the direction of flow and a hole drilled down the center axis of the tube aligned parallel to the flow. The holes on the outside are used to calculate the static pressure of the flow, and are connected to one port of a pressure transducer. The center hole is used to determine stagnation pressure and is connected to a separate port of the pressure transducer. From there the pressure difference can be calculated. There are a few different options for the shape of the tip of the probe, and the designs vary for subsonic or supersonic flow. For use in supersonic flow, the ideal tip shape is a National Physical Laboratory modified ellipsoidal Pitot tube which provides the most accuracy results at higher velocities. Once the difference of static to stagnation pressure and the air density ρ (relative to the probe location) is known, the velocity can be calculated using Bernoulli's equation (4.3, 4.4) if the flow is subsonic [14]. A correction factor denoted by K is required to account for the variation of the kinetic energy of the fluid. The specific heat ratio is denoted by γ (1.4 for air).

$$p_0 - p = K \frac{\rho V^2}{2} \tag{4.3}$$

$$V = \left[\frac{2\gamma}{\gamma - 1} \left(\frac{p_0}{\rho_0} - \frac{p}{\rho} \right) \right]^{\frac{1}{2}} \tag{4.4}$$
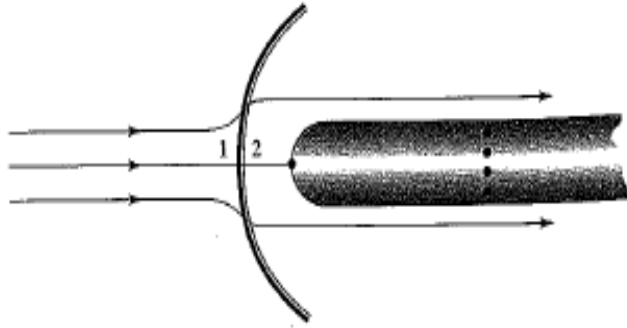
Figure 16: Pitot-static tube in supersonic flow (Ref. [14], ©2006, Pearson Prentice Hall)

For supersonic flow, the determination of the free stream velocity is slightly more difficult to calculate because of the inevitable formation of a detached bow shock ahead of the nose of the probe, as shown in Figure 16. It is beneficial to have a static pressure measurement upstream of the bow shock, where the size of the port hole perpendicular to the flow is approximately 20% of the local laminar boundary layer thickness [14]. This gives a true measurement of the free stream static pressure behind of the shock. This measurement should be ideally equal to the static pressure measured by the holes around the perimeter of the probe, which can be used to help calibrate the probe. The alignment of the probe must be within 5° parallel to the direction of flow in order to minimize the disturbance of the flow and maximize the accuracy of the static pressure readings (the stagnation pressure is much less sensitive to probe alignment) [15]. In order to calculate the Mach number of a supersonic flow, a combination of normal shock relations and isentropic flow relations must be used in order to calculate the fluid properties on both sides of the shock wave. The *Rayleigh-Pitot Formula*, shown in Equation (4.5), was derived for just this reason [7].

$$\frac{p_{02}}{p_1} = \frac{\left(\frac{\gamma+1}{2}M_1^2\right)^{\frac{\gamma}{\gamma-1}}}{\left(\frac{2\gamma}{\gamma+1}M_1^2 - \frac{\gamma-1}{\gamma+1}\right)^{\frac{1}{\gamma-1}}} \qquad (4.5)$$

In order to find the Mach number using this equation, the Newton-Raphson or similar procedure must be used. Using a spreadsheet program, this method of extracting the Mach number from the Rayleigh-Pitot formula is very straightforward. However, the critical pressure ratio must first be calculated using Equation (4.6), which determines if the flow is subsonic or supersonic [14].

$$\left(\frac{p_{02}}{p_1}\right)_{crit} = \left(\frac{\gamma+1}{2}\right)^{\frac{\gamma}{\gamma-1}} \qquad (4.6)$$

If the actual pressure ratio is less than this critical value, the subsonic Mach number is calculated using Equation 4.7.

$$V = \left[\frac{2\gamma}{\gamma-1}\left(\frac{p_0}{\rho_0} - \frac{p}{\rho}\right)\right]^{\frac{1}{2}} \qquad (4.7)$$

If it is larger than the critical value, then the Mach number must be calculated from the Rayleigh-Pitot formula using the Newton-Raphson procedure, as shown below in Equations (4.8) to (4.13).

$$f(M) = AM^{2\gamma} - BM^2 + C = 0 \qquad (4.8)$$

$$A = \frac{(\gamma+1)^{\gamma+1}}{2\gamma-1} \qquad (4.9)$$

$$B = 4\gamma\left(\frac{p_{02}}{p_1}\right)^{\gamma-1} \qquad (4.10)$$

$$C = 2(\gamma-1)\left(\frac{p_{02}}{p_1}\right)^{\gamma-1} \qquad (4.11)$$

$$\frac{df}{dM}(M) = 2\gamma AM^{2\gamma-1} - 2BM \tag{4.12}$$

$$M_{new} = M_{old} - \frac{f(M_{old})}{\frac{df}{dM}(M_{old})} = \frac{(2\gamma - 1)AM_{old}^{2\gamma} - BM_{old}^2 - C}{2(\gamma AM_{old}^{2\gamma-1} - BM_{old})} \tag{4.13}$$

A spreadsheet was created which can easily compute both the subsonic or supersonic Mach number for any given static and stagnation pressures.

4.2 Implementation of Diagnostics

A thorough understanding of the theory behind the use of a Pitot probe pressure measurement system lead to the design and implementation of a system that meets the needs of supersonic wind tunnel. The design not only incorporates the requirements of the current wind tunnel design, but also allows for the possibility of future expansion.

4.2.1 Pressure Probe Mount

While designing the mounting interface for the pressure probe, it was important to keep in mind that future studies which use this tunnel may wish to implement different diagnostics or mounting points for supersonic testing. Initially, the stagnation pressure probe was to be inserted through the bottom face of the aluminum contour. Although one could still interchange different mounting systems through this configuration, it would fix the location of the probe for all future testing which may limit the abilities of future groups to test. The solution to this was to insert the probe through the acrylic sidewall, due to its low cost and ease of removability. The probe was accurately aligned and epoxied so that it is centered within the channel and parallel to the flow, perpendicular to the static pressure taps drilled in the bottom face of the aluminum contour. This allows for multiple sidewalls to be manufactured with various probes/mounting rods to

accommodate future testing requirements. These different sidewalls with integrated diagnostics can easily be swapped out as needed by unbolting the acrylic from the aluminum tunnel.

Since the four static pressure taps are less critical and can easily be capped off, they are permanently drilled into the aluminum contour. Each static tap has a Swagelok NPT to compression tube fitting, where a 1/16" tube with a 1/50" ID was press fit into the tap of choice, and adjusted so it is flush with the aluminum contour (test section bottom). Flexible tubing was connected to the end of the stainless steel probe tube and to a pressure transducer. For any static taps which are not being used, a 1/16" diameter welding rod was inserted in the same manner in order to cap off the holes which are not being used, as shown in both Figure 17 and Figure 18. This allows for more flexibility in the designs of future groups, since a 1/16" NPT is a very standard size for most fittings and various changes could be made while still using the same holes.
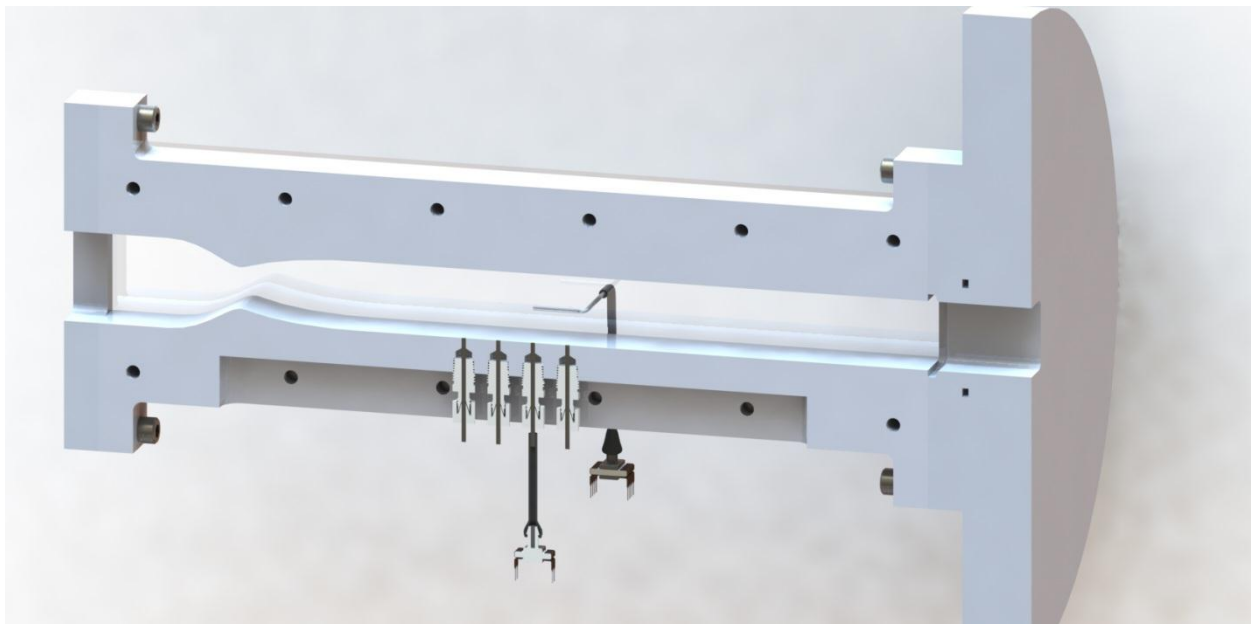
Figure 17: Cross-section of wind tunnel assembly
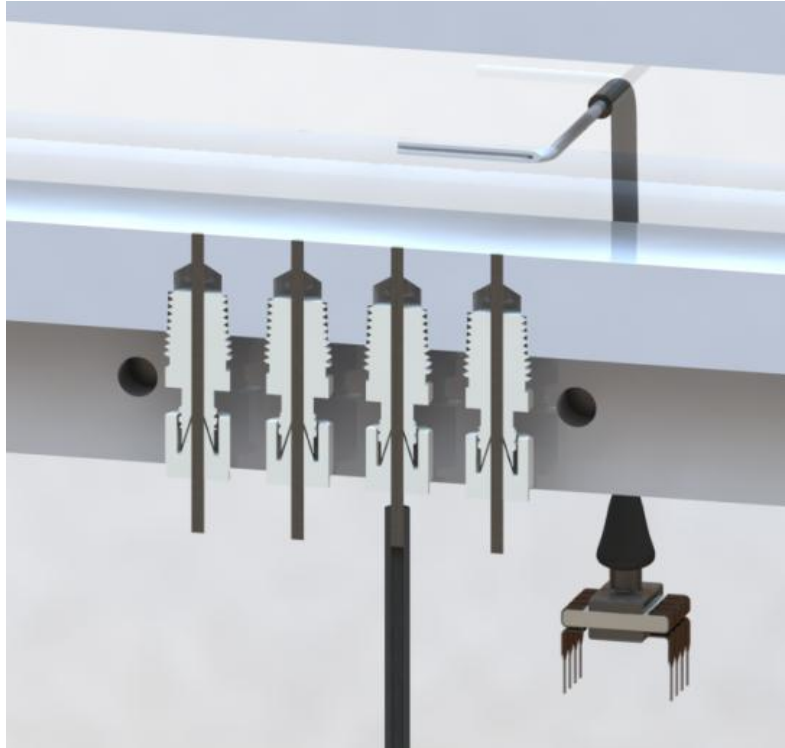
Figure 18: Pressure port close-up

4.2.2 Pressure Transducer Selection

The pressure transducer discussed in the previous section converts the measured pressure into a voltage that can be analyzed by a data acquisition system. In order to function properly, the static and stagnation pressure ranges of the tunnel during run-time needed to be fully encompassed within the transducer's range. These pressures were calculated in MATLAB for Mach numbers within an uncertainty range about the design Mach number. A Mach number range of ±0.3 was chosen to account for possible errors introduced by variations in atmospheric conditions, leaks, and channel roughness. The MATLAB script used in the 2009-2010 Supersonic Wind Tunnel MQP incorporated isentropic flow and normal shock relations to calculate the range of static and stagnation pressures at Mach numbers of 2.0 ±0.3 [2]. These absolute pressures ranged from 58-88 kPa for the stagnation pressure and 8-20 kPa for the static

pressure. The transducer also introduces an uncertainty in its pressure measurement accuracy. The transducer configuration necessitated a small inlet port, close to the size of the probe inner diameter and static tap, as well as a location as close as possible to the probes. The requirements on transducer inlet port size and proximity resulted from the need to minimize delay caused by large volumes of air in the pressure lines between the transducer pressure ports and the probes. In addition, because of the available data acquisition hardware in the lab, the transducer also requires analog outputs.

Based on the required specifications, Honeywell Sensing's TruStability High Accuracy Silicon Ceramic (HSC) series transducers provided the best match to the needs of the project (model #: HSCDANN001BAAA3). The HSC series offers a ±1% full scale (FS) error-band, i.e. ±1% of the measurement range, which would allow for calculation of a Mach number with an uncertainty of ±0.1 (see calculations in Section 4.1.2 Pitot-Static Probe). The transducer series also offers rapid response time (~1ms), a variety of port options, internal signal amplification that eliminates the need for the team to build an amplifier, and good resolution of measurement (~0.03% FS). To simplify calibration and the required circuitry, the same transducer with a range of 0-1 bar (0-100kPa) was selected for both measurements. A single barbed port for the transducer was chosen to facilitate making connections and to insure interchangeability between ports.

Project Box Design

After the transducer had been selected, a semi-permanent circuit (that could be modified as needed by future teams) was required to provide the transducer with power and to relay the voltage output to the DAQ. The circuit was housed in a project box (Jameco ValuePro Manf. No.

SY0206-R) in order to protect the circuit, power, and signal connections. The transducer requires 3.3V with a very low maximum current draw of 2.1 mA each. Improper use of the transducers would run the risk of burning out the transducers, making them not function properly. In order to provide this specific power, the team used an AC/DC wall outlet transformer (12VDC 500mA, Jameco DCU120050) and a DC/DC converter to attenuate the voltage down to the required 3.3V at an acceptable current.

The DC/DC converter was made by TracoPower. The converter takes in a range of voltages and adjusts them to a constant output. Since the AC/DC converter had an output of 12V, the TracoPower TMR 1210 was selected since it operates nominally at an input of 12V and converts the input to a 3.3V output. This power supply will automatically adjust the current level to what is drawn by the transducers above 50 mA. However, error would be introduced into this value if the circuit draw was less than this, but it was determined experimentally that this error was insignificant in our circuit, so the transducers were wired directly to the output of the TMR 1210 without additional signal conditioning. These transducers were connected to the TMR 1210 in parallel to keep the excitation voltage constant, and therefore, the team was able to leave empty chip sockets as placeholders that can be used later, (should future teams wish to add transducers for the other three static tap channels) without affecting the rest of the circuit. To protect the leads of the transducer chips, they were mounted on chip sockets after soldering them to the protoboard. Finally, the outputs from the transducers are connected to individual male BNC style connections that carry the signal to the DAQ. The final project box can be seen in Figure 19.

Figure 19: Project box holding transducer circuitry

In order to protect the parts, a simple series of breadboard tests were conducted to ensure that the components would not be exposed to current/voltage overloads. Circuit elements were simulated with their equivalent impedance.

4.2.3 Data Acquisition System

A LabVIEW program was constructed that collects both static and stagnation pressure measurements through the Pitot-static probe installed inside the wind tunnel. The program then calculates the free stream Mach number of the flow from the collected data. The first step of the program is converting the voltage output to pressure measurements. Since the signal input is a voltage (Volts), the VI has to convert the input into pressure (Pascals). The equation is given by Honeywell Company [16].

$$V_{output} = \frac{0.8 \times \text{Voltage Supply } (V_s)}{P_{max} - P_{min}} \left[P_a - P_{min} \right] + 0.1 \times V_s \qquad (4.14)$$

In this equation, the output voltage (V_{output}) is the measured voltage and the voltage supply (V_s) is the magnitude from a battery used to power the pressure transducer. The equation can be rearranged to solve for the applied pressure.

$$V_{output} = \frac{0.8 \times V_s}{P_{atm} - 0}(P_a - 0) + 0.1 \times V_s \qquad (4.15)$$

$$V_{output} - 0.1 \times V_s = \frac{0.8 \times V_s}{P_{atmx}} P_a$$

$$P_{atm} \frac{(V_{output} - 0.1 \times V_s)}{0.8 \times V_s} = P_a$$

$$P_a = P_{atm} \frac{V_{output}}{0.8 \times V_s} - P_{atm} \frac{0.1 \times V_s}{0.8 \times V_s}$$

$$P_a = 1.25 P_{atm} \times \frac{V_{output}}{V_s} - 0.125 P_{atm} \qquad (4.16)$$

The calculation above is evaluated in LabVIEW, as shown in Figure 20. Each measurement gathered by the probe and DAQ is passed through this part of the program.
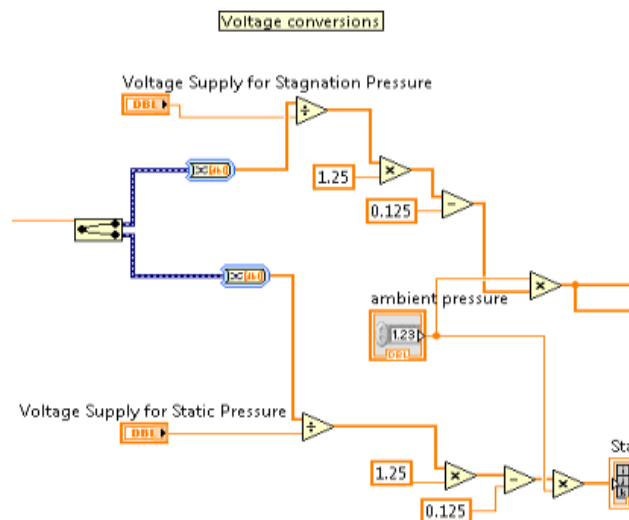
Figure 20: Conversion process from voltage to pressure

After this process, the stagnation pressure is compared with the atmospheric pressure. Based on the expected pressures, the VI has set the range of from -5 to 20 Pa. This means, if the difference between a stagnation pressure and an atmospheric pressure lies within the range, the true loop will be processed. On the other hand, if the difference between a stagnation pressure and an atmospheric pressure does not lie within the range, the false loop will be processed. The range can be redefined if necessary. This range set up is shown in Figure 21 below which is a part of the LabVIEW block diagram.
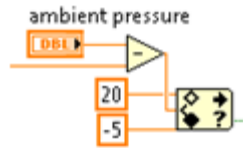
Figure 21: Range of numerical differences

After the comparison, the LabVIEW scheme will automatically process either the true or false loop. The true loop is defined as a subsonic flow case, so if the value of the difference between stagnation pressure and ambient pressure is within that range, the data will be processed with the subsonic equation and the program will calculate the Mach number of the flow at the break point of the loop. The equation of the subsonic flow is derived with the isentropic flow equation relating the ratio of stagnation pressures to the Mach number [3].

$$\frac{P_{t1}}{P_{t0}} = [\frac{(\gamma + 1) \times M^2}{(\gamma - 1) \times M^2 + 2}]^{\frac{\gamma}{\gamma-1}} \times [\frac{(\gamma + 1)}{2 \times \gamma \times M^2 - (\gamma - 1)}]^{\frac{1}{\gamma-1}} \qquad (4.17)$$

$$\frac{P_{t1}}{P_{t0}} = [\frac{2.4 \times M^2}{0.4 \times M^2 + 2}]^{\frac{1.4}{0.4}} \times [\frac{2.4}{2.8 \times M^2 - 0.4}]^{\frac{1}{0.4}}$$

$$\frac{P_{t1}}{P_{t0}} = [\frac{1.2M^2}{0.2M^2 + 1}]^{\frac{7}{2}} \times [\frac{6}{7M^2 - 1}]^{\frac{5}{2}} \qquad (4.18)$$

$$\frac{P_0}{P_{to}} = (1 + \frac{\gamma - 1}{2}M^2)^{\frac{-\gamma}{\gamma - 1}}$$

$$\frac{P_0}{P_{to}} = (1 + 0.2M^2)^{\frac{-7}{2}}$$

$$\frac{P_{t0}}{P_o} = (1 + 0.2M^2)^{\frac{7}{2}}$$

$$(\frac{P_{t0}}{P_o})^{\frac{2}{7}} = 1 + 0.2M^2$$

$$M = \sqrt{5(\frac{P_{t0}}{P_o})^{\frac{2}{7}} - 5} \qquad (4.19)$$

These steps of calculation are shown in Figure 22 below. P_{to} is stagnation pressure and P_o is static pressure. Each pressure is supplied by a probe.
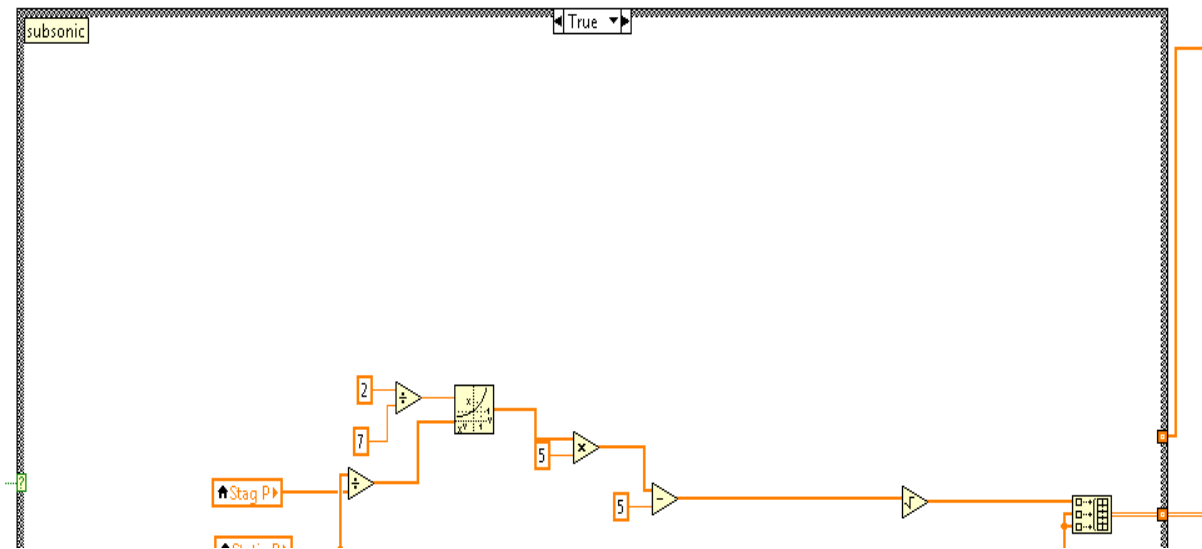
Figure 22: True (subsonic) loop

The false loop is then defined as the supersonic flow case, so if the stagnation pressure calculated by Eq. 4.16 lies between the ranges defined in Figure 21, the pressure ratio will be processed with the supersonic equation and the program will calculate the Mach number of the

flow at the break point of the loop. The equation of the supersonic flow is derived by applying normal shock wave relations and isentropic flow relations, multiplying Eq. 4.18 with the equation used to derive Eq. 4.19.

$$\frac{P_{t1}}{P_0} = \frac{P_{t1}}{P_{t0}} \times \frac{P_{t0}}{P_o} \tag{4.20}$$

$$\frac{P_{t1}}{P_0} = [\frac{1.2M^2}{0.2M^2+1}]^{\frac{7}{2}} \times [\frac{6}{7M^2-1}]^{\frac{5}{2}} \times (1+0.2M^2)^{\frac{7}{2}} \tag{4.21}$$

$$\frac{P_{t1}}{P_0} = [1.2M^2]^{\frac{7}{2}} \times [\frac{6}{7M^2-1}]^{\frac{5}{2}}$$

$$(\frac{P_{t1}}{P_0})^{\frac{2}{7}} = 1.2M^2 \times [\frac{6}{7M^2-1}]^{\frac{5}{7}}$$

$$M^2 = \frac{1}{1.2}(\frac{P_{t1}}{P_0})^{\frac{2}{7}} \times [\frac{6}{7M^2-1}]^{-\frac{5}{7}}$$

$$M = \sqrt{\frac{1}{1.2}(\frac{P_{t1}}{P_0})^{\frac{2}{7}} \times [\frac{6}{7M^2-1}]^{-\frac{5}{7}}}$$

$$M = 0.913(\frac{P_{t1}}{P_0})^{\frac{1}{7}} \times [\frac{7M^2-1}{6}]^{\frac{5}{14}} \tag{4.22}$$

Since the calculation of the Mach number cannot be directly calculated using just the pressure ratio, a loop had to be implemented to perform the iterative procedure to calculate the Mach number. An initial guess for the numerical value of Mach number was arbitrarily established as 1.2. As long as the initial guess is above one, and the flow is supersonic, the iteration automatically converges to the appropriate Mach value. The VI uses a sampling rate of the pressure transducer voltages per every 50 milliseconds. The program is set up to run for 10 seconds or until the user enables the stop button. The steps in the calculation are shown in Figure 23 below. P_{t1} is stagnation pressure and P_o is static pressure. Each pressure is supplied by a probe.
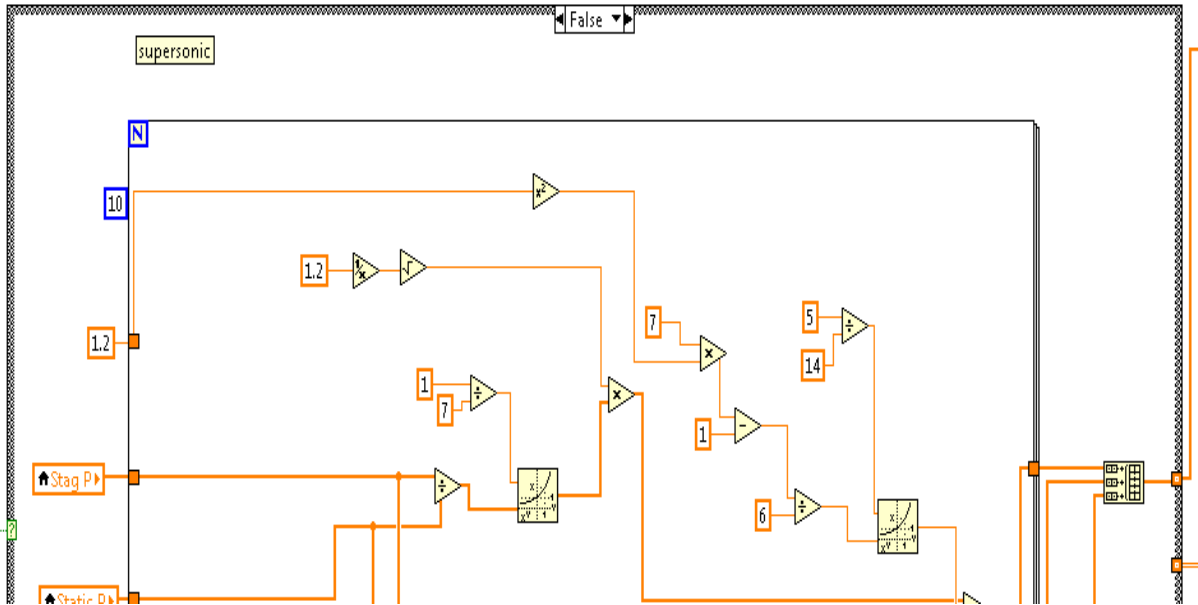
Figure 23: False (Supersonic) Loop

Upon completion of the program, it will save the data to an Excel file with numerical values of Mach number, stagnation pressure, and static pressure. The VI will use the average value of each value to calculate the stream Mach number of the flow inside of the tunnel.

4.2.4 Data Acquisitioning System Initial Tests

A series of tests were performed to check the DAQ system. The goal of these tests was to calculate an expected numerical value for the Mach number based on voltage inputs used to simulate output from the transducer. The data points used in the tests are given below. The first numerical value of the data point represents the stagnation voltage which will be converted to the stagnation pressure, and the second numerical value of the data point corresponds to the static voltage which will be converted to static pressure according to the conversion equation from Section 4.2.3 Data Acquisition System. After these points are converted to the pressures, these values will be calculated either with the subsonic equation loop, if the difference of the

51

stagnation and the ambient pressure is true for the range (which means the difference lies between the range), or to the supersonic equation loop if the difference is false for the range. The purpose of this mock test is to verify the accuracy and performance of the processes and equations by comparing these values to the expected numerical Mach numbers.

Data Points:

A. (2.52, 0.6708) Volts

B. (2.612, 0.8702) Volts

C. (2.066, 0.5597) Volts

D. (2.437, 0.7598) Volts

Since the power supply could not show the precise numerical values on the screen, a circuit was used to gather more precise values of the two voltages. This was accomplished by connecting fluke multimeters in parallel, as shown in Figure 24.
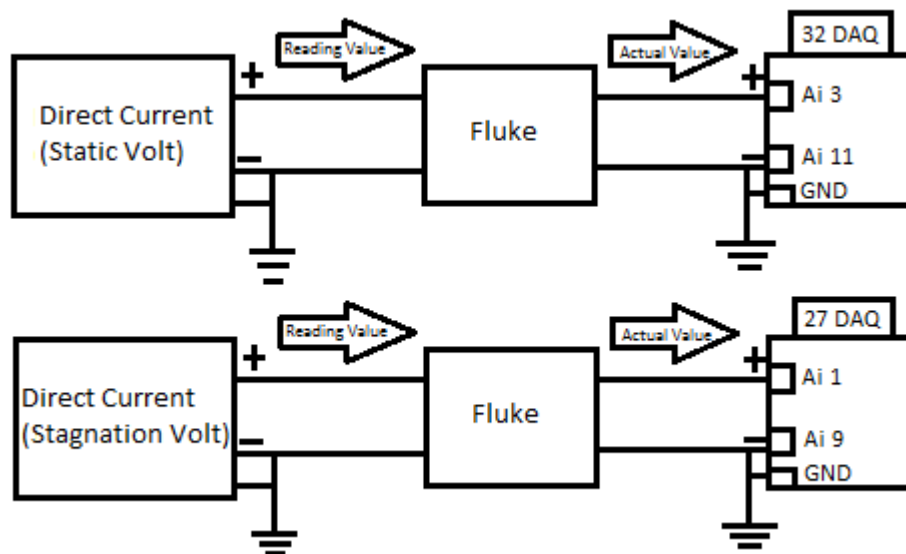
Figure 24: Circuit diagram of parallel connection

Figure 25 and Figure 26 show the connections from the DAQ channel to the battery supply.
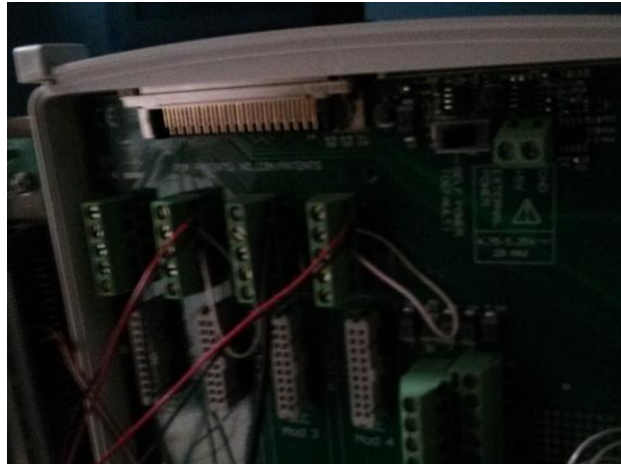
Figure 25: DAQ channel connection
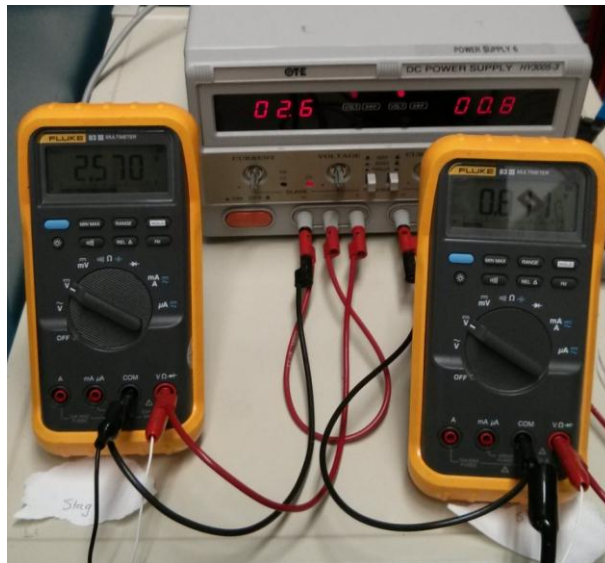
Figure 26: Connection between fluke and battery supply

Figure 27 shows the front panel of the DAQ system. The left side of the panel shows the initial inputs for calculating two pressures and Mach number, and the right side of panel shows the current Mach number of the flow inside of the tunnel.
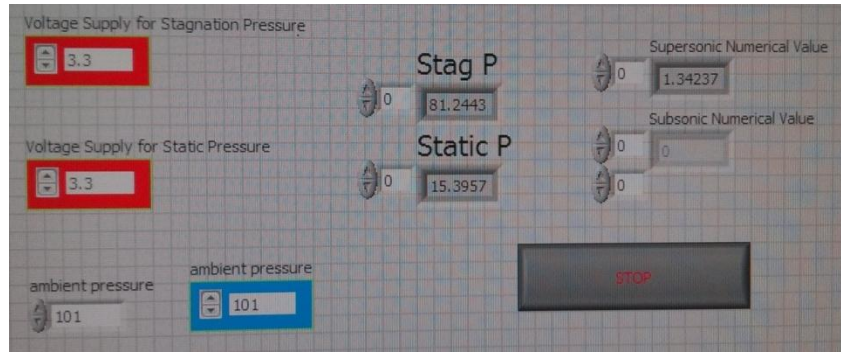
Figure 27: Front panel of DAQ system

5 Schlieren Imaging Flow Visualization

The schlieren imaging technique is a non-intrusive flow visualization method that can be used to visualize the density gradient in a flowing fluid. This technique has been used for centuries to study the distribution of density gradients within a transparent media. Robert Hooke is a pioneer of the schlieren technique [17]. In 1665, he used a convex lens and two candles that displayed the density gradients of the air on a projection screen. After that, the schlieren technique was further developed into a visualization system by Toepler in 1864 [17]. Since then, many kinds of schlieren arrangements have been developed, such as single-lens, dual-lens and z-type schlieren systems. The z-type system was selected for this project to visualize flow in the wind tunnel. The relevant background and the methodology to implement this system are discussed in the subsequent sections.

5.1 Schlieren Background

In homogeneous media such as a vacuum, light propagates uniformly. This means that the light rays are undisturbed, and they travel in straight lines. However, as light travels through our atmosphere, it does not travel uniformly. This is because our atmosphere is not homogeneous due to turbulence, thermal convection, weather phenomena, and other disturbances [18]. The reason that these phenomena affect traveling light is because of a change in refractive index. As light interacts with these changes in refractive index, distortions are produced that can be observed. Although this phenomenon can occur in solids, liquids, and gases, this project focuses on how distortions are produced in gases.

There are many refractive properties that change as light travels through inhomogeneous media. For example, light is slowed when passing through transparent matter. The refractive index given for this property is simply:

$$n = \frac{C_0}{C} \tag{5.1}$$

where C_0 is the universal speed of light and C is the speed of light in the medium [18]. For air and other gases, a linear relationship exists in terms of the density ρ:

$$n - 1 = k\rho \tag{5.2}$$

where k is the Gladstone-Dale coefficient (about 0.23 cm^3/g for air at standard temperature and pressure). In common gases the refractive index varies very little; the refractive index is weakly dependent on ρ. Therefore, to detect changes in the refractivity, sensitive optics must be used. The refractivity $(n - 1)$ depends on the substances' properties such as temperature differences, varying density, and mixing of dissimilar materials, as well as the wavelength of illumination [17]. Flowing gases with variable density can arise from temperature differences or high speed flows. These changes can all lead to disturbances in the gas which can lead to light refraction. For solids, the equations involved are much more complex. The refraction is also much greater, as such the optical sensitivity needed to view these refractions reduced.

There are special cases of refraction that can occur in inhomogeneous mediums. One such case that can be taken advantage of is the fact that k is directly proportional to and increases with light wavelength, λ. Therefore infrared light can be used to detect smaller changes in refraction. Likewise, the sensitivity can also be increased by using ionized gas.

General geometric properties of light diffraction through inhomogeneous media can be predicted. This refraction of light caused by inhomogeneities has been shown to be proportionate to the gradients in refractive index. The resulting ray curvature is given by:

$$\frac{\partial^2 x}{\partial z^2} = \frac{1}{n}\frac{\partial n}{\partial x}; \quad \frac{\partial^2 y}{\partial z^2} = \frac{1}{n}\frac{\partial n}{\partial y} \tag{5.3}$$

\where x, y, and z refer to the standard Cartesian directions, and *n* refers to the refractivity. Integrating once, the resulting angular ray deflection in the x- and y- direction are:

$$\varepsilon_x = \frac{1}{n}\int \frac{\partial n}{\partial x}\partial z; \quad \varepsilon_y = \frac{1}{n}\int \frac{\partial n}{\partial y}\partial z \tag{5.4}$$

These two equations are the fundamental equations used for schlieren and shadowgraph techniques [17]. Both equations illustrate that light rays are bent toward the region of higher refractivity, and as indicated by the equation, higher refractivity corresponds with higher density. These gradient disturbances of inhomogeneous transparent media are the principles behind schlieren [19]. They consist of relatively small differences of refractivity, and by definition bend light in the z-direction. Schlieren may occur in one, two, or three dimensions. For schlieren occurring in one and two dimensions, typical schlieren and shadowgraph techniques can be used. Typical techniques are further explained in the later section, Schlieren Systems. For schlieren that occur in the third dimension, holographic[1], tomographic[2] and stereoscopic[3] methods are ways of fully characterizing the refraction.

Through the use of laser interferometry and holography, reconstruction of schlieren phase optics can be achieved. A reconstruction hologram yields both the amplitude and phase of the

---

[1] Holographic method – Technique involving lasers interference, and diffraction to produce a three dimensional image

[2] Tomographic method – Uses a similar technique to an MRI, where multiple section images are used to gain a three dimensional image.

[3] Stereoscopic method – Technique for creating the illusion of depth from a two dimensional image, using separate images for each eye

original light beam, while capturing the three-dimensional image. Tomographic schlieren methods have also been used to image complex shock wave shapes. This is achieved by the addition of a second parallel schlieren beam rotated perpendicular to the original. Stereoscopic schlieren, similar to tomographic methods uses a second beam, however they are crossed at angles between 10° to 15° to achieve "left" and "right" eye views.

Techniques and Applications

There are several techniques for observing schlieren effects and then quantitatively obtaining results. The two primary techniques of observing schlieren effects are the schlieren and shadowgraph techniques. Both methods are most appropriate for the two-dimensional phenomena, but are still useful qualitatively for three-dimensional schlieren.

Shadowgraph methods focus on a shadow rather than an image of the refractions. The shadowgraph illuminance level is dependent on the second spatial derivative, or Laplacian e.g:

$$\frac{\partial^2 n}{\partial} = \partial x^2 \tag{5.5}$$

This results in the shadowgraph method displaying the ray displacement resulting from the deflection. In other words, when the displacement occurs, rather than being re-focused and cut-off like in schlieren technique, the rays continue to disperse from their point of origin. In terms of the apparatus and setup, shadowgraphy is considerably easier than using schlieren technique since fewer components are necessary. Because of this ease, shadowgraphy is used for large scale visualizations. However, it has a lower sensitivity than schlieren imaging, as the shadowgraph method is a higher order derivative than the schlieren method. Still, when investigating shock waves and turbulence in flows, shadowgraphy can be more sensitive than the

schlieren technique. An example of a flow in which shadowgraphy is more sensitive would be shock waves created by supersonic projectiles.

The schlieren method, on the other hand, generally observes a conjugate image[4] of the test section formed by the refracted light through a lens. Another requirement of the schlieren technique is that a knife edge or some other cutoff of the refracted light must be used. The illuminance level in the schlieren image responds to the first spatial derivative of the refractive index, e.g. $\frac{\partial n}{\partial x}$. Therefore the schlieren image displays the deflection angle ε. Therefore, the superior sensitivity and adaptability of the schlieren technique results in it being the most preferred method.

Various applications such as Moiré and interferometry applications can be used to achieve more quantitative data than available from schlieren and shadowgraph techniques. The Moiré technique uses a similar setup to that of the schlieren technique; it uses a grid to filter the light source. In contrast, interferometry applications rely on using multiple angles to capture the full schlieren effect. This is accomplished by using two to three schlieren designs from these different angles. The Moiré technique is popular because it can produce a quantitative image from a shadowgraph technique without the use of a second image, which would be required from other techniques. A quantitative image, being one that can be measured with a known value of size distortion, is achieved by use of a grid. These measurements can then be extrapolated to calculate the magnitude of change in the test section.

---

[4] Conjugate image - The "real" image is often called the conjugate image; in comparison, a virtual image is also created simultaneously

5.1.1 Schlieren Definition

Due to the shape and size of the supersonic wind tunnel built for this project, a two dimensional schlieren system will provide enough information about the velocity gradient inside the test section.

Obtaining the Schlieren Image of a Test Subject

There are many different variations of schileren image setups, and the equipment required for each varies slightly. However, there are a few key components that are common amongst most systems [17]. They include a light source, a screen or camera, an assortment of lenses or mirrors, and a light cut-off device. These objects are displayed in Figure 28.
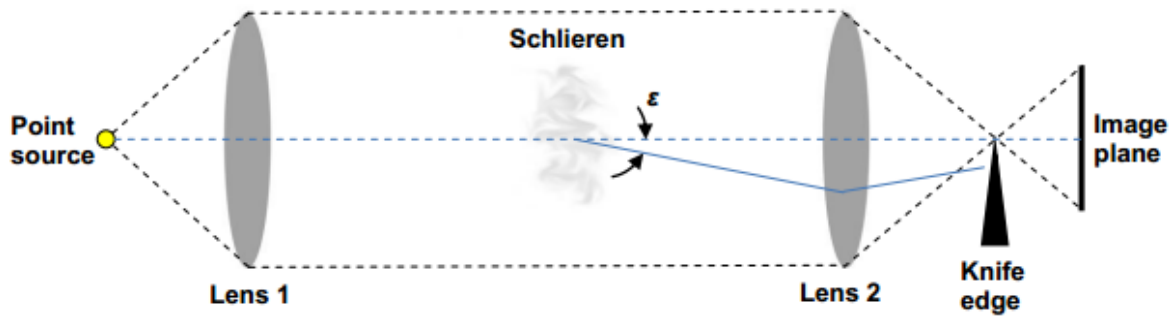
Figure 28: Simple duel lens schlieren system with point light source ©TAMU Aerospace Department (Ref [17] © 2001, Springer)

The Light Source

In order to gain an understanding of how a schlieren system works, perhaps it is easier to analyze a basic duel lens system in Figure 28 in terms of its light source. Though this system wouldn't be very practical for obtaining a good quality schlieren image, it incorporates the basic principles of all schlieren systems.

Point Light Source

In a duel lens system, the light from a point source is collimated to encompass the test area where the schlieren object[5] is present. This is accomplished through the use of a lens. Another lens at the opposite end of the test section will refocus the point source light and project it upside-down on a screen. This setup, without a cutoff, would be analogous to a simple projector. The key to making this a schlieren system is the cutoff, shown in Figure 28 as a knife edge, located either before or after the focus point. Light rays that are refracted by the schlieren object do not pass through the focus therefore averting the cutoff; these rays reach the screen. For simplicity, only the two refracted light rays shown in Figure 28 will be discussed, but in reality, there are an infinite number of light rays that can be refracted. The knife edge blocks refracted light rays, thus creating a corresponding dark spot on the screen. By blocking 'half' of the refracted light, the rays will not cancel each other out ensuring that there will be dark and light spots, i.e. a visual gradient [17].

If the knife edge is directly on the focus, the entire image will be blocked and the visual useless. This gives two options for the cutoff – either place it before or after the focus. By placing it right before the focal point, one obtains a bright screen, or what is known as a brightfield. Placing it after the focal point, one obtains the opposite, a darkfield [17].

Despite being good basic representations of schlieren systems, point source setups are impractical in the sense that they are only "on-off", binary systems [17]. They cannot produce a 'greyscale' image that effectively portrays the gradient – each point on the image will either be black or white.

---

[5] Schlieren object – the density gradients creating inhomogeneities in the test section
Note: does not necessarily guarantee the projection of a schlieren image

Extended Light Source

Extended light sources on the other hand provide a more realistic and practical methodology for developing schlieren images. An extended light source can be created through the use of a slit; the design of which can vary according to desired usage [17]. Extended light source systems act as if they were an array of point sources. Thus each point in the test area is illuminated by multiple arrays, lending to a more complex and true image of the schlieren object visualized using this technique. A third lens is needed to refocus the rays onto the screen. If a camera was being used the camera lens could act as this focusing lens. This system is shown in Figure 29.
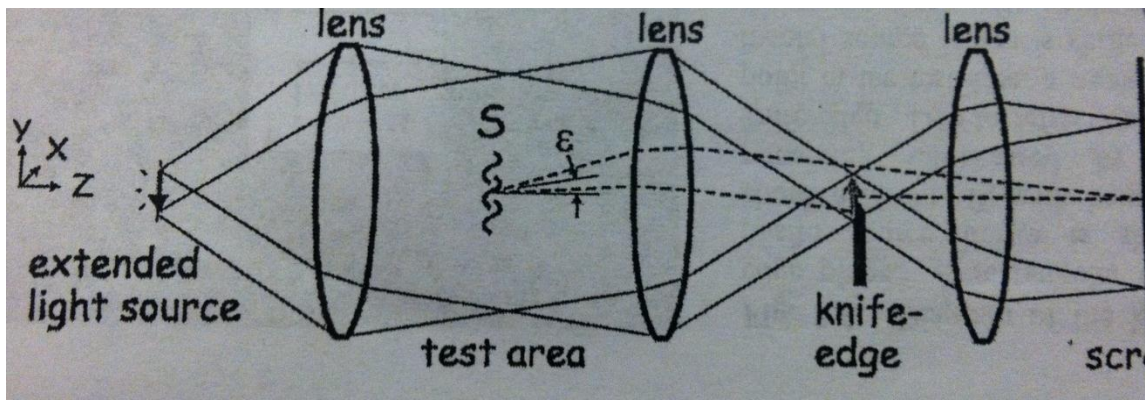
Figure 29: Extended light source schlieren system (Ref [17] © 2001, Springer)

It is important to note that these systems have a definable measuring range. This concept is defined in more detail in the Schlieren Characteristics section. The measuring range is the range of illuminance in a schlieren image, and is linearly proportional to the amount of knife-edge cutoff. Knife edge cut-off can be quantitatively measured as the percentage of light source rays that are blocked off [17].

The knife edge cuts off rays in a single direction. Changing the orientation of the knife edge will change the type of cutoff, thus altering the results. Figure 30 shows three different types of cutoffs – point, vertical, and horizontal respectively. Each provides a different orientation view of the gradient created by the cutoff. Choosing the type of cutoff right for one's system is an important step in obtaining a useful schlieren image.
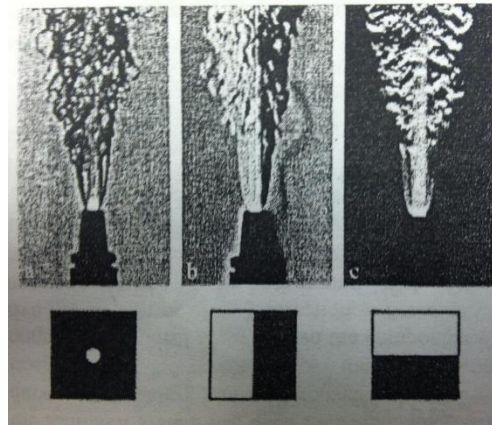
Figure 30: Schlieren images of an oxy-acetylene torch with various cutoffs (Ref [17] © 2001, Springer)

Although the extended light source provides a more practical approach to imaging a flow, it is important to note that often, including in this project, a mirror based setup is utilized. Although these systems are more common, mirror schlieren systems are more complex to set up compared to lens systems [17].

5.1.2 Types of Schlieren Systems

Optics

The principle of the schlieren technique is based on the refraction of light. If the light goes through inhomogeneous media, the light beam will be distorted by the variations of refractive index caused by density gradients in the media. This distortion creates a spatial

variation in the intensity of the light, which can be visualized directly on a viewing screen [17]. If the refractive indices between two media are different, the original direction of the light will be changed. Snell's Law indicates that the angle changed depends on the refractive index difference. This relationship is given in Equation (5.6):

$$n_1 \sin(\theta_1) = n_2 \sin(\theta_2) \tag{5.6}$$

where n_1 and n_2 are the refractive indices of the two regions and θ_1 and θ_2 are the angles the ray makes with the plane of intersection. Using this relationship and assuming that the front and back surfaces of a lens are close together and planar, the thin lens approximation, given in Equation (5.7), can be demonstrated.

$$\frac{1}{f} = \frac{1}{d_i} + \frac{1}{d_o} \tag{5.7}$$

where f is lens focal length, d_i is the distance from the lens to the image and d_o is the distance from the lens to the object. Equation 1.2 relates the position of an image for a lens based on the lens focal length and its position relative to the object [20]. The object plane and the image plane form "conjugate[6]" optical planes. That is, anything in either plane is focused to a corresponding position in its conjugate plane. This idea of conjugate planes is particularly useful in multi-element lenses and lens systems.

Equation (5.7) can be used to estimate the location of the lens relative to the object and image however it loses accuracy with thick or multi-element lenses. For accurate optical component design the "paraxial theory" is much better and can now be done using a computer [21]. Paraxial theory uses Snell's Law at each lens/air or lens/lens interface to calculate image positions. For this work, the thin lens approximation is adequate.

---

[6] Two planes within an optical system are said to be conjugate planes if the intensity distribution across one plane is an image (generally magnified or de-magnified) of the intensity distribution across the other plane.

Despite modern lens manufacturing techniques, most lenses have some form of aberration. The most common two are chromatic aberration and spherical aberration. Other aberrations, coma, astigmatism, and distortion, are less common though no less significant when they do occur [17].

Chromatic aberration occurs because the refractive index of most substances is a function of the wavelength of light. This means that blue light and red light have different ray deflections, and the index in Snell's Law [20] is a function of wavelength. The net result is that the blue light has a focal point which is closer to the lens than the focal point for red light because it deflects more. Achromatic lenses solve this by having two or more elements of different focal lengths and different refractive indices. The lenses are designed so that the chromatic aberration of the first element is cancelled by the equal and opposite aberration of the second.

Spherical aberration is caused by the fact that most lens surfaces are ground to a spherical surface, hence the name. A spherical surface does not bring all the light to one clear focal point [20]. Instead, the rays striking the rim of the lens typically focus closer than those near the center. Aspheric lenses are ground to a slightly different shape which makes parallel light rays pass through the same focal point.

Z-Type Schlieren System

A modern z-type schlieren system is shown in Figure 31. It is by no means the only method but is one of the most common/conventional implementations of the technique.
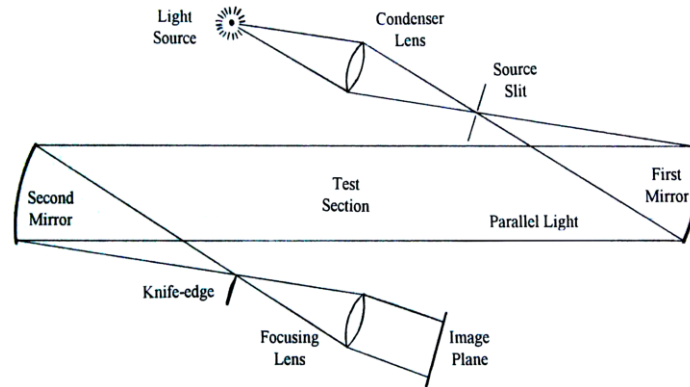
Figure 31: Conventional z-type schlieren system (Ref [17] © 2001, Springer)

In a z-type schlieren system, a light source is focused by a condenser lens onto a source slit, usually about 1 mm wide and several millimeters long [17]. This makes the system more sensitive in the 1 mm direction. The knife-edge is placed parallel to the source slit. The condenser lens should be chosen to project as much light as possible onto the first mirror.

The source slit is placed at the focal length of the first mirror in order to obtain a parallel beam of light from the mirror. After the test section, a second, usually identical mirror is placed to focus the light down to an image of the source slit at its focal point. A knife edge is placed at the source slit image so that it blocks part of the image. The z-shape of the optical axis prevents the light source and imaging components from blocking the test section. By keeping the off-axis angles small and equal, most optical aberrations are kept to a minimum [17].

Finally another lens is used to focus the light that has passed through the test section onto the image plane. This lens is necessary to make a sharp image on the image plane. While a point light source would have infinite depth of field, a finite light source requires this lens to focus the test section image sharply. The depth of field is very large though, so the exact position of the lens is not that critical.

The z-type arrangement developed from a system using lenses instead of the mirrors. The use of mirrors increases the diameter of the test section for a given cost, since mirrors are less expensive than similar sized lenses. Mirrors also prevent chromatic aberrations due to their reflective, rather than refractive, nature [17].

Mirrors also have several drawbacks. They are prone to coma[7] and astigmatism[8]. This can be minimized by making the angles between the incident and reflected light rays as small as possible and by making the two mirrors identical. Also, they tend to be very far apart to prevent interference between the test section and the non-parallel sections of light. This allows air currents to become a problem, since they cause small density fluctuations which can be picked up in sensitive systems [17]. Space for the system can also be a problem, though plane mirrors can be used to fold the optical axis. The size of the test section that is imaged is limited to the diameter of the mirrors [17].

Focusing Schlieren

There have been two main methods of achieving a sharply focused image when using schlieren systems. What is interesting is that very little attempt is made to separate them in the literature even though they are quite different. The two methods are described below, multiple source schlieren and focusing schlieren.

---

[7] Coma- a wave-front aberration occurs either due to the incident wave front being tilted, or decentered with respect to the optical surface. Hence, it is either an aberration affecting off-axis image points, or the result of axial misalignment of optical surfaces, respectively.

[8] Astigmatism- an off-axis point wave-front aberration, caused by the inclination of incident wave-fronts relative to the optical surface. However, while coma always originates at the optical surface, astigmatism, in its simplest form, for mirror with the stop at the surface, results simply from the projectional asymmetry arising from wave-front's inclination to the surface.

The Multiple Source Schlieren System

The multiple source system is similar to z-type schlieren with the exception of the light source and knife-edge. The light source is replaced by a set of light sources making up a pattern. Generally speaking this is a set of grid lines, though it can also be as few as two point sources [20]. Each source must have a corresponding knife-edge or negative grid. This can also be thought of as a z-type system with multiple sources, hence the name used here of multiple source schlieren. The basic system layout for a simplified system with two light sources is shown in Figure 32.
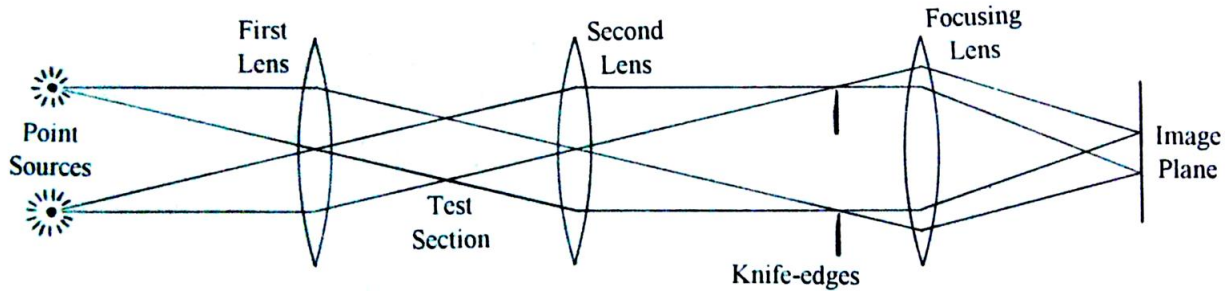
Figure 32: A multiple source schlieren system arrangement (Ref [20] © 2006, Hanenkamp)

The light from each source can be regarded as passing through a separate schlieren system, however an object placed in the test section will be focused on the image plane by the focusing lens. Thus, while each system has infinite depth of field, the images from each source are only superimposed at the image plane. This gives the system its focusing effect, since there is a unique image plane for each refracting plane for which the two images superimpose one another [20]. In addition, by adding more sources, such as a grid, the quality of focus as well as the clarity can be improved.

Due to this arrangement's similarity to the z-type schlieren, many of its characteristics are similar too. Like the z-type schlieren, the test section size is limited by the size of the optics.

Depending on the size of the light source, the test section is usually about two thirds of the diameter of the lenses [20]. The sensitivity equations for a z-type system will hold for a multiple source system, though there are added equations for depth of field. These equations are explained in more detail in the following section.

The differences are in the focusing effect and in the range, the distance from the lenses to one another, of the system. Normally, once the range is exceeded, a z-type system can no longer distinguish angles of deflection. However, with a multiple source schlieren system, if the sources are close together, such as with a grid type source, it is possible for the light source of one system to interact with the knife-edge and gap of an adjacent system [17].

The advantages and disadvantages of a multiple source schlieren system are summarized in Table 1 below:

Table 1: Advantages and disadvantages of multiple source schlieren system

Advantages	Disadvantages
1. Focuses on a 2D plane within the test section, thus reducing noise from out of test section disturbances.	1. Sensitivity is theoretically as good as a conventional system.
2. Similar to the z-type schlieren from a design and mathematical point of view.	2. Lenses (or mirrors) must be good quality, particularly with regards to off-axis aberrations.
	3. Setting up conjugate knife-edges to their sources can be difficult, particularly to get uniform cutoff at both knife edges. Grids can be used to simplify alignment matters but then construction and accurate positioning of suitable grids becomes a problem.

The Focusing Schlieren System

The second focusing system is a more commonly used method to achieve the focusing effect than the multiple source schlieren and works on a slightly different principle than the z-type schlieren. A schematic of the arrangement is shown in Figure 33:
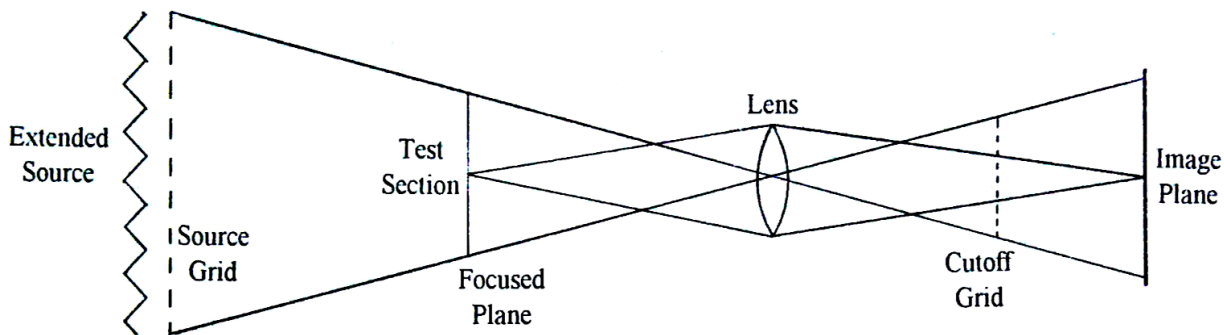
Figure 33: A focusing schlieren system arrangement (Ref [20] © 2006, Hanenkamp)

An extended light source is used to backlight a source grid. The source grid generally consists of closely spaced black and transparent stripes evenly spaced. The light passes through the test section to the lens, which focuses the source grid onto a cutoff grid, which is an image of the area from the test section. Ideally this image is a perfect negative of the source grid image. Each bright band of the source grid is like a source slit and each corresponding black band in the cutoff grid is the corresponding knife-edge. By adjusting the position of the cutoff grid minutely, varying cutoff between 0% and 100% is possible [20].

There are several advantages to using grids. These are that the construction and alignment is greatly simplified, the percentage cutoff can be varied easily and constantly over the whole area and provides clarity in the images [20]. The disadvantage is that the system can only detect density gradients in one direction.

The advantages and disadvantages of the system are summarized in Table 2 below, as compared to the z-type schlieren system:

Table 2: Advantages and disadvantages of focusing schlieren system

Advantages	Disadvantages
1. Focuses on a 2D plane within the test section, thus reducing noise from out of test section disturbances.	1. The construction of the light source and knife edge is a problem, due to the very high accuracy required over a large area.
2. The size of the test section is independent of the optics, thus very large fields of view are possible at relatively low cost.	2. Alignment of the cutoff is difficult, particularly with respect to achieving constant cutoff over the whole area.
3. The light source does not have to be a very bright point-like source.	3. The sensitivity is typically not as good as a conventional system. This is related to the lens quality and the difficulty of alignment.
4. Less space is required on either side of the test section than for the z-type system.	

5.1.3 Schlieren Characteristics

Sensitivity

Sensitivity is the quality or clearness of the density gradients in a schlieren image. Sensitivity is influenced by the quality of the components in the system, including the light source, mirrors, focusing lens, and camera [17]. It is also dependent on the proper positioning of the components to focus the schlieren image on the gradients in the test section. The setup of the schlieren system to optimize sensitivity will be discussed in more detail in the Methodology. Sensitivity can be quantitatively determined based on certain measureable parameters, such as mirror focal lengths or light source height. The calculation of the sensitivity shows the parameters that are maximized or minimized for optimized results.

A light source has a certain luminance[9], B. The light source is channeled through a slit of dimensions b and h, which are the width and height of the slit, respectively. Illuminance[10] of this light source on a mirror, E_0, is a function of B, b, h, and the focal length[11] of the mirror, f_1.

$$E_0 = \frac{B \times b \times h}{f_1^2} \qquad (5.8)$$

This same equation can be applied to determine the background illuminance of a schlieren image, E, or the measure of illuminance in the background of a schlieren image. Because refracted, or bent, light rays infringe upon the knife edge, a fraction of the light slit height will be "cut out". The resulting smaller height, a, is given as a ratio of the focal lengths of the two mirrors multiplied by the slit height [17].

$$a = \frac{f_2}{f_1} \times h \qquad (5.9)$$

The background illuminance of a schlieren image can be estimated by solving Equation (2) for h and substituting the result into Equation (5.8). After this is done, a magnification factor, m, is multiplied in to correlate the true size of the test section gradients with that displayed in the image output.

$$E = \frac{B \times b \times a}{m^2 \times f_1 \times f_2} \qquad (5.10)$$

An illuminance at a particular point in the schlieren image can be determined with respect to E, where the difference between these values is the differential illuminance for a given section, ΔE [17]. A light ray at this point will be refracted by a distance Δa, which can be defined as the refraction angle, ε, multiplied by the focal length of the second mirror.

---

[9] Luminance – the amount of light that passes through a given area in a certain direction, [candela/m^2]
[10] Illuminance – the amount of light that is incident on a given surface, quantitative measure of brightness [lumens/m^2]
[11] Focal length – the length over which a mirror bends rays to a single point of focus [m]

$$\Delta a = \varepsilon \times f_2 \tag{5.11}$$

Equation (5.11) can be used to determine the height, a, which is then substituted into Equation (3) to obtain ΔE.

$$\Delta E = \frac{B \times b \times \varepsilon}{m^2 \times f_1} \tag{5.12}$$

The contrast, C, is a characteristic of the image produced by a schlieren system, which is characterized as the ratio of the differential local illuminance to the background illuminance [17].

$$C = \frac{\Delta E}{E} \tag{5.13}$$

Substituting Equations (5.12) and (5.10) into Equation (5.13), contrast is now defined in terms of refraction angle.

$$C = \frac{\varepsilon \times f_2}{a} \tag{5.14}$$

Sensitivity, S, is a ratio of the output to the input, which can be given as the first order derivative of the contrast with respect to refraction angle.

$$S = \frac{dC}{d\varepsilon} \tag{5.15}$$

When substituting Equation (5.14) into Equation (5.15), sensitivity is given by an output of focal length and an input of height as defined by the placement of the knife edge.

$$S = \frac{f_2}{a} \tag{5.16}$$

Overall, the sensitivity of a schlieren image can be maximized by minimizing the height difference between the slit and knife edge and selecting a mirror with the longest possible focal length. Increasing sensitivity in a schlieren image is shown in Figure 34.
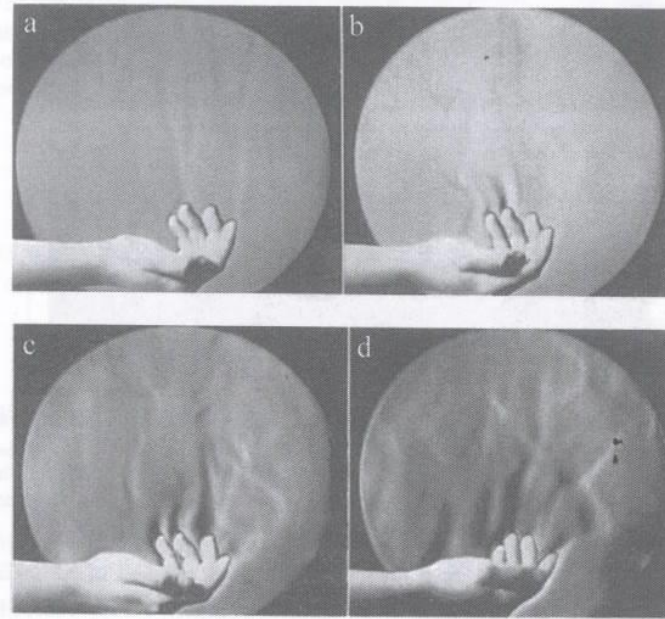
Figure 34: Thermal convection shown through schlieren imaging with increasing sensitivity (Ref [17] © 2001, Springer)

The parameters in the derivation have physical limits that hinder the highest achievable sensitivity. According to Settles, as a general principle, most schlieren users find that a contrast of 0.05 is minimally detectable [17]. When maximizing focal lengths, cost limits must be addressed when selecting a mirror for an application. The size of the mirror chosen, as well as the focal length, must also be reasonable for the dimensions of the system layout. When minimizing the height of the slit, the effects of diffraction[12] will limit sensitivity due to the obstruction of the edge of the slit. Diffraction distorts the quality of the schlieren image by creating bright shadows in the image, as shown in the right picture in Figure 35 [17]. Diffraction can also occur in the test section, creating halos[13] in the image, but these distortions can often be overlooked or eliminated with image post-processing [17].

---

[12] Diffraction – the phenomena where bent light rays encounter an obstacle or area of a different refractive index, thus distorting the schlieren image

[13] Halos – light circles, arcs, or spots in an image due to the effects of diffraction

74
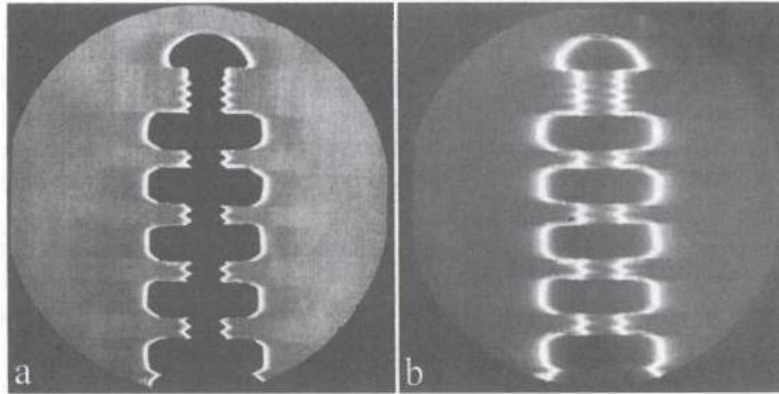
Figure 35: Diffraction in schlieren image as light slit height is minimized by knife edge (Ref [17] © 2001, Springer)

Post-processing is used to improve the contrast in a schlieren image, which then inherently improves the sensitivity. Some of the capabilities available in present-day digital software include edge detection, smoothing and sharpening, image correction, and image restoration [17].

Measuring Range

The measuring range of a schlieren system is the range of illuminance where the density variations are visible in the test section when projected onto an image. The measuring range directly corresponds to the range over which the knife edge cuts off any of the refracted light rays from the test section [17]. The end points of the measuring range are when the knife edge is fully removed from the light source image (0% cutoff), and when the knife edge is completely blocking the image (100% cutoff). The former is considered the bright limit or over-ranged condition, while the latter is the dark limit or under-ranged condition [17]. The measuring range for a gas jet is shown in Figure 36. The range is considered equal in both directions if the knife edge cuts off 50% of the light source image in the test section. However, most applications use

about a 90% cut-off range in order to maximize sensitivity. This makes sensitivity and range inversely proportional, where one characteristic is minimized when the other is maximized [17].
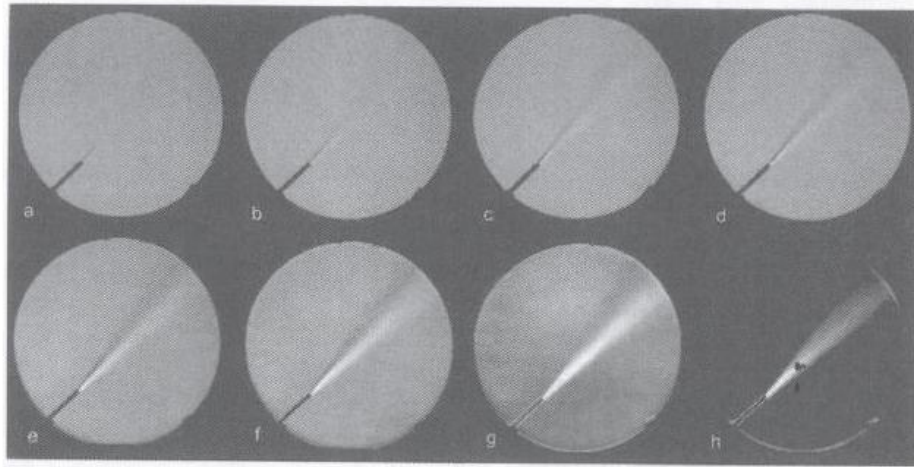
Figure 36: Schlieren image of a gas jet at a) 0%, b) 20%, c) 40%, d) 60%, e) 80%, f) 90%, g) 95%, and h) 100% of the measuring range (Ref [17] © 2001, Springer)

There are two main abnormalities that can affect measuring range. If the light source slit is too narrow, the images will become "binarized" in black and white, rather than have a continuous grayscale color gradient. In high speed flows with shock waves, refractions of light rays can be strong enough to over-range the system and create dark regions where it is normally bright. Over-ranging the system occurs when light rays are refracted beyond the range of the knife edge, and are therefore not registered in the formation of the image [17].

Resolution

The resolution of a schlieren system, or resolving power, is the amount of detail that an image is capable of producing. Resolution is measured in lines per millimeter (lines/mm) or arcseconds of separation between observable points by the given optical equipment [17]. The range of lines/mm found in most schlieren systems is between only 10 and 30 lines/mm, making

it unlikely that the resolution limit in a medium will be reached. This makes resolution less important to maximize than sensitivity or measuring range. The images in these systems produce images that are sharp enough for the application, despite their low resolution [17].

5.2 Schlieren System Implementation

For use in this MQP, the team decided on a conventional z-type schlieren mirror system. The design includes a light source, condenser lens, optical slit, two parabolic mirrors, a knife edge, a focusing lens, a camera, and various mounting equipment.

5.2.1 Mounting

In order to minimize any possible effects of vibration from the tunnel on the schlieren system, the entire setup needs to be mounted separately from the wind tunnel and vacuum chamber. This has been accomplished through the design and construction of an optical mounting table. The table is made up of standard x-channel components for ease of construction and has two acrylic shelves. The top shelf has tapped holes to allow mounting of the z-frame for the system. The bottom shelf provides rigidity and a surface for the light source during operation. The four legs have adjustable feet to compensate for any unevenness in the floor of the lab. By keeping the entire system fixed on the table, it can be moved to different testing locations without disrupting the precise placement of the optics required for the schlieren imaging.

The optical components themselves are mounted on z-frame made from three pieces of x-channel. The x-channel pieces are fashioned together using adjustable, locking hinges as seen in Figure 37. This adjustability helped maintain the critical offset angles, θ_1 and θ_2. The values of

these angles can be set based on physical constraints as long as the angles are set equal to each other to limit the effects of coma and astigmatism.
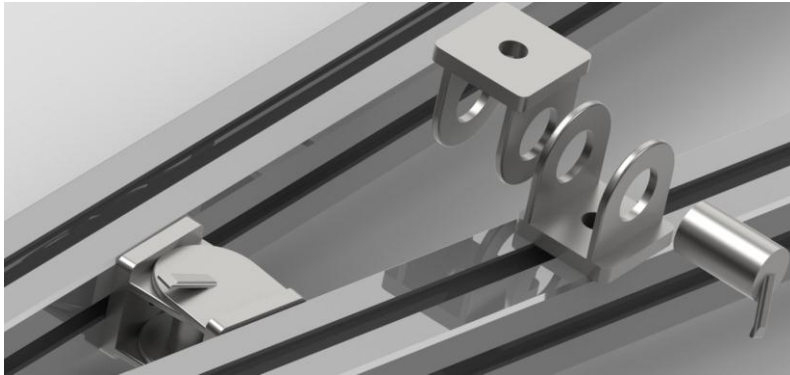
Figure 37: SolidWorks kinematic hinge in z-type system to set offset angles

All of the optical elements fit into custom mounts that have 8-32 threaded holes for mounting. In order to make the optical mounts compatible with the common ¼ - 20 threaded optical rails, custom adapters, shown in   Figure 38, were made. These adapters have an 8-32 threaded hole on one side to allow for connection to the optical mounts through an 8-32 threaded rod. The other side of the adapter is not threaded, but allows for the non-threaded portion of a partially threaded ¼ - 20 rod to be attached and secured using a 4-40 set screw.

Figure 38: Z-system mount adapters

This provides the ¼ - 20 connection along with vertical adjustability of the optical components which is critical to developing a schlieren image, especially with respect to the knife edge. These mounting set ups, consisting of the optical mounts, 8-32 rod, adapter, ¼ - 20 rod, and 4-40 set screw are fastened to the x-channel rails using a t-nut which is compatible with the ¼ - 20 rod. These t-nuts are custom shaped to fit the x-channel groves.

5.2.2 Component Selection

Once all parts needed for the system to operate as a cohesive unit were identified, they were ordered. These included: condenser lens and mount, Mirror and mount x 2, knife edge and mount, and the focusing lens and mount. The rest of the components were purchased locally, or lent to us by our advisor. This section will provide a brief overview of the parts used, including a description of the part, specifications, and role in the system.

Light Source

The light source used, shown in Figure 39, is a Stocker Yale Imagelite Mite Model 20 light source. It uses 150 Watts, 100 Volts, and has a range of 50 to 60Hz. This light source, as shown in the picture, uses fiber optics to direct the light created in the block shaped part, to the end of the adjustable wand. The light source includes an adjustable knob to control the illumination level of the light produced. As discussed in the background section, the light source produces the light of which we are observing the diffraction. Because of the small, controlled light source that is emitted from the end, little to no manipulation was needed from the slit.

Figure 39: StockerYale Imagelit Model 20 light source

Condenser Lens

The condenser lens that was chosen, shown in Figure 40, is a standard aspheric condenser lens. The lens has a diameter of 20mm, and has focal length of 18mm. The main parameter of this lens was a relatively small focal length. The glass lens, is used to collect all ambient light, and that of the light source, and distribute it evenly onwards towards the rest of the system. Also

in the picture, surrounding the lens, is the mount for the lens. The mount, designed to hold the lens in place, was purchased for the lens, as it was the corresponding sized mount. This mount includes an adjustable ring which clamps the lens into place. The condenser lens and condenser lens mount were purchased from Thor Labs and have part numbers of ACL2018 and LMR20 respectively.

Figure 40: Condenser lens and mount used in z-type schlieren system

Slit

The slit, shown in Figure 41, is section of eraser shield, with additional construction paper taped around the edge to block extraneous light from entering the system. The slit is used to ensure that the light source emits a rectangular beam that is ideal for cutoff by the knife edge. This change to the beam of light qualifies the source as an extended light source. This, as explained in the background section improves the results generated. The slit is oriented in the vertical direction so that the horizontally mounted knife edge can provide effective cutoff.
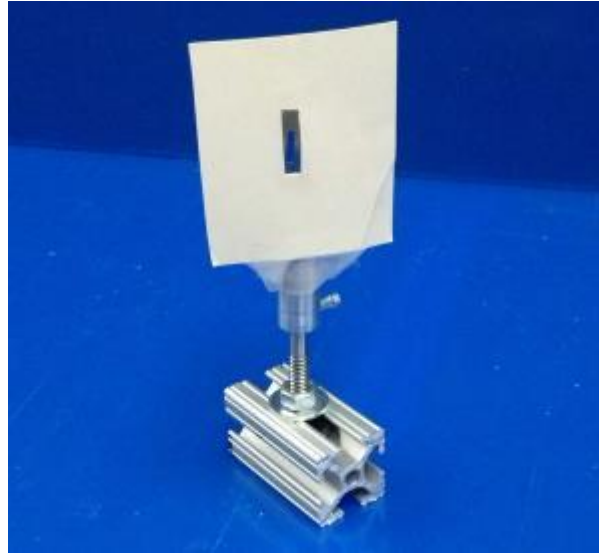
Figure 41: Slit used in z-type schlieren system

Mirror

The mirrors, shown in Figure 42, are parabolic, aluminum coated, UV enhanced mirrors – CM508-200-F01 from Thor Labs. This mirror has a 50.8mm diameter, and a focal length of 200mm. This mirror was chosen based on price and size. As the diameter increases, so does the observable area, but so does the price. Based on our budget, and the wind tunnel channel size, a 50.8mm diameter was determined to be sufficient. A focal length of 200mm was acceptable as the design uses a much greater distance between the two mirrors. The mounts for the mirrors, from Thor Labs, correspond directly to the diameter of the mirrors selected. The mounts include a small set screw which is used to tighten the mirrors into place so they stay rigidly within the mount. The part number for the mirror mounts is FMP2.

Figure 42: Concave mirror and mount used in z-type schlieren system

Knife Edge and Vernier

For the knife edge, a razor blade was used, as shown in Figure 43. The knife edge's purpose is to cut off a percentage of the light being reflected from the second mirror, as the light comes to a single point. This cut off is essential for good results. If the knife edge was not used, and all of the light rays were allowed to pass, the distortion would not be visible because the lower 50% of light carries the "opposite distortion" as the top 50%, resulting in the canceling of both distortions. This principle acts in the vertical direction due to the vertical nature of the slit. Therefore it is possible to cut off the top 50%; however it is not commonly done because the mount needed for the knife edge would be far more complex. Although 50% was used for the previous example, more than 50% cut off achieves higher contrast, yielding better, but darker results. The darkness can be an issue if the test section includes too many layers of material which the light must pass through, or the light source is not bright enough. Initially the knife

edge was held up by a kinematic mount discussed in Section 5.2.1 Mounting. This mount did not offer the precise adjustment needed to finely tune the knife edge's cut off. Therefore, a manual vernier stage was purchased. This Manual Lab Jack Stage, travels a total of 13mm vertically, and has a 2kg load capacity. Because the vernier stage is tall to begin with, the need for additional height is minimal. In addition, only the knife edge, and possibly a mounting converter will be on the stage, a total weight well below the weight capacity. The knife edge mount was purchased from Thor Labs and has a part number of DH1. The linear adjuster came from Produstrial and has a part number of 124704.
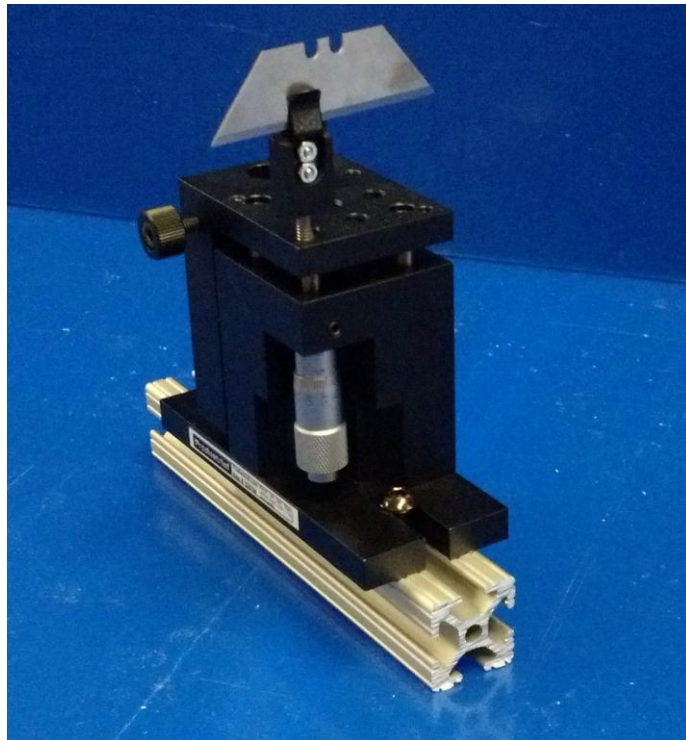
Figure 43: Knife edge & vernier used in z-type schlieren system

Focusing Lens

The focusing lens, shown in Figure 44, is used at the end of the system for focusing the light passing the knife edge. The focusing lens chosen has a focal length of 250mm, and a

diameter of 2in. The focusing lens was placed within the focal length of the mirror to ensure that the lens captures the entire diameter of the light beam reflected by the mirror. The focusing lens is useful because it condenses the results to a smaller area while preserving the image quality. The mount used for the lens was an LMR2 from Thor Labs. It is used to hold the focusing lens in place, so that it may be positioned correctly. The lens, AC508-250-A, was also purchased from Thor Labs.
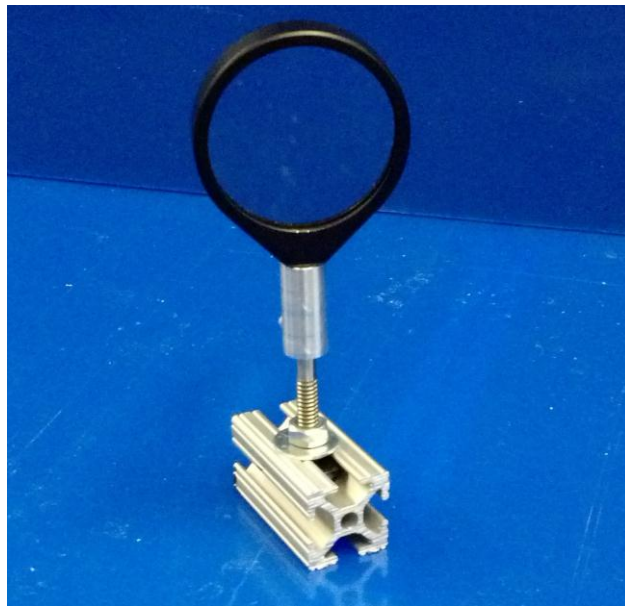
Figure 44: Focusing lens and mount used in z-type schlieren system

Screen

The screen that the team used to project the image onto, apparatus shown in Figure 45, uses high quality Dell Premium Photo Paper, held flat and in place by a clipboard. The higher quality paper ensures a whiter and smoother surface than regular printer paper. The smooth surface reduces the amount of light that is scattered when it hits the paper, producing a crisper result. The specifications for the high gloss photo paper are 9lb stock and a brightness of 90.

Figure 45: Screen used in z-type schlieren system

Camera

The camera used, illustrated in Figure 46, is a Lumix DMC-GF3 equipped with a Lumix G Vario 14-44mm adjustable zoom lens. After testing, it was concluded that a $\frac{1}{125} sec$ shutter speed was to be used with the largest available focal length. This gave the least blurry pictures, as the schlieren image is changed during testing due to airflow, and the highest quality pictures are captured with the most zoom available.

Figure 46: Camera used in z-type schlieren system

5.2.3 Modified Z-System Bench Top Test

The layout of the modified z-system is shown below in Figure 47.
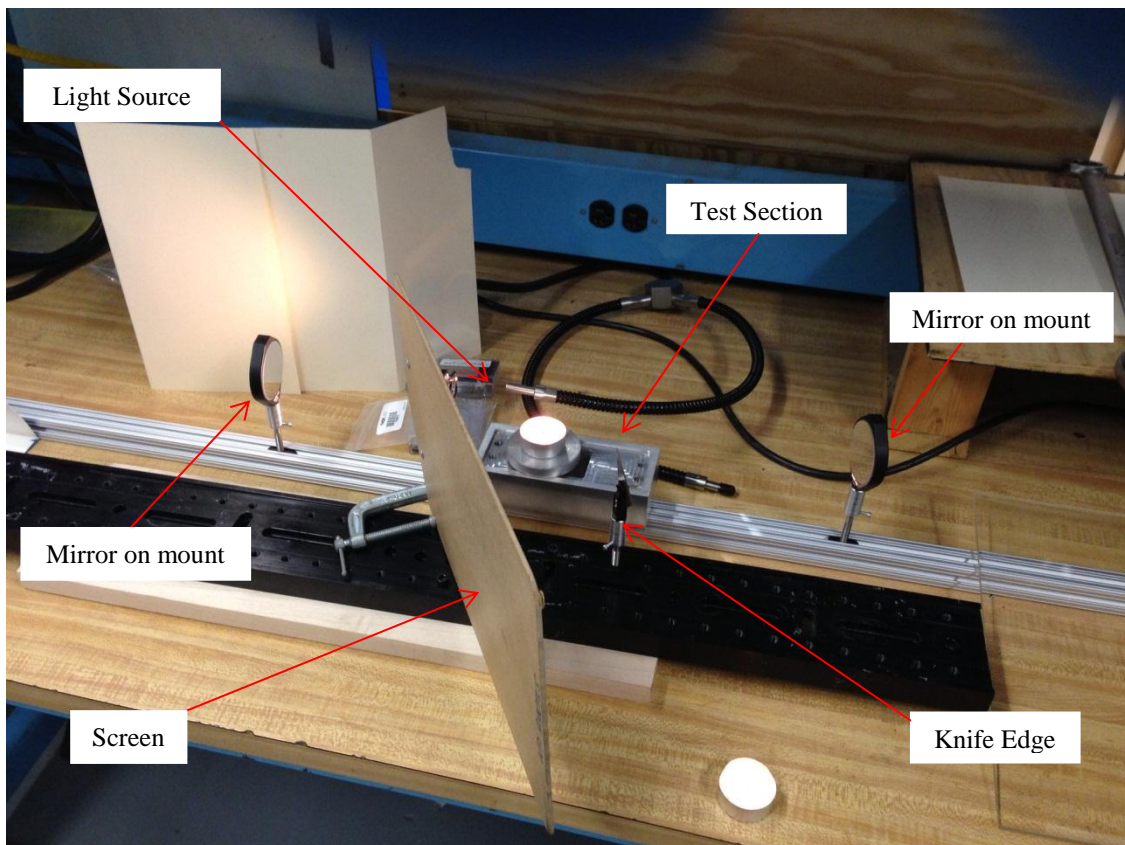
Figure 47: Modified z-system setup

The components[14] used in the modified z-system design were the light source, 2 mirrors and mounts, knife edge, and screen. The set-up of the design is to have both mirrors and mounts located on the same axis, with the test section in between them. The light source and knife edge are located at a set angle of 15° on either side the axis along which the mirrors and mounts are placed. The modified design works by using the light source to provide light to the first mirror from which the light is reflected across the test section to the other mirror. The second mirror is placed so that the reflection is directed to the knife edge, which is set to certain height to cut-off some of the light and produce a more clear and focused image on the screen.

5.2.4 Results of Modified Bench Top Tests

The following objects were used in the modified z-type system bench top tests to produce a density gradient in surrounding air: (1) a candle, (2) a soldering iron, (3) a heat fan, and (4) a blow torch. These objects generated a heat source that created visible density gradients in the test section of the schlieren system. The images of the schlieren results were imported into Adobe's Lightroom Version 4.0 program in order to enhance the contrast of the gradient lines with respect to the rest of the picture.

Candle

The observed image from a candle flame is shown in Figure 48. The image in the test section is inverted, making it appear as if it were upside down. During testing, density gradients moved from the wick of the candle to the bottom of the projected image. The gradient lines were smooth when the flame was not flickering. However, the gradient lines became rougher and more defined when the flame flickered or was disturbed by an outside velocity.

---

[14] A more detailed description of the components is provided in Section 5.2.2
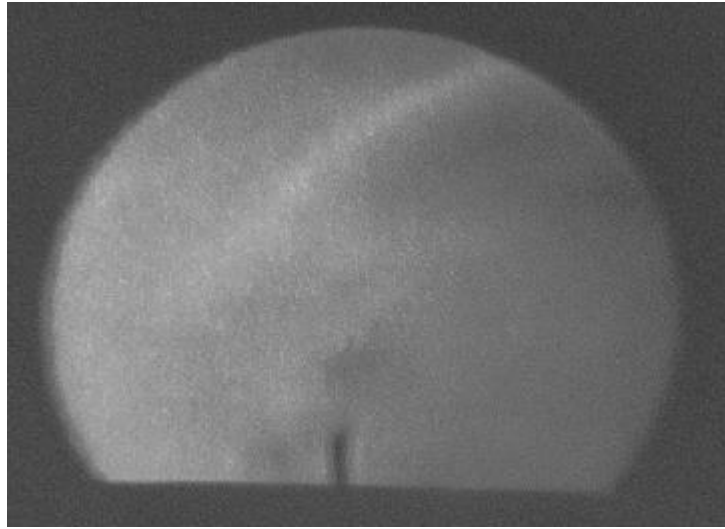
Figure 48: Schlieren image of candle flame in modified z-type system re-inverted to appear "right-side-up"

Soldering Iron

The image created due to the heat generated from a soldering iron is shown in Figure 49. Despite the fact that the soldering iron did not produce a flame, the results of the density gradients appear as clear as the schlieren image of the candle. Again, the image inverted since the heat rising off of the iron is depicted as traveling to the bottom of screen. For ease of view the images were un-inverted in Microsoft Word. As with the candle, the density gradient lines were smooth when no air passed over the surface of the iron. However, when disturbed by surrounding air with some velocity, heat was convectively transferred to the flow, causing the gradients to become more pronounced and rougher in form.
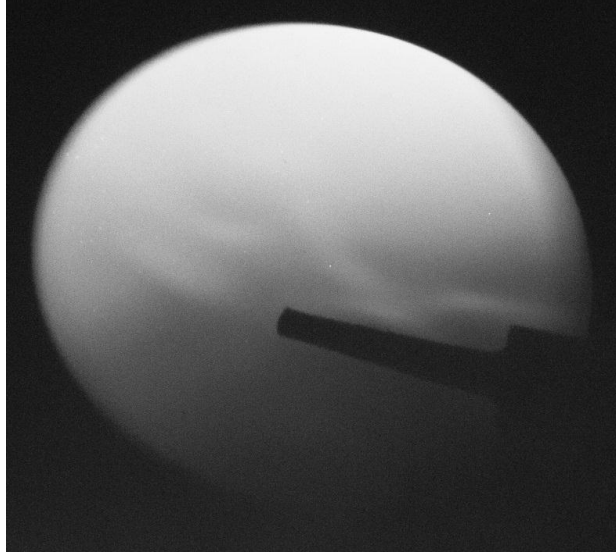
Figure 49: Schlieren image of soldering iron heat in modified z-type system

Heat Gun

The image created by the flow from a heat gun, as used for applying heat shrink tubing, is shown in Figure 50. Like the soldering iron, the heat fan did not produce a flame yet has the same level of quality in the schlieren image. The fan itself creates a flow to the ambient air, where the density gradients appear as smooth streamlines in the flow.
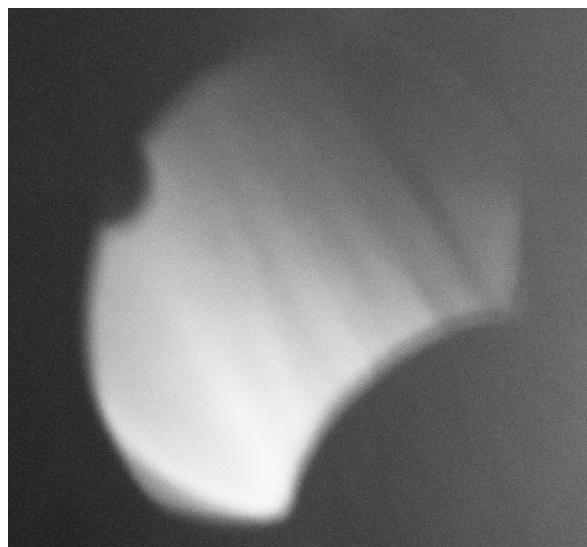
Figure 50: Schlieren image of flow from heat fan in modified z-type system

Blow Torch

The effect created by the flame of a blow torch can be seen in Figure 51. The blow torch combines the effects of the candle and heat fan, where a flame is produced and is subjected to a constant flow from the torch. During testing, the density gradients moved swiftly from the torch to the edge of the projected image. As a result, the gradients show the stream itself clearly distinguishable from the image background, however, it was difficult to acquire a fast enough shutter speed to capture the torch streamlines in more detail.
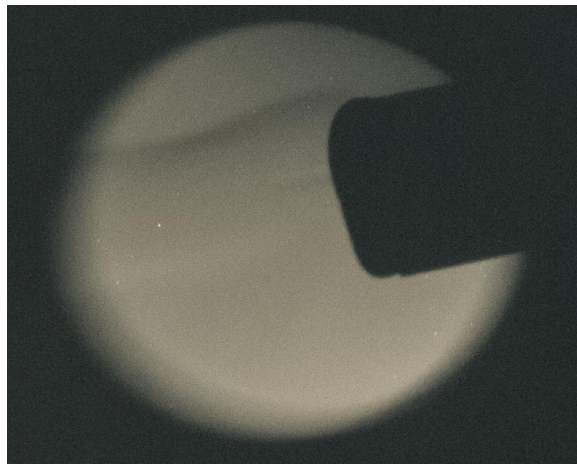
Figure 51: Schlieren image of heat from the blow torch flame in modified z-type system
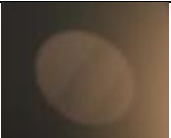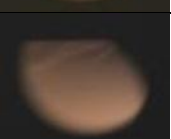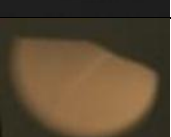
5.2.5 Z-type System Optimization

An optimization exercise was performed in order to transition from testing on a modified benchtop layout to testing on the z-type system rails. The goal of this exercise was to finalize the dimensions of the optical rails. The overall distance between mirrors and the angles that the mirrors were set at towards the light source and knife edge were varied to determine the values that resulted in optimal performance. The values selected for this had to take into consideration the potential interference between the wind tunnel and diagnostics systems. The wind tunnel test section must be suspended in the test section of the schlieren system, and the diagnostics system

is mounted onto the wind tunnel. Due to these factors, the schlieren system needed to allow for a large enough passage that would properly interface with the other components in the project.

The results of the optimization exercise are given in Table 3. The first three columns list key dimensions of the z-type system. The next column shows a picture of the schlieren results using the chosen dimensions. The final column details the observations taken during testing.

Table 3: Results of the z-type system optimization exercise

Trial	Length Between Mirrors [mm]	Mirror Angle [°]	Results	Observations
1	200	15	N/A	Schlieren equipment interfered Too much interference to run trial
2	400	15		Schlieren equipment interfered Unwanted light polluted results
3	600	15		Good results with minor polluting light
4	800	20		Good results without polluting light
5	800	15		Good results without polluting light
6	800	10		Good results without polluting light
7	800	30		Lopsided circle (astigmatism) Results were not as clear
8	800	45		Eye-like shape (severe astigmatism) Results poor quality

9	1200	15		Difficult to align mirror Results slightly blurry
10	1600	15		Difficult to align mirror Results slightly blurry

The results in the trials with shorter distance between the mirrors did not produce optimal results. Light from the light source would pollute the image on the projection screen. Also, components of the system physically interfered with the test section, thus obstructing light rays from passing through the system. The results in the trials with longer distance between the mirrors also did not produce optimal results. As the mirrors were placed further apart, it became difficult to align the mirrors with each other in order to pass light rays through the system. The results in the trials with larger angles between the mirrors and the knife edge did not generate strong results. As the angle of the mirror to the knife edge became larger, the image projected on the screen was no longer circular and suffered from the effects of astigmatism and coma. As a result, the density gradients found in these images were no longer distinctly observed.

The results that produced the highest quality schlieren images had mirrors distanced 800mm apart with the light source and knife edge railings placed at 15 degree angles. The z-type system rails were then cut to the appropriate lengths to replicate the quality of the results when tested on the t-slotted extrusion rails.

5.2.6 Final Z-System Set Up

After refinements were made to our part designs and final dimensions were calculated, a full z-system could be constructed. This full system is a more complete version of the modified system with stricter dimensional tolerance. Having the system hard mounted to x-channel made

duplication of results easier. Figure 52 illustrates the system using the help of SolidWorks. This three-dimensional representation helps visualize the complete design and allow one to understand the dimensions when calculated.
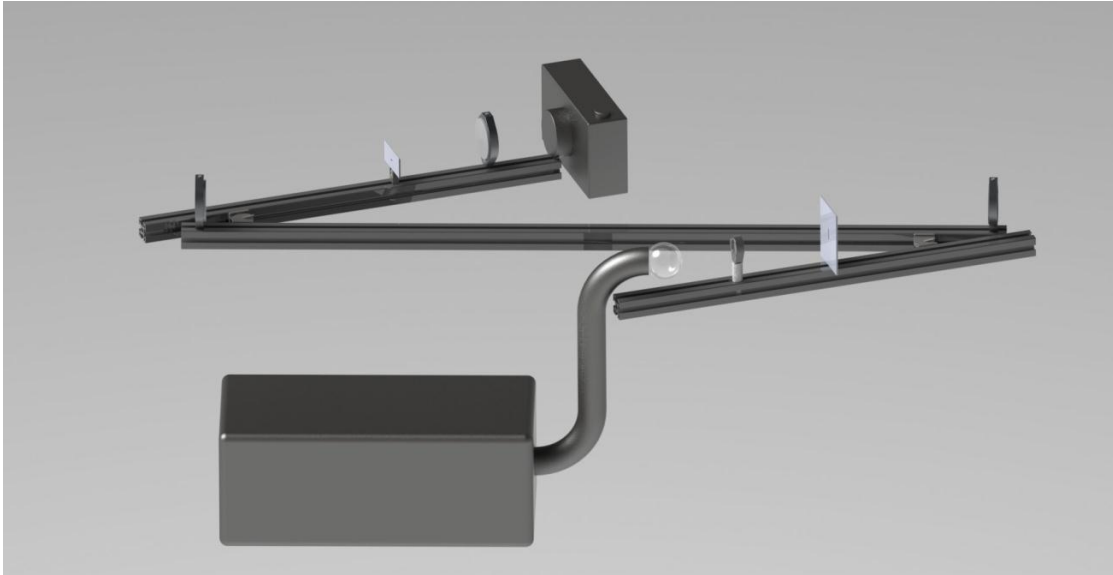
Figure 52: Conceptual design of the z-system prepared in SolidWorks

Shown in Figure 53 is the fully constructed z-system. The main difference from the modified z-system layout is that the full z-system contains adjustable dynamic mounts at the joints, and all of the components are in line due to their mounting on the x-channel. The advantage of this is having the majority of the components attached in one unit, making it easier to move, or alter the angle at made by the smaller legs of the "z." When finished with testing, the dynamic mounts holding the legs can be loosened and folded together making it easy to transfer between tables. During set up, if multiple angles of the z are desired, they can easily be changed; and once changed, minimal work is needed to run the system at the new angle. In addition, the components only need minute adjustment when recalibrating. Therefore, the work involved when operating the full z-system is reduced, and the margin for error is minimized.

Figure 53: Fully constructed z-system

The objects used in the full z-system include: a light source, a condenser lens, a slit, two mirrors, a knife edge, a focusing lens, a screen, and a capturing device (a camera). The use and description of these components are all described in Section 5.2.2 Component Selection. The components follow the same order as before, with the addition of a test section between the two mirrors. This stand-alone z-system was tested with a candle, a soldering iron, a compressed air can spray, and the cross section of a supersonic wind tunnel; all of which performed well. These results are presented in the next section.

5.2.7 Results of Stand Alone Testing

After constructing the full z-type system without a vernier style adjuster, the team was able to achieve clearer results than with the bench top test. However, the improved schlieren images required a great deal of fine adjustment to component heights and distances. This increased the estimated set up time for a successful run longer than initially anticipated. Though trial and error, the team was able to determine the best locations for each optical component that

would provide a clear image without disturbing the test section or the future location of the wind tunnel. These components were then secured into place using nuts and washers on the optical rails. Despite this, the vertical adjustment of the cut-off proved to be very difficult and time consuming with the original adjustable mounts. Due to the relatively small run time of the tunnel as designed, and the limited amount of activated desiccant available, a vernier style linear adjuster was purchased. Figure 54 shows the differences of the z-type system with various component changes.
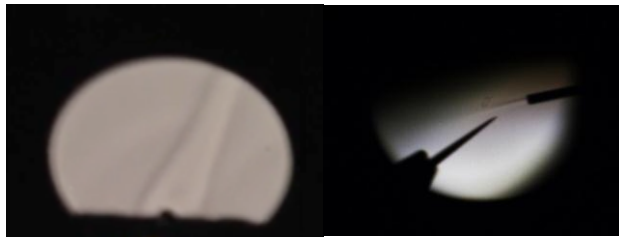
Figure 54: From left to right - schlieren images of z-type system (1) without vernier or focusing lens and (2) with vernier and focusing lens

Although each test produced schlieren images, the addition of the focusing lens, which was added in the bench top test helped produce a clearer image, and the vernier style linear adjuster allowed for the tiny adjustments necessary to balance detail and brightness of the images.

6 Humidity Measurement and Control

In order to design a wind tunnel that with reliable flow diagnostics, it is important to monitor and control the humidity of the inlet flow. The acceleration through a converging-diverging nozzle, from subsonic to supersonic flow, results in substantial temperature and pressure gradients, which can lead to condensation. This causes the flow to become saturated, resulting in the formation of water vapor, which would appear in the form of fog in the tunnel. Fog in the tunnel would negatively affect the quality of visual flow data. The formation of water vapor is also accompanied by latent heat release, which changes the flow properties and pressure distribution in the test section. This results in a decrease in the maximum possible Mach number achievable. The change in Mach number and static pressure as a function of this heat release are related in the following equations (6.1 and 6.2) from Pope [7]:

$$\frac{dM^2}{M^2} = \frac{1 + \gamma M^2}{(1 - M^2)}\left[\frac{dQ}{dx} - \frac{dA}{dx}\right] \tag{6.1}$$

$$\frac{dp}{p} = \frac{\gamma M^2}{(1 - M^2)}\left[\frac{dQ}{dx} - \frac{dA}{dx}\right] \tag{6.2}$$

In these equations γ represents the ration of specific heats (C_p/C_v) and Q represents the amount of heat added per unit mass. These equations show that Mach number and pressure are both functions of heat interaction in the flow. These are two critical measurements that will be made with the flow diagnostic tools. Therefore, it is very important to monitor and control the humidity of the flow entering the wind tunnel.

There are several ways to solve the problem of humidity. The first would be to create a tunnel dimensioned and contoured such that the flow would not induce condensation. Through multiple experiments and calculations, Alan Pope determined the maximum Mach number achievable without condensation is 1.6 [7]. The MQP group in the academic year of 2009-2010

determined this number to be closer to 1.2 for the operating conditions of this project [2]. Using the MATLAB code to implement the method of characteristics, a tunnel with these specifications could be easily generated.

Another option would be to control the humidity of the air entering the channel. One way of doing this would be to dry air slowly over time, store it in a settling chamber, and pump this air into the tunnel. The problem with this option, as it pertains to this project, would be the cost and operational complexity of the storage chamber. The chamber would have to be able to hold at least as much air as the vacuum chamber powering the wind tunnel and remain air tight. This option would be too difficult and expensive for the duration and budget of this project.

The second option to explore is to dry the air continuously as it flows into channel. This would require a filter containing a desiccant to remove moisture from the air. A common design for an air drier utilizing a desiccant is provided in Figure 55. When the tunnel is operating with the dampers at position 1, the ambient air passes through a dust screen and a desiccant bed before it enters the tunnel. The dampers are switched to position 2 after the run to heat up and remove the moisture from, or "reactivate," the desiccant, so it can be used again in the next run [7].
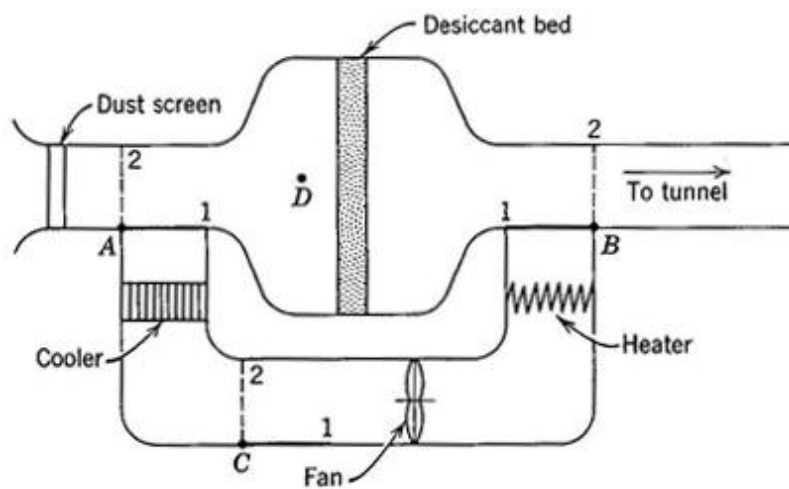
Figure 55: Typical air drying system for an indraft tunnel
(Ref. [7], © 1965, John Wiley & Sons, Inc.)

Two commonly used desiccants for wind tunnels are activated alumina and silica gel. A summary of relevant characteristics of these substances is provided in Table 4. From the information in the table, activated alumina would be a better choice for this project. It is capable of absorbing almost the same amount of moisture as silica gel and has a lower reactivation temperature, which means there is less work required to prepare it for re-use.

Table 4: Characteristics of Activated Alumina and Silica Gel
(Ref. [7], © 1965, John Wiley & Sons, Inc.)

	Activated Alumina	**Silica Gel**
Suggested moisture capacity (lb of water/ lb of desiccant)	0.02	0.03
Reactivation Temperature	275°F	325°F
Max. Temp without Damage	600°F	400°F
Specific Heat (Btu/lb-°F)	0.21	0.22
Typical Density (lb/ft^3)	50	40

The first step in building a filter like the one shown in Figure 55 is to calculate the amount of desiccant required to dry the air in the flow. First, it is first necessary to know the amount of moisture that has to be removed from the flow. To calculate this one must first know the amount of moisture in the air, which can be obtained using Figure 56. The graph in the figure plots the amount of moisture in pounds per pound of dry air as a function of both relative humidity and dry bulb temperature[15].

---

[15] Dry bulb temperature is the temperature of air measure by a thermometer not subject to the moisture of the air
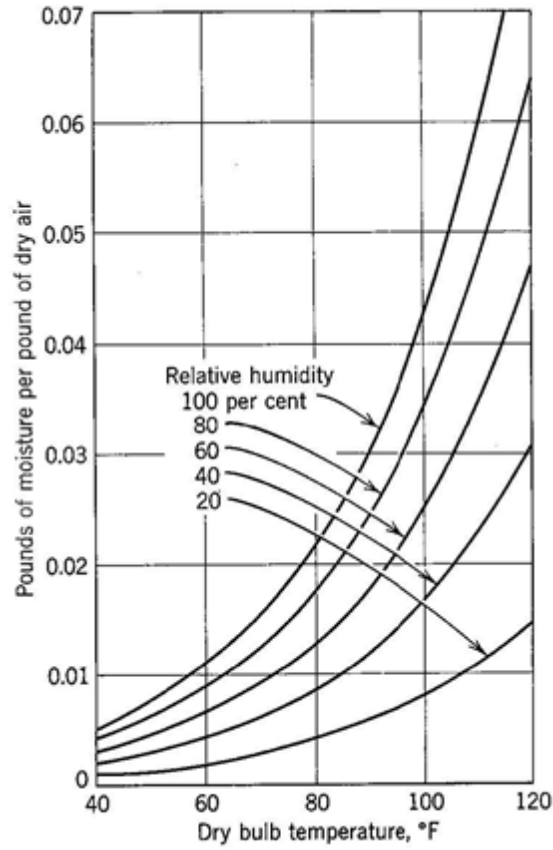
Figure 56: Moisture content of air at various relative humidities
(Ref. [1], © 1965, John Wiley & Sons, Inc.)

Multiplying this number by the total mass of air that passes through the tunnel in one run will yield the total number of pounds of moisture that must be absorbed by the desiccant. Finally, dividing this number by the suggested moisture capacity of the desiccant provided in Figure 56 yields the total mass of desiccant needed.

The volume of the desiccant can then be calculated using its density and the total number of pounds needed. Pope suggests a desiccant bed thickness of twelve inches as a starting point. This is long enough to ensure that the air passes over a sufficient length of desiccant to remove the desired amount of moisture, and also short enough to keep the pressure differential over the

length of the bed to a minimum [7]. Finally, knowing the volume of the desiccant and the proposed thickness, the cross-sectional area of the flow passage can be calculated.

The next consideration in designing the air drier is the pressure drop Δp over the length of the desiccant bed expressed in inches of mercury. The pressure drop can be calculated using the following equation from Pope [7]:

$$\Delta p = 0.0883(1.715U)^{1.38} \tag{6.3}$$

In this equation, U represents the maximum air velocity in the duct approaching the bed. The air velocity can be calculated using the continuity equation, since the mass flow rate remains constant throughout the tunnel. Driers have operated successfully with pressure drops as high as 1.5 inches of mercury, which corresponds to a velocity of about 4.5 ft/s [7]. These values should be used as the maximum design condition.

6.1 Operating Conditions

The wind tunnel is designed to take into account the following operating parameters and conditions. First, the tunnel must reach and sustain a supersonic flow of Mach 2, as verified by onboard diagnostic equipment. Secondly, it must operate at a supersonic flow for a period of 15.2 seconds. The humidity of the air entering the tunnel shall not exceed 40% to prevent a condensation shock wave from forming and destabilizing the supersonic flow, based on our target Mach number. When operating in conjunction with the schlieren system, the humidity must be further reduced to $< 25\%$ to prevent fog from appearing.

All of the operation conditions of the vacuum chamber itself must also be adhered to while running the wind tunnel. The entire wind tunnel assembly must not release any gases or particles that could damage the vacuum tank or pump.

6.2 Initial Air Drier Calculations

In order to create a functional air drier, numerous calculations must first be performed to ensure its compatibility with the facility and wind tunnel. These calculations include the amount of desiccant needed for each run and the pressure drop resulting for a given bed thickness. An Excel spreadsheet was made to compare the results at various room temperatures and relative humidity levels.

To calculate the amount of desiccant required it is first necessary to identify the amount of moisture needed to be removed from the air for each run. This can be obtained by determining the moisture content of the air (pounds of moisture per pound of dry air) and the amount of air passing through the tunnel in each run. For the chosen tunnel design, there is a mass flow $\dot{m} = 0.14$ kg/s $= 0.3051$ lb/s and a test time t $= 12.605$ seconds (Adding a diffuser resulted in a slightly larger test time than this number, which results in a slight increase in amount of moisture to be removed, but over-compensation later in the calculations makes up for this loss). Multiplying these two values yields a mass of 3.846 lb of air to be removed each run. The moisture content, which varies according to temperature and relative humidity, is obtained from Figure 56. By multiplying this moisture content and the amount of air passing through the tunnel in each run, the amount of moisture that needs to be removed per run is found.

Finally, to calculate the amount of desiccant required for each run, the "moisture capacity" (pounds of moisture removed per pound of desiccant) of the desiccant must be known. The desiccant of choice for this project is Activated Alumina, which has a moisture capacity of

0.02 [7]. Simply dividing the quantity of moisture by the moisture capacity yields the weight of desiccant necessary measured in pounds. Figure 57 below is a plot generated using the Excel calculation, which shows the weight of desiccant required for a temperature range of 50 - 100˚F at relative humidity levels of 60 and 80 percent.
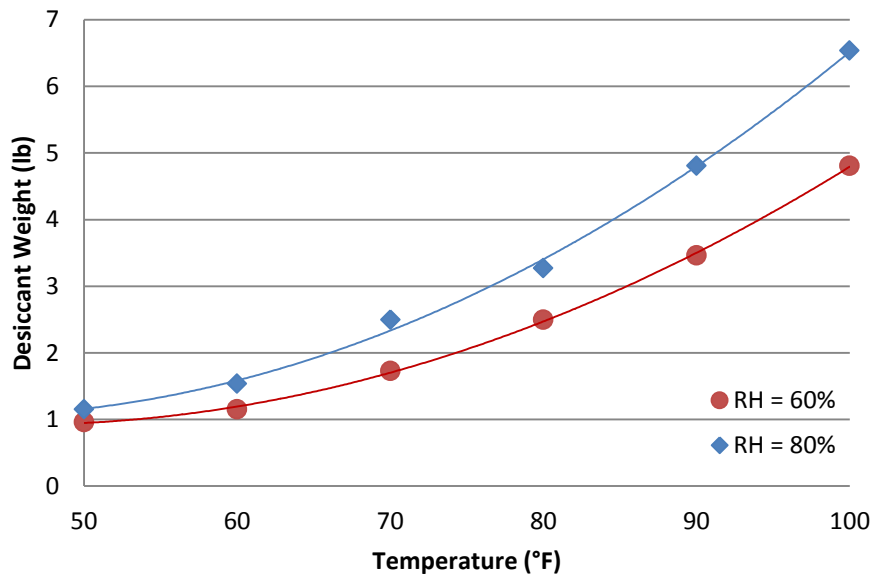
Figure 57: Desiccant weight vs. temperature for two values of relative humidity

Assuming a room temperature of 70˚F would mean that 1.7 and 2.5 pounds of Activated Alumina is required for 60% and 80% relative humidity levels respectively. The goal is to properly dimension the air drier to both fit the necessary quantity of desiccant while maintaining a low enough pressure differential (Δp) such that the flow remains supersonic in the channel. This pressure differential can be calculated by using Equation (6.3). In order to use this equation, however, it is necessary to know the velocity of the flow through the desiccant bed.

As long as the flow in the nozzle is choked, the mass flow is constant throughout the entire tunnel. This is the only time frame that we are interested in drying the air, because this is when data will be collected using the flow diagnostic tools. For this reason, the previously calculated mass flow of the tunnel can be used to calculate an average velocity of the flow through the air drier. We will neglect when the flow becomes unchoked toward the end of the run time. For the purpose of this calculation the following relation for mass flow is given in Equation (6.4):

$$\dot{m} = \rho A U = const. \tag{6.4}$$

In this equation ρ represents the density of the operating fluid (air), *A* is the cross-sectional at the given axial location in the tunnel, and *U* the corresponding mean velocity of the flow. The density of air at standard atmospheric conditions is approximately 0.15 lb/ft^3. This can be considered constant, because the flow through the air drier is subsonic. Therefore only the cross-sectional area has an effect on the velocity of the flow. Because, there is a constant desiccant weight, and therefore constant desiccant volume, the only way to make changes to the cross-sectional area of the bed is to change the bed thickness. So, reducing the bed thickness increases the cross-sectional area, and vice versa.

First the volume of the enclosed desiccant was calculated using the density of activated alumina, which is 50 lb/ft^3. Simply dividing the weight of the desiccant by its density yields the volume in cubic feet. The cross-sectional area is now easily manipulated by selecting various bed thicknesses. The corresponding flow velocity can then be calculated by solving Equation x for velocity, which is then used in Equation x to solve for the pressure drop.

Recall from earlier in this section that the air velocity through the desiccant bed must remain under 4.5 ft/s to guarantee a pressure differential of less than 1.5 inches of Mercury. Pope

[7] also suggests a bed thickness of 12 inches for optimal results. This was the starting point for finding the appropriate dimensions of the desiccant bed. In our case, a 12 inch thickness results in a small cross-sectional area, a high flow velocity through the bed, and therefore a high pressure drop. Steadily decreasing the bed thickness allows for a larger cross-sectional area, smaller flow velocity, and similarly a smaller Δp.

Using the Excel spreadsheet the process above was modeled for various bed thicknesses. Reducing the bed thickness to 1 inch resulted in an acceptable pressure drop of 1 inch of Mercury. This more than 30 percent less than the maximum allowable pressure drop of 1.5 inches of Mercury. The calculated values correspond to the 70˚F and 80% relative humidity case and are shown in Table x. Choosing the higher humidity level makes up for the earlier reduction in test time and also allows for a large enough cross sectional area, such that the Δp is low enough to sustain supersonic flow in the test section.

Table 5: Dimensions and flow considerations for 1 inch bed thickness

Volume (ft^3)	Cross-sectional Area (ft^2)	Velocity (ft/s)	ΔP (in. of Mercury)
0.05	0.60	3.39	1.00

The cross-sectional area given in Table 5, if modeled as a cylinder, would yield a desiccant bed 10.5 inches in diameter and 1 inch thick. The 1 inch thickness is much lower than the 12 inch recommendation, but the tunnel in this project is very small in comparison to other wind tunnels, and that recommendation was likely for a tunnel of larger size. Now that the proper dimensions of the desiccant bed have been determined, designing the air drier is possible.

6.3 Initial Air Drier Design

The necessary components for constructing an air drier to use with the tunnel in this project are the following: a piece of copper tubing to separate the drier from the ball valve such that they do not interfere with each other, a reducer fitting (funnel) to bring the flow from the cross-sectional area of the desiccant bed to the size of the copper fitting, durable fine-mesh screens of proper diameter to enclose the desiccant, aluminum stock to create the necessary fittings, and a stand to support the structure.

Using the calculated values from Section 6.2 Initial Air Drier Calculations and the design considerations mentioned in the background of this section a CAD model was constructed, which can be seen in Figure 58.

Figure 58: Initial design of air drier (outer diameter of funnel entrance (large end) is 13.13 inches for scale)

The design consists essentially of one large funnel attached to the copper fitting that transitions the 10.5 inch diameter of the desiccant bed down to the 1.5 inch diameter of the

copper tubing. The desiccant bed is one removable piece, so it is easy remove and replace the desiccant between runs. The resulting structure will be too heavy to support itself and will thus require a stand. A simple tripod will be used for this purpose.

6.4 Air Drier Assembly

The major components that of the air drying system are the desiccant bed made out of aluminum rings and stainless steel screens, activated alumina desiccant, the reducer coupling, the copper tube connection, and the support stand. The entire air drier system needed to clear the table that was required to hold the schlieren system components directly under the tunnel. Not one piece of the tunnel can be in contact with the table because it would create unwanted table vibrations that would ruin the schlieren system's flow visualization. In order to clear the table, a 16 inch piece of 1.5 inch O.D. copper tubing was brazed to the ball valve and connected to the tunnel inlet to give it the extra length that was necessary. The opposing side of the ball valve is a 6 inch piece of 1.5 inch O.D. copper tube that fits into the air drier's reducer coupling.

The air drier not only needs to clear the schlieren table completely, it must also support itself as well. The increased length of the tunnel system results in a greater moment, which creates more stress on the flange connection to the vacuum chamber's door port. Therefore, the air drier had to be as light and short as possible. In order to relieve the additional stress, an adjustable tripod was used to support it from underneath. A machined aluminum adapter was utilized as the mate between the tripod and copper tubing.

The exact calculations pertaining to the size, thickness, and amount of desiccant needed for the desiccant bed can be found in Section 6.2 Initial Air Drier Calculations. These calculations called for a circular desiccant bed that was 10.5 inches in diameter, with a thickness

of 1 inch to hold the activated alumina desiccant pellets. As a result, we needed a section of the air drier to expand from a 1.5 inch diameter (copper tube) to at least a 10.5 inch diameter (desiccant bed) and could enclose the desiccant beds screens and rings within it. The first idea was to have a custom aluminum funnel made at an external machine shop, and secondly to use the 3D printer at WPI to create it out of a plastic material. The problem with the 3D printer is that it was not large enough to make the funnel, so it would have required the components to be broken up into three separate pieces and connected to each other afterward for the final product. In addition to that, neither of these options fit within the budgets constraints. Consequently, a large plastic funnel was purchased that cost less than half of either of the first two options.

Located at the large mouth of the funnel is a 2.75 inch deep circular ring that proved to be ideal for holding the desiccant bed. The goal was to create an easily removable desiccant bed using two stainless steel screens pressed against either side of a 1.5 inch thick aluminum stock in the shape of a ring, and finally held together by quarter-twenty screws. The outer ring of the desiccant bed clips onto the external surface of the funnel, holding it in place. The purpose of an easily removable bed is to replace the desiccant pellets after each run in order for the humidity to be completely removed from the tunnel. To reuse the saturated desiccant pellets, they are heated in an oven to 300°F for 20 minutes to revert back to their activation state. The screens must tightly contain the desiccant pellets without letting any pellets get loose, so based on the screen's mesh size, a ¼ inch diameter desiccant was chosen so it would not slip past the screens. It is vital that no desiccant pellets are sucked past the screens, into the tunnel, and eventually into the vacuum chamber at high speed, because they could seriously damage the chamber. With that said, a back-up mesh screen was placed at the base of the funnel, right before the copper tubing.

In its final state the air drier system is completely removable from the wind tunnel system at the copper tube joint. When running the tunnel without the air drier, the schlieren system will able to determine how effective the air drying approach actually is. Observations and suggestions were taken to improve the air drier design for possible future iterations.

6.5 Air Drier Testing Procedure

In order to ensure that the air drier is functioning properly, a preliminary testing procedure was developed. The air dryer has two major functions. It must remove moisture from the air before it enters the tunnel, and it must also allow sufficient mass flow such that the flow remains supersonic in the test section. A testing procedure was proposed that will verify if these goals were being met.

In principle, the removal of moisture from the air using a desiccant is very straightforward. The amount of moisture in the air will decrease as it passes through the desiccant. Testing this function of the air drier will involve mostly qualitative analysis. The wind tunnel will be run two times, first without the air drier attached, and then with the air drier attached. Conditions in the test section will be observed and recorded on both runs, noting any condensation or fog visible to both the naked eye and the schlieren visualization system. Without an effective way of measuring the humidity levels within the tunnel itself, this will be the most reliable method to test the air drying capabilities. Developing a humidity measurement system would be a good recommendation for future work.

The second air drier function that needs to be verified is its ability to pass the required air flow rate to sustain supersonic flow. As mentioned earlier, the air drier must remove moisture without altering the free stream conditions in the test section. In order to make sure that this is

happening, the tunnel will once again be run with and without the air drier attached. Static and stagnation pressure readings will be recorded for each run, from which a Mach number can be determined. These values will be compared to each other, and adjustments will be made as necessary.

7 Integrated Testing

Once the systems were developed individually, they were integrated into the full assembly to be tested in unison as per the project goals. This was to ensure that not only each component could fulfill its intended function, but that the whole assembly could interact and operate as a cohesive unit. Figure 59 shows the integrated setup of all components in the project. The channel is attached by the flange to the vacuum chamber with the air drier connected to the entry point of the tunnel. The probe system is connected with the Pitot-static probe on the side panel of the wind tunnel and static ports on the bottom contour surface. The schlieren system is positioned under the tunnel with the mounted optical equipment interfacing with the desired area of the test section.
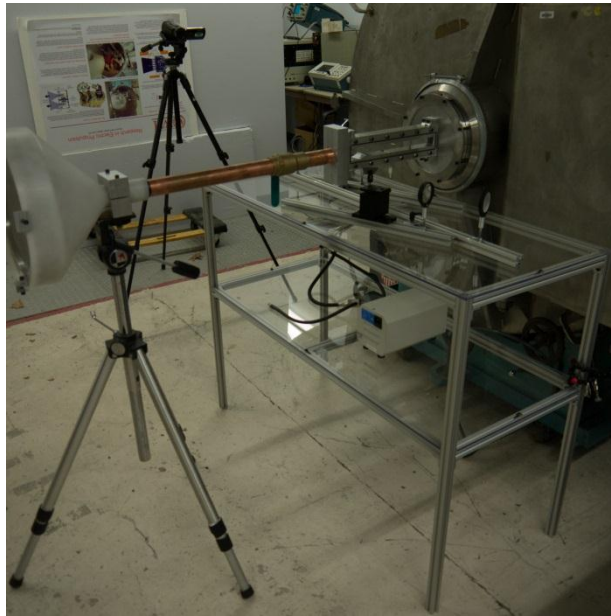
Figure 59: Setup of components in integrated testing

7.1 Testing Without Diagnostics

Several improvements were made over the previous MQPs to account for problems that arose during testing in those earlier projects. The biggest problem encountered in previous MQPs was leakage of the tunnel itself. This prevented the tunnel from being tested due to the inability of the tunnel to seal sufficiently and allow the vacuum system to pump down. To mitigate this problem the tunnel was redesigned to use O-rings placed in specially designed grooves. The grooves restrict the movement of the O-rings and prevent them from entering or interfering with the airflow in the tunnel. This also simplifies the assembly procedure and means that sealing the tunnel can take place on a piece by piece basis, instead of requiring the entire tunnel to be assembled at the same time. The sides of the wind tunnel have one continuous O-ring which mates with the two clear windows. The end blocks of the wind tunnel also have a single O-ring that seal the tunnel and the valve and flange assemblies. These end blocks are secured to the tunnel contour by means of a high strength silicone epoxy. Once the tunnel was completed, preliminary vacuum testing began to ascertain whether the new sealing design was sufficient to allow the tunnel to reach a maximum vacuum of 50 milliTorr.

Sound was also an issue that the previous MQP experienced. This was a result of gaskets being pulled into the air stream by the vacuum, causing them to vibrate like a reed, producing a very loud noise. The design of the current wind tunnel uses O-rings placed in grooves instead of gaskets which should prevent this problem by constraining the movement of the O-rings.

Initial testing of the wind tunnel using the procedure outlined in Section 7 gave satisfying results. The tunnel was able to reach its design vacuum without developing leaks. During the testing a "knee" in the pumping process was observed where the pressure in the chamber appeared to rise despite the fact that the displacement pump was still evacuating the chamber.

The exact cause of this is unknown but it did not hinder the pump down procedure, and the design vacuum pressure was still achieved. It was also noted that after the pump was shut off, the pressure in the tank would rise albeit by an insignificant amount. This was completely normal and within the operating conditions of the vacuum chamber. Typically the chamber is pumped down multiple times to allow the desired vacuum to stabilize but as the increase in pressure was on the order of hundreds of milliTorr, a single pump down was considered sufficient for our initial test.

After the vacuum check was concluded, the valve was opened and a qualitative analysis of the operation of the wind tunnel was performed. While the tunnel was running, it emitted a high pitched sound which appeared to emanate from the ball valve assembly. This conclusion was drawn based on the fact that the sound was heavily mitigated once the funnel and air drier assembly was attached, bringing the sound level down to more comfortable levels.

7.2 Testing with Diagnostics

During testing, pressures measured by the static and stagnation probes did not reach expected levels. During chamber evacuation, the instrumentation followed the expected pressure values (from Equation 4.14 in Section 4.2.3 Data Acquisition System), until the pressure lines fully pinched closed below 10 kPa. Upon running the tunnel, the average measured stagnation and static pressures were 89 kPa and 68 kPa, respectively. However, it is important to note that the average was taken after the tunnel reached a "steady state" with only minor variations from turbulence and electronic noise. This short delay after startup is required to allow the flow to settle and to compensate for pressure loss from the overly compliant pressure lines inflating. The averaged measurements were much higher than expected of a Mach 2.0 flow and when analyzed,

correspond to a Mach number of approximately 0.17 (according to the process described in Section 4.2.3 Data Acquisition System).

Because the programming errors in the subsonic LabVIEW code were not resolved, the measured pressures were incorrectly processed to the supersonic equation but showed the subsonic Mach number. This issue may be caused from the miscalculated range to determine the characteristic of the flow (refers to Figure 21: Range of numerical differences. Also, the measurement of stagnation and static voltages from the pressure transducers was not precise enough to establish an accurate Mach number. As it went through a supersonic loop, a subsonic numerical Mach number was erroneously assessed. These calculations used the same conceptual methods as outlined in the LabVIEW scheme (refers to 4.2.3 Data Acquisition System). In addition, the writing-to-file process was not fully implemented within the system's code to record each data point (stagnation and static pressures and Mach number) which made the group was not able to analyze the characteristic of the flow. The pressure calculations indicated that a shock was never formed at the designed throat of the tunnel and thus the tunnel did not achieve supersonic flow in the test section.

The testing results of the fully integrated wind tunnel system were gathered during the preliminary commissioning. Consequently, it is unclear whether errors in the quantitative results are due to problems with the diagnostics, the geometry of the channel contours, or a combination of both areas. The most likely cause of this would be boundary layer separation of the flow from the channel walls due to the sharp transition between the testing section and the downstream adapter for the flange. This could have decreased the effective cross-sectional area at the end of the tunnel, causing the flow to choke at the exit plate rather than at the designed throat. Since the flow did not choke at the designed throat, the designed diverging section of the nozzle is located

114

before the actual throat at the exit plane. This causes deceleration, rather than acceleration of the flow, resulting in a reduced Mach number.

7.3 Testing with Schlieren Flow Visualization

The schlieren system was set up to perform in the same manner as the bench top tests that utilized heat sources as objects in the test section. The presence of the vacuum chamber and other components of the wind tunnel presented additional challenge upon set up and alignment of the z-system. The system was set up in such a way to avoid physical interference with the vacuum chamber or other components of the wind tunnel, which resulted in a more limited region of the test section that could be visualized qualitatively.

The test section regions that were visualized with the system included the channel throat and the region in front of the Pitot probe. The group expected to see turbulent flow structures at the throat, as well as a bow shock in front of the Pitot probe. The preliminary testing yielded no observable density gradients in either of these regions in the test section with the optical equipment selected for this MQP. These issues led to a troubleshooting assessment that verified the ability of the interfaced schlieren system setup to yield results when presented with a stronger gradient. A butane lighter was introduced on either side of the channel walls to create a density gradient in the same region as air flow through the channel. The results of this assessment confirmed that the schlieren system operated properly when presented with a large enough change in the density gradient from the ambient conditions. Because the density gradient produced in the wind tunnel was not strong enough to be observed with the current equipment, more sensitive optical equipment from the holographic laboratory was implemented. Flow

structures were then observed after the throat of the tunnel with the improved optics in the schlieren system, as shown in Figure 60.

Figure 60: Schlieren results (a) before introducing flow, (b) and (c) during testing

These results showed the presence of a flow structure after the throat, as seen in the upper portion of the image.

There was uncertainty regarding the flow speed due to the possible presence of leaks. There is also the prospect that the geometry of the channel contours is incorrectly calculated. As a result, this makes the tunnel unable to produce a choked flow that can create and swallow a shock wave for proper testing.

8 Recommendations for Future Work

Over the course of testing it was determined that the wind tunnel was unable to reach a supersonic airflow. It is unclear as to what exactly caused this so this team recommends further work into the following areas which were identified as possible problems.

8.1 Tunnel Geometry

It is highly possible that the contour geometry was preventing the wind tunnel from reaching the designed Mach number. During the polishing of the contour surface some material was removed, causing the throat to widen slightly. The impact of this on the Mach number is unknown but it should be taken into consideration when designing a new contour. To assist the next MQP involving this system, this group created and machined a redesigned core section of the tunnel. Instead of two contoured halves the top and bottom pieces have been modified to accept a separate contoured part while preserving the airtight nature of the wind tunnel. This design is shown in Figure 61. The red contoured sections are separate from the upper and lower halves and can be removed to expand the functionality of the wind tunnel. This should make it easier to design test specific contours and install them in the wind tunnel.
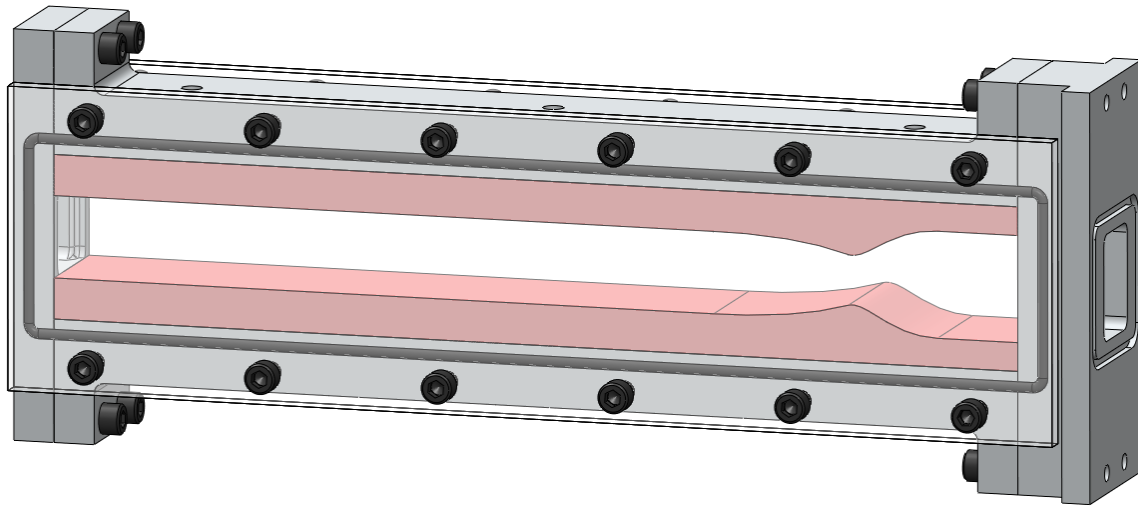
Figure 61: New wind tunnel design

8.2 Pressure Measurements

Future projects can be designed to incorporate more measurements throughout the wind tunnel. The project box left room for three more pressure transducers to be added to the circuit. This allows up to four channels of static pressure measurements to be taken simultaneously, which can be used to find a Mach number distribution around the Pitot probe in the test section. The box can be improved with addition a lid to enclose the transducers and associated hardware. The box should also be relocated to minimize the interference with the schlieren system. One of the problems encountered during testing involved errors in the LabVIEW VI. Future work on the true-or-false process of subsonic and supersonic equations for more precise establishment of subsonic Mach number needs to be improved. Another concern found was that the transducers require further calibration in order to confirm their performance and enhance the accuracy of the measured values. This would entail confirming that the pressure readings obtained via the LabView VI match those from the vacuum chamber gauge. Testing also showed that the rubber

tubing connecting the transducers to the pressure ports pinched shut during chamber evacuation. It is recommended to use stiffer pressure lines that are capable of withstanding the full vacuum process. This phenomenon may have caused deviation from the actual readings and reduced the usable data time for each run. The steel tubing used for the static taps was also slightly oversize which presented a problem when installing them in the SwageLok fittings.

8.3 Schlieren System

Testing the schlieren system showed that improvements can be made to the mirror mounts. These were designed by the group to lower costs of the overall system. However, the mounts were not as stable as desired, had limited adjustability in height, and could not be smoothly adjusted or locked into place when aligning the system. These problems can be solved by purchasing professional kinematic mounts that incorporate these design challenges. Another improvement to the schlieren system would have been including a mount to support the light source. This mount would accelerate alignment of the system and improve overall stability. A third improvement to the system includes the addition of a hole in the top shelf of the table for the light source. The fiber optic cable of the light source is too rigid to turn in the space limited by the wind tunnel, so mounting the light source below the top shelf would allow greater flexibility in positioning the cable. Alternatively, a different fiber optic attachment could be purchased that has greater mobility and reach. The dynamic hinges holding the z-system together should be either filed down, or replaced with other hinges. Currently the bolt holding the hinge together protrudes slightly below the x-channel, thus preventing the two smaller pieces of the z-system from lying perfectly flat on the table.

Another area potential area of improvement is the interfacing of schlieren system with the other tunnel components. The limitations of the z-system cause some problems viewing regions of the tunnel closer to the flange because the edge of the z-system interferes with the door of the vacuum chamber. Solutions to this problem include reconfiguring the shape and size of the z-system, or inclusion of additional length between the end of the channel and the vacuum chamber.

8.4 Humidity Control

Recommendations for future work regarding the air drier system are entirely related to the assembly of the components. The first problem encountered was the actual size and dimensions of the plastic funnel that was purchased. The aluminum rings and clips were machined based off of dimensions provided by the funnel's manufacturer. Upon assembly of the drier it was determined that the provided dimensions were not consistent with the CAD drawing, which resulted in faulty mates and issues with assembly. Therefore this group recommends that future groups design and construct their own funnel in order to guarantee precise mates and a quick and simple assembly.

Another issue faced was the unexpected stretching of the screens due to the tight packing of the desiccant beads. The stainless steel screens were very fine and thus lacked the rigidity necessary to prevent the beads from packing down and bulging out, leaving a significant air gap through which untreated air could flow into the tunnel. Uniform thickness of the desiccant bed is vital to ensure that the pressure calculations are consistent with the air drier assembly. The picture below depicts the assembled air drier with the enclosed desiccant beads displaying the aforementioned air gap.

Figure 62: Assembled air drier showing flaw in desiccant bead packing

The most obvious solution to this problem is to fill the bed with more desiccant beads, but this would result in a greater thickness, which would in turn cause a higher pressure differential over the air dryer. Another solution would be to incorporate two or more cross members on each side of the desiccant bed that span the diameter. This would reinforce the screens and help to maintain the uniform thickness throughout the desiccant bed, while limiting the obstruction of air flow through the air drier. Alternatively, stiffer screens can be employed to reduce the deflection.

References

[1] Moore P. Design of a Supersonic Wind Tunnel. Major Qualifying Project. Worcester Polytechnic Institute 2009. ME-JB3-SWT1.

[2] Butler K, Cancel D, Earley B, Morin S, Morrison E, Sangenario M. Design and Construction of a Supersonic Wind Tunnel. Major Qualifying Project. Worcester Polytechnic Institute 2010. ME-JB3-SWT2.

[3] Balachandran, P. *Fundamentals of Compressible Fluid Dynamics*. New Delhi: Prentice-Hall of India, 2007. Print.

[4] Drikakis D. Introduction to Compressible Flows. Encyclopedia of Aerospace Engineering: John Wiley and Sons, 2010.

[5] Michel A. Saad, "*Supersonic flow*," in AccessScience, ©McGraw-Hill Companies, 2008, <http://www.accessscience.com>. Accessed September 23, 2012.

[6] Huang, J.C. (2008). "Humidity Effect in Transonic Windtunnel Tests". *46th AIAA Aerospace Sciences Meeting and Exhibit.* AIAA 2008-358.

[7] A. Pope and K. Goin, *High-Speed Wind Tunnel Testing.* New York, NY, USA: John Wiley and Sons, 1965.

[8] "NPTEL: Mechanical Engineering - Gas Dynamics." NPTEL: Mechanical Engineering - Gas Dynamics. <http://nptel.iitm.ac.in/courses/112103021/34>. Accessed October 3, 2012.

[9] International Organization for Standardization. Standard Atmosphere. ISO 2533: 1975. 1975. <http://www.iso.org/iso/catalogue_detail?csnumber=7472>. Accessed November 4, 2012.

[10] Series 1700 Mechanical Booster Vacuum Pumps, Series MB Two-Stage Vacuum Pumps.Bulletin 536. Penwalt Corp.; 1980.

[11] Devenport, William J. *Nozzle Applet*. 01/03/01. EngAPPLETS. Virginia Tech.

[12] *efunda.com.* (n.d.).
<http://www.efunda.com/designstandards/sensors/hot_wires/hot_wires_intro.cfm>.
Accessed October 9, 2012.

[13] P.C. Stainback and K.A. Nagabushana, "Review of hot-wire anemometry techniques and the range of their applicability for various flows," Electronic Journal of Fluids Engineering, Transactions of the ASME., vol. 167 (1993).
<http://scholar.lib.vt.edu/ejournals/JFE/data/JFE/DB96-DEC/S&N/hot-wire.pdf >. Accessed September 12, 2012.

[14] John J, Keith T. Gas Dynamics, 3rd Ed., Ch 15. New Jersey: Pearson Prentice Hall; 2006.

[15] M.R. Emami, *Supersonic Flow and Shockwaves*, Ch. 6. University of Toronto, Canada; 2008.

[16] Honeywell Sensing TruStability Silicon Pressure Sensors: HSC Series-High Accuracy
<http://sensing.honeywell.com/index.php/ci_id/44482/la_id/1/document/1/re_id/0>.
Accessed February 5, 2013.

[17] Settle, Gary S., *Schlieren and Shadowgraph Techniques: Visualizing Phenomena in Transparent Media*. New York: Springer-Verlag; 2001.

[18] Kontis K, Zare-Behtash H. Optical Flow Visualization. Encyclopedia of Aerospace Engineering, Online 2010. DOI: 10.1002/9780470686652.eae069. Accessed October 7, 2012.

[19] Jebsen-Marwedel, H. "Schlieren" als Wort, Gebilde und Begriffe. *Glastechniche Berichte*, 33(12):475-477, 1960.

[20] Hanenkamp A, Merzkirch W. Investigation of the properties of a sharp-focusing schlieren system by means of Fourier analysis. Optics and Lasers in Engineering 2006 0;44(3–4):159-169.

[21] Venkatesh Gopal and Julian L Klosowiak and Robert Jaeger and Timur Selimkhanov and Mitra,J.Z.Hartmann. Visualizing the invisible: the construction of three low-cost schlieren imaging systems for the undergraduate laboratory. European Journal of Physics 2008;29(3):607.

Appendix A: Derivation of Equation for Test Time

Derivation of Mass Flow Rate

$\dot{m}$ = mass flow rate, ρ^* = Density at throat, A^* = Area at throat, V^* = Velocity at throat,

P^* = Pressure at throat, R = Perfect Gas constant, T^* = Temperature at throat,

M^* = Mach number at throat, γ = specific heat ratio

T_0^* = Stagnation Temperature at throat, P_0^* = Stagnation Pressure at throat

These are initial definitions of mass flow rate, density, and velocity taken at the throat of the

tunnel.

$$\dot{m} = \rho^* A^* V^*$$

Where $\rho^* = \dfrac{P^*}{RT^*}$ and $V^* = M^* \sqrt{\gamma R T^*}$

When put together, the mass flow rate equation then becomes the following.

$$\dot{m} = \frac{P^* A^*}{\sqrt{T^*}} \sqrt{\frac{\gamma}{R}} \times M^*$$

Here are basic stagnation to static ratio equations of temperature and pressure dependent on

Mach number and the specific heat ratio. Also any Mach number at a choked throat will be 1.

Where $\dfrac{T_0^*}{T^*} = 1 + \dfrac{\gamma-1}{2} M^{*2}$, $\dfrac{P_0^*}{P^*} = \left(1 + \dfrac{\gamma-1}{2} M^{*2}\right)^{\frac{\gamma}{\gamma-1}}$,   and $M^* = 1$

The $\dfrac{P^*}{\sqrt{T^*}}$ in the above mass flow equation has been redefined using the ratio equations.

$$\frac{P^*}{\sqrt{T^*}} = \sqrt{\frac{P_0^{*2}\left(\frac{2}{\gamma+1}\right)^{\frac{2\gamma}{\gamma-1}}}{T_0^*\left(\frac{2}{\gamma+1}\right)}} = \frac{P_0^*}{\sqrt{T_0^*}}\sqrt{\left(\frac{2}{\gamma+1}\right)^{\frac{2\gamma-(\gamma-1)}{\gamma-1}}}$$

Placing the $\frac{P^*}{\sqrt{T^*}}$ back into the mass flow equation, one can get the following.

$$\dot{m} = \frac{P_0^* A^*}{\sqrt{T_0^*}}\sqrt{\frac{\gamma}{R}\left(\frac{2}{\gamma+1}\right)^{\frac{\gamma+1}{\gamma-1}}}$$

Since the process from atmosphere to the throat is isentropic, it can be assumed that $P_0^*=P_{atm}$, and

$T_0^*=T_{atm}$.

$$\dot{m} = \frac{P_{atm} A^*}{\sqrt{T_{atm}}}\sqrt{\frac{\gamma}{R}\left(\frac{2}{\gamma+1}\right)^{\frac{\gamma+1}{\gamma-1}}}$$

This is the final equation for mass flow, which is used in this project, and used in the following

derivation of the test time.

Derivation of the Test Time
Generic Continuity Equation:

$$\frac{\partial}{\partial t}\iiint_{CV(t)} \rho d\forall_{chamber} + \oiint_{CS(t)} \rho\vec{V_r}\cdot\hat{n}dS = 0$$

After integrating the vacuum chamber volume $\forall$ and the control surface about the throat of the

nozzle, it becomes the following.

$$\frac{\partial}{\partial t}\rho\forall_{chamber} - \rho^*V^*A^* = 0$$

The vacuum chamber volume $\forall$ is constant with respect to time, and $\dot{m} = \rho^*V^*A^*$, which was

derived previously. This becomes the following equation after moving the mass flow to the other

side and integrating, assuming the volume doesn't change with density, and mass flow rate at the

throat does not change with respect to time during supersonic flow.

$$\forall_{chamber} \int_i^d d\rho = \dot{m} \int_0^t dt$$

The integration of density is from the initial vacuum chamber air density, right before the valve

to the wind tunnel is opened, to the diffuser air density downstream of a shock wave at the point

in time when the shock wave is about to enter the test section. When the shock wave enters the

test section, the test section becomes subsonic.

At this point in the calculation, the filling process of the vacuum chamber is generically

established as a polytropic process. The definition of a polytropic process is as follows.

$$Pv^n = C_1 \ \text{or} \ \frac{P}{\rho^n} = C_1$$

The variable pressure and air density is equated to the initial pressure and density.

$$\frac{P}{\rho^n} = \frac{P_i}{\rho_i^n} \ \text{or} \ \rho(t) = \rho_i \left(\frac{P(t)}{P_i(t)}\right)^{\frac{1}{n}}$$

Here is the differential form of the equation.

$$d\rho = \frac{\rho_i}{P_i^{1/n}} \times \frac{1}{n} \times P(t)^{\frac{1-n}{n}} dP$$

Placing the air density differential back into the Continuity equation, where ρ_d is the air density

at the diffuser.

$$\dot{m}t = \forall_{chamber} \frac{\rho_i}{P_i^{1/n}} \times \frac{1}{n} \int_{\rho_i}^{\rho_d} P(t)^{\frac{1-n}{n}} dP$$

Integrating the equation, and pulling out a P_d.

$$\dot{m}t = \forall_{chamber} \times \frac{\rho_i}{P_i^{\frac{1}{n}}} \times P_d^{1/n} \left(1 - \left(\frac{P_i}{P_d}\right)^{1/n}\right)$$

Here is an altered polytropic relation.

$$\rho_d = \frac{\rho_i}{P_i^{1/n}} \times P_d^{1/n}$$

Substituting in the altered polytropic relation.

$$\dot{m}t = \forall_{chamber} \times \rho_d \left(1 - \left(\frac{P_i}{P_d}\right)^{1/n}\right)$$

A definition from the ideal gas law.

$$\rho_d = \frac{P_d}{RT_d}$$

The final Test Time Formulation

$$t = \frac{\forall_{chamber} P_d}{\dot{m} R T_d} \left(1 - \left(\frac{P_i}{P_d}\right)^{1/n}\right)$$

Assuming an isothermal process, n=1, for a conservative approach.

$$t = \frac{\forall_{chamber} P_d}{\dot{m} R T_d} \left(1 - \frac{P_i}{P_d}\right)$$

The derivation of this equation can be found in Pope [7]

Appendix B: Air Drier Assembly Procedure

For the purpose of this project the air drier system is not crucial to the operation of the wind tunnel. The air drier does however provide a valuable function for the schlieren's flow visualization by removing the moisture from the incoming air. For future use it is very important that one knows the proper assembly and components of the air drier so it operates correctly.

There are several components that are meant to be permanently mated. The first set of components that are fixed at all times are the white plastic funnel (Figure 58), copper piping, tripod adapter and tripod. The second set of components that stay connected are the ½ inch aluminum ring, 20-mesh stainless steel, and 1 inch aluminum ring held together by ¼ -20 hex screws. The third set of fixed components is a ½ in. aluminum ring with a 20-mesh stainless steel screen glued to it.

Materials and Tools needed for assembly:

Item #	Description	Quantity
1	Plastic Funnel / Copper Pipe / Tripod assembly	1
2	¼ -20 hex screws (½ in. length)	4
3	¼ -20 hex screws (1 in. length)	4
4	Al funnel clip	4
5	½ in. thick Al ring with fixed S.S. screen assembly	1
6	½ in. thick Al ring / 1 in. thick Al ring / S.S. screen assembly	1
7	Strainer screen	1
8	¼ in. Activated Alumina Desiccant Pellets	2 lbs.
9	Allen wrench	1
10	Level	1

Air Drier set up and desiccant filling Instructions:

1. Insert item #1 into the open end of the ball valve (attached to wind tunnel), and adjust the tripod until level by placing item #10 on top edge of the copper pipe.

2. Pour approximately 2 lbs. of desiccant pellets onto the strainer screen and shake out all loose particles.

3. Place item #6 on a flat surface with the 1 in. thick ring placed on top.

4. Carefully take the sifted desiccant pellets and place them within the desiccant bed onto the screen surface until the desiccant pellets are flush with the top of the 1 in. ring.

5. Gently place item #5 onto the filled desiccant bed with the screen of item #5 on the bottom.

6. Align item #4 on the 4 holes. Using items #3 and #9, fasten the assembly together until tight.

7. Lift assembly into a vertical position. If the desiccant pellets compact down so much that you can see through a window greater than ½ in. at the top of the screen, then you must repeat steps 3 thru 6.

8. Once the desiccant bed is properly assembled, carefully insert the bed into the large mouth of the funnel such that the clips grab the outer edge.

9. With an Allen wrench tighten the ½ in. hex screws (Item 2) onto the outer diameter of the plastic funnel until they are snug.

Only once all of these steps are completed successfully, the Air Dryer is ready to be used.

Appendix C: Set-up & Alignment of Z-System

Set up

- Ensure all components are present
    - 2 x mirrors, 1 x condenser lens, 1 x focusing lens, 4 x pre-assembled mounts, folded z-system
- Un-fold z-system
- Using gloves carefully remove optical mirror and lenses and insert them into their respective optical mounts
- Gently tighten the optical mounts and ensure that the mirrors / lenses are securely fastened
- Attach to adapter mount
- When loosened the mount should be able to slide freely through the X-channel
- Place mounts in designated areas, marked on X-channel for optical mirrors only (lens can vary in location)
- When in place both the rod from the adapter mount and the hex nut can be tightened to secure the optical component in place
- When transporting remove all optical components
- When finished with testing all optical components should be covered with plastic sleeves to ensure dirt or other contaminates do not reach the optical components

Alignment

- Start with light source (using goose neck)
    - Place light source block on lower shelf
    - Secure goose neck separation point with a clamp
    - Position one fiber optic tube around one inch behind the condenser lens
        - Try to achieve a level position parallel to the x-channel
    - Using a piece of paper, or other large surface, place behind first mirror to ensure proper positioning of light source
        - Position center of light coming through condenser lens at mirror
        - (Adjustment of the light source will most likely be needed)
- Align first mirror
    - By carefully turning the mirror aim the light reflected to second mirror
    - Again, using a piece of paper, or other large surface, place behind second mirror to ensure proper positioning
        - Light coming from first mirror should be centered over second mirror
- Align second mirror
    - By carefully turning the mirror aim the light towards the focusing lens and knife edge

- o As long as the knife edge is able to cut off light proceed to knife edge alignment
  - o If the knife edge is un able to reach the desired height, re-alignment of the light source may be needed
- Align focusing lens
  - o This component alters the point of cut off for the knife edge
- Align knife edge
  - o The point of cut off can be found by moving a piece of paper back and forth parallel to the x-channel
  - o The location at which the light beam is the smallest is cut off point
  - o Position the knife edge along the x-channel at this point
  - o Through raising and lowering of the linear adjuster more and less cut off can be achieved
  - o Minute adjustments may therefore be made to the cut off throughout testing
- During testing, use photo quality paper to view results